CENTER FOR CONNECTED AND AUTOMATED TRANSPORTATION

CCAT-NU-2025-3
October 2025

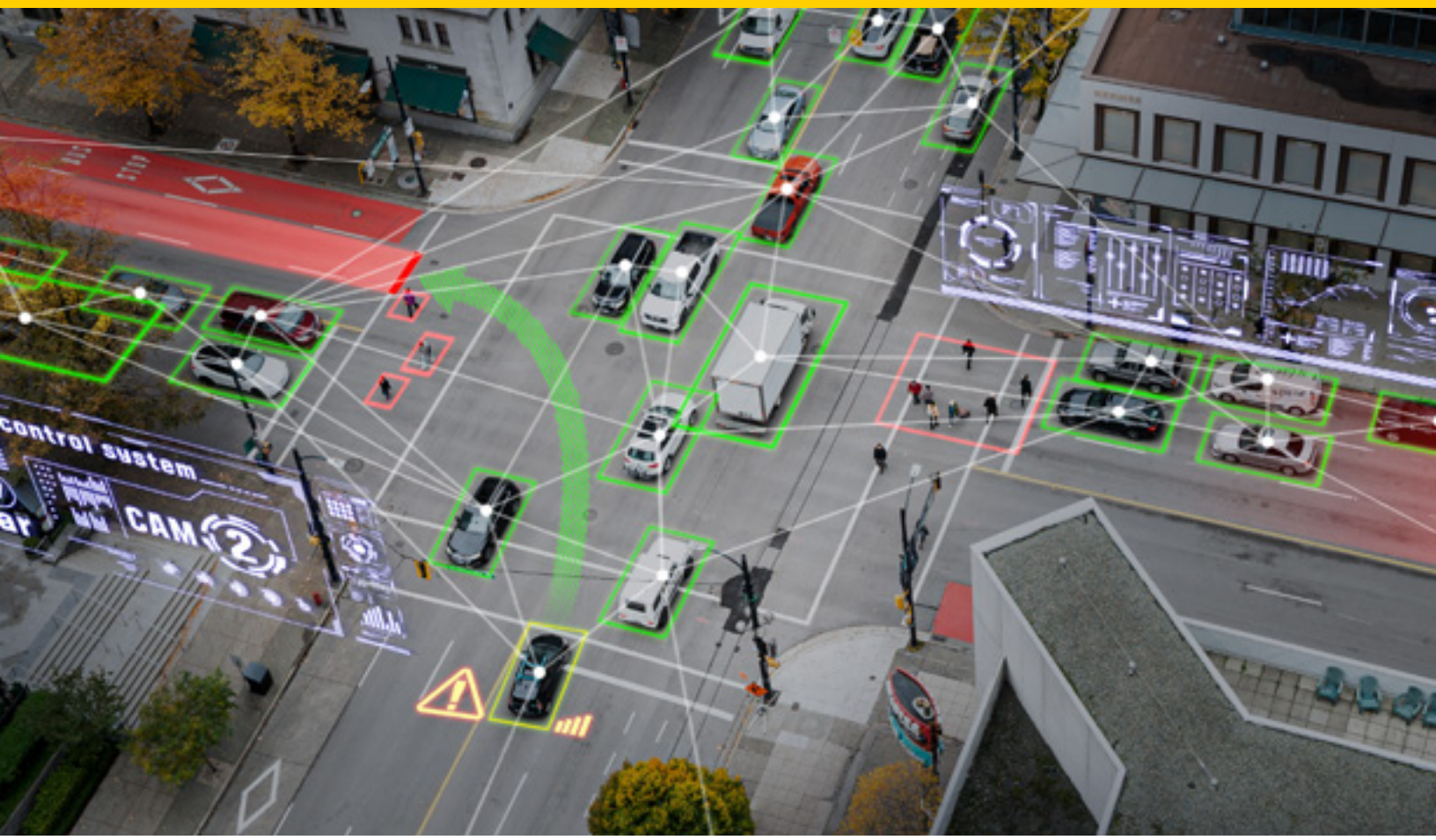

Making CAV Deployments Compatible with Complete Streets Objectives for Safe and Efficient Operation Phase I

Hani S. Mahmassani
Sharika J. Hegde
Meredith Raymer
Amirmohammad Khakpour

Northwestern

CENTER FOR CONNECTED AND AUTOMATED TRANSPORTATION

Report No. CCAT-NU-2025-3 September 2025

Project Start Date: 12/1/2023

Project End Date: 9/30/2025

Making CAV Deployments Compatible with Complete Streets Objectives for Safe and Efficient Operation

Phase I

Hani S. Mahmassani
Professor

Sharika J. Hegde
Graduate Researcher

Meredith Raymer
Graduate Researcher

Amirmohammad Khakpour
Graduate Researcher

Northwestern University

DISCLAIMER

Funding for this research was provided by the Center for Connected and Automated Transportation under Grant No. 69A3551747105 of the U.S. Department of Transportation, Office of the Assistant Secretary for Research and Technology (OST-R), University Transportation Centers Program. The contents of this report reflect the views of the authors, who are responsible for the facts and the accuracy of the information presented herein. This document is disseminated under the sponsorship of the Department of Transportation, University Transportation Centers Program, in the interest of information exchange. The U.S. Government assumes no liability for the contents or use thereof.

Suggested APA Format Citation:

Mahmassani, H., Hegde, S., Raymer, M., & Khakpour, A. (2025). Making CAV deployments compatible with Complete Streets objectives for safe and efficient operation, Phase I (Final Project Report). Northwestern University, Center for Connected and Automated Transportation (CCAT).

Contacts

For more information:

Brett Johnson

Northwestern University
600 Foster St
Evanston, IL 60208

bretj@northwestern.edu
(847) 491-7287

CCAT

University of Michigan Transportation Research Institute
2901 Baxter Road
Ann Arbor, MI 48152

umtri-ccat@umich.edu
(734) 763-2498

Technical Report Documentation Page

1. Report No. CCAT-NU-2025-3	**2. Government Accession No.**	**3. Recipient's Catalog No.**
4. Title and Subtitle Making CAV Deployments Compatible with Complete Streets Objectives for Safe and Efficient Operation – Phase I		**5. Report Date** September 2025 **6. Performing Organization Code** N/A
7. Author(s) Hani S. Mahmassani (orcid.org/0000-0002-8443-8928), Sharika J. Hegde (orcid.org/0000-0002-8822-3844), Meredith Raymer (orcid.org/0000-0003-2138-0842), Amirmohammad Khakpour (orcid.org/0009-0002-2441-5481)		**8. Performing Organization Report No.** N/A
9. Performing Organization Name and Address Northwestern University Transportation Center 600 Foster St. Evanston, IL, 60201		**10. Work Unit No.** **11. Contract or Grant No.** Contract No. 69A3551747105
12. Sponsoring Agency Name and Address U.S. Department of Transportation Office of the Assistant Secretary for Research and Technology 1200 New Jersey Avenue, SE Washington, DC 20590		**13. Type of Report and Period Covered** Final Report (December 2023 – September 2025) **14. Sponsoring Agency Code** OST-R

15. Supplementary Notes
Conducted under the U.S. DOT Office of the Assistant Secretary for Research and Technology's (OST-R) University Transportation Centers (UTC) program.

16. Abstract
This research examines how Connected and Autonomous Vehicle (CAV) deployments can be made compatible with Complete Streets objectives through strategic infrastructure design and systematic interaction management to optimize urban space utilization. Urban transportation systems face increasing pressure to accommodate both autonomous vehicle technology and human-centered design principles within limited street space.Three analytical approaches were employed to address this challenge. Network-level analysis using area-based Network Fundamental Diagrams quantified multimodal traffic flow through SUMO microsimulations across varying infrastructure configurations. Microscopic interaction modeling used extended Drift Diffusion Models to analyze pedestrian-CAV encounters in two-lane environments, examining how different behavioral parameters affect safety and efficiency. A probabilistic space utilization framework employed Monte Carlo simulations to identify conflict hotspots and evaluate competing demands for street space. Results demonstrate that modal separation produces substantial efficiency gains, with network throughput increasing from 0.09 to 0.18 veh/min/m² when transitioning from shared to separated infrastructure. Pedestrian separation through sidewalks generates the largest initial benefits across all modes. However, in space-constrained environments where complete separation is impossible, managing interactions between different modes becomes critical for maintaining both safety and efficiency. Optimal pedestrian-CAV interaction parameters minimize conflicts while preserving reasonable crossing opportunities, and the probabilistic framework successfully identifies areas where systematic management strategies are most needed.The research concludes that infrastructure separation provides optimal outcomes, but effective management of modal interactions is essential for maximizing space utilization efficiency in real-world urban environments. Transportation planners can apply this methodological toolkit to evaluate design alternatives, prioritize separation where feasible, and implement evidence-based strategies for managing unavoidable conflicts in space-constrained locations.

17. Key Words Connected and Autonomous Vehicles, Complete Streets, Network Fundamental Diagram, Conflict management, Multimodal transportation	**18. Distribution Statement** No restrictions.

19. Security Classif. (of this report) Unclassified	**20. Security Classif. (of this page)** Unclassified	**21. No. of Pages** 86	**22. Price**

Form DOT F 1700.7 (8-72) Reproduction of completed page authorized

Making CAV Deployments Compatible with Complete Streets Objectives for Safe and Efficient Operation

Phase I

Hani S. Mahmassani
https://orcid.org/0000-0002-8443-8928

Sharika J. Hegde
https://orcid.org/0000-0002-8822-3844

Meredith Raymer
https://orcid.org/0000-0003-2138-0842

Amirmohammad Khakpour
https://orcid.org/0009-0002-2441-5481

Northwestern University

Table of Contents

List of Figures

List of Tables

Abstract

The deployment of Connected and Autonomous Vehicles (CAVs) promises significant improvements in traffic flow efficiency and safety through enhanced connectivity and automation. Simultaneously, the Complete Streets movement advocates for human-centered urban design that prioritizes accessibility, safety, and comfort for pedestrians, cyclists, and micromobility users. These seemingly divergent objectives have evolved on separate tracks, resulting in fragmented policy approaches that may compromise both technological efficiency and vulnerable user safety. This Phase I report presents a methodological framework that systematically examines the compatibility of CAV deployments with Complete Streets objectives through three integrated analytical approaches.

First, we develop network-level analysis tools using area-based Network Fundamental Diagrams (NFDs) to quantify how Complete Streets infrastructure affects multimodal traffic flow. Through SUMO microsimulations of varying street configurations, we demonstrate that increased modal separation benefits all users, with network efficiency improvements of up to 100% when transitioning from shared to separated infrastructure.

Second, we turn to the reality that modal separation is not always feasible, particularly in dense urban environments where space is limited and shared use is unavoidable. In these contexts, managing conflicts and interactions becomes essential for balancing efficiency and safety. We examine microscopic encounters between CAVs and pedestrians using an extended Drift Diffusion Model for pedestrian crossing decisions in two-lane environments. Our integrated simulation platform captures how pedestrian behavior disrupts CAV flow and highlights the importance of understanding interaction dynamics when space cannot be fully segregated. Sensitivity analysis further identifies parameter ranges where conflicts can be minimized without compromising reasonable pedestrian crossing opportunities, offering insights into how shared space can be managed more effectively.

Third, we propose a unified probabilistic framework for multimodal space utilization that uses Monte Carlo simulations to identify spatial and temporal conflict hotspots, enabling systematic evaluation of competing demands for limited street space.

The integration of these approaches yields a methodological toolkit that enables scenario analysis balancing technological efficiency with human-centered design principles. Key findings indicate that strategic infrastructure separation can achieve both CAV flow optimization and Complete Streets safety objectives but requires careful attention to pedestrian-vehicle interaction dynamics and space allocation efficiency. This work provides planners and engineers with evidence-based tools for designing urban streets that accommodate both autonomous vehicle deployment and vulnerable user needs, establishing a foundation for Phase II implementation and real-world validation.

Introduction

Urban transportation systems stand at a critical juncture where two powerful and seemingly contradictory forces are reshaping street design and operation. On one side, the rapid advancement of Connected and Autonomous Vehicle (CAV) technology promises unprecedented improvements in traffic flow efficiency, safety, and network throughput through enhanced vehicle coordination, reduced reaction times, and optimized routing algorithms. On the other side, the Complete Streets movement advocates for fundamental changes in urban design philosophy, prioritizing human-scale environments that provide safe, accessible, and comfortable mobility options for pedestrians, cyclists, and emerging micromobility users across all ages and abilities.

The tension between these paradigms reflects deeper questions about the future of urban mobility. CAV deployment strategies typically emphasize system-wide efficiency metrics such as vehicle throughput, travel time reduction, and network capacity optimization. These objectives align with traditional traffic engineering approaches that have historically prioritized motorized vehicle flow. In contrast, Complete Streets principles challenge this vehicle-centric paradigm by demanding that street design accommodate the full spectrum of urban users, with particular attention to vulnerable populations who have been marginalized by conventional transportation planning.

This fundamental incompatibility has manifested in fragmented policy approaches and ad-hoc implementation strategies that fail to address the underlying conflicts between technological efficiency and human-centered design. Cities implementing Complete Streets retrofits often do so without considering how these changes might affect future CAV operations, while CAV deployment pilots typically ignore existing or planned active mobility infrastructure. The result is a patchwork of investments and interventions that may inadvertently create new safety risks, particularly for pedestrians and micromobility users who must navigate increasingly complex technological environments.

CAV technology offers genuine opportunities to improve urban mobility through reduced congestion, enhanced safety, and more efficient use of existing infrastructure. However, these benefits risk being undermined if deployment strategies conflict with broader urban livability goals or exacerbate existing inequities in transportation access. Conversely, Complete Streets implementations that ignore technological realities may fail to achieve their safety and accessibility objectives if they create operational conflicts with emerging vehicle technologies.

This Phase I report addresses these challenges through the development of a systematic analytical framework that enables rigorous investigation of scenarios combining CAV deployment with Complete Streets objectives. Rather than treating these as competing paradigms, our approach seeks to identify design principles and operational strategies that can achieve both technological efficiency and human-centered urban environments. The methodology integrates three complementary analytical approaches: network-level performance modeling using extended Network Fundamental Diagrams, microscopic interaction modeling of

pedestrian-CAV decision-making, and probabilistic frameworks for multimodal space utilization analysis.

The research objective is to develop a methodological toolkit that enables planners and engineers to evaluate street design alternatives based on comprehensive performance metrics spanning safety, efficiency, and equity considerations. This toolkit addresses the critical gap between transportation engineering approaches focused on system optimization and urban planning approaches emphasizing livability and accessibility. By providing quantitative methods for assessing trade-offs and identifying synergistic solutions, this work establishes a foundation for evidence-based policy making in the era of autonomous vehicles and Complete Streets.

The report demonstrates that the apparent conflict between CAV efficiency and Complete Streets objectives can be resolved through careful attention to infrastructure design, interaction dynamics, and space allocation strategies. Our findings suggest that strategic separation of transportation modes can simultaneously improve CAV flow characteristics and enhance safety for vulnerable users, but success requires sophisticated understanding of how different user groups interact within shared urban spaces. The methodological framework developed here provides the analytical foundation for this understanding, enabling systematic evaluation of design alternatives and operational strategies.

Literature Review

In 1980, in a seminal contribution, Donald Appleyard wrote Livable Streets, which aimed to define the characteristics by which streets should be designed for human, rather than vehicle use, in addition to analyzing current neighborhood design practices (*1*). He considers streets of the time to be "dangerous, unlivable environments," yet most people live on them. This philosophy, influenced by other urbanists like Jane Jacobs, remains a popular motivation for current urban interventions like Complete Streets (CS), slow streets, and traffic calming that continue to be implemented in cities today. These motivating theories have been further encouraged by the United States Department of Transportation's policy statement encouraging the equal planning of space for all modes (*2*).

More recently, it has been found that decreasing the level of traffic stress decreased the motorized mode share and increased the non-motorized mode share (*3*). There is also a positive effect on retailing and economic benefits without increasing housing prices (*4–6*). In terms of cost, a case study of Charlotte, N.C. found that the cost of CS elements made up a small percentage of total project costs (*7*). However, defining CS still has limitations, and additional work is required to define the priorities and performance objectives for different types of streets (*8*). Some of these priorities include the allocation of space, but some authors argue that without better guidance for negotiating tradeoffs, existing institutional frameworks may simply maintain the status quo, where streets foremost accommodate motor vehicles (*9*).

To ensure the success of these implementations, they need to be studied from a traffic perspective as well. In order to understand the full impacts of CS, the network-level characteristics of the system before and after these changes should be measured. Some network-level performance measures proposed could include average speed, concentration, flow, the fraction of vehicles stopped in the network, and the two-fluid running time: stopped time and trip time variables (*10*). From these studies of network performance indicators, a macroscopic relationship between flow and density was found and derived under certain homogeneity conditions (*10*, *11*). Subsequent work has provided ample evidence of fundamental diagrams for networks and subnetworks under both stationary and dynamically changing conditions (*12*).

Beyond vehicle traffic, this relationship has also been found in pedestrian and cycling networks. On the link level for bicycles, the shape of the fundamental diagram appears to depend on the shape of the area and the size and shape of any obstacles in that area (*13*). In single-file ring experiments, circle single-file experiments of different modes to extend the relationships seen in vehicle traffic flow to pedestrians and bicycles (*14*, *15*). When the single-file requirement is lifted, it was found that as density increased, more lanes were formed by the cyclists, allowing a consistent flow rate to be maintained at a wide range of densities. These "extra lanes prevent the longitudinal density from increasing as quickly as in single-file bicycle flow" (*16*).

At the network level, there are only a few implementations of network-wide bike dynamics. The impacts of bicycle traffic on the network fundamental diagram of cars has been investigated with a mixed traffic model, finding that in a shared network, bike spilling can slow

cars down (*17*, *18*). This is quantified in the NFDs, where the maximum flow rate of the network decreases as the bike congestion level increases (*18*). Additionally, different road types were separated into sub-networks with variations between car-only roads, car and bike shared roads, and roads with dedicated lanes (in which spilling may occur). Car-only roads exhibited a higher network throughput, while shared roads had significantly lower throughput (*18*).

The literature on bike networks and micromobility has developed along two main directions, with some studies using bike-sharing data to optimize the placement of facilities and manage rebalancing, while others focus on evaluating bike lane networks through connectivity measures or stress indices. Although these evaluation methods are widely applied, there is growing skepticism about their usefulness due to the continuous introduction of new indices with only marginal differences. Reviews of connectivity research indicate a steady increase in publications, but they also highlight a persistent gap in linking connectivity measures to actual travel behavior, which undermines the validity of these approaches (*19*). This gap is addressed in part by modeling the marginal impact of bike lane miles and bike share stations on the number of trips (*20*). This work is further extended into a forecasting model (*21*). From a behavioral perspective, cyclists were surveyed to update level of service measures to be more reflective of actual preferences explained by latent user classes (*22*). Further work shows that for commuters, increased investment in active mobility infrastructure through sidewalks, bike lanes, and protected bike lanes increases the likelihood of choosing an active mode for commuting (*23*). Additional factors that increase active mode commuting likelihood include connectivity and directness of the infrastructure (*24*).

Work that explicitly addresses the design of a network of bike lanes is more limited. Early work in this area focuses on improving bike level of service by connecting origin and destination demand locations (*25*). While demand location can serve as a starting point for the design, the network design can be extended to creating a connected network regardless of demand, allowing for the capture of latent demand (*26*). Further advances in optimization strategy incorporate the use of a Genetic Algorithm (GA) with custom crossover and mutation functions based on the topology of the network (*27*). Since these foundational works, there has been an uptick in research on bike lane network design and solution algorithms.

The first set of expansions formulates the bike-lane selection as a graph optimization to minimize travel cost or maximize coverage under budget and width constraints. Some objectives of these formulations minimize the travel costs of users, apply the formulation to clusters of the network, and maximize the number of riders who commute via bike or shift to cycling (*28–31*). With some focus on the multi-modal impacts, these graph optimization formulations can be used to assess trade-offs in bike and car space investments (*32*) and generate solutions that are desirable for all modes (*33*).

The second set focuses on filling gaps and ensuring network connectivity. This is done by finding links that overlap or intersect in sets of OD trips (*34*, *35*). Similar objectives include maximizing coverage and connectivity by identifying and adding bike lanes to critical links (*36*). These links can be identified as those that increase connectivity if added (*37*), those selected

through clustering approaches (*38*), or those necessary to connect an origin to a destination within a threshold distance (*39*). Algorithmic strategies improve the connectivity outcomes when combined with design frameworks to connect isolated bike infrastructure (*40*).

While the existing literature provides valuable insights into the design and evaluation of multimodal networks at the macroscopic scale, understanding how these infrastructures are actually used requires attention to human decision-making at the microscopic level. Pedestrian and cyclist choices, particularly in environments shared with vehicles and emerging autonomous systems, strongly influence both the safety and efficiency of networks. Modeling these decisions is challenging because they are shaped not only by infrastructure availability and connectivity but also by cognitive and behavioral factors.

To capture these dynamics, researchers have developed models of pedestrian decision-making, ranging from psychophysics-based gap acceptance approaches and game-theoretic formulations to cognitive models such as the Drift Diffusion Model (DDM). These models allow the integration of behavioral realism into traffic microsimulations, bridging the gap between infrastructure-level planning and user-level interactions.

A gap acceptance model is used in (*41*) called Psychophysics-based Gap Acceptance (PGA) that leverages visual looming cues. Furthermore, a game theory-based approach is developed in (*42*) which incorporates factors including vehicle speed, pedestrian-vehicle distance, vehicle length, and time pressure. Other research introduces a multi-input fusion model to predict pedestrian crossing intentions (*43*). This model combines pedestrian bounding boxes, pose information, bounding box coordinates, and surrounding context to enhance prediction accuracy and reliability. Models based on cognitive theory have received significant attention in predicting human traffic behavior, with promising results (*44*). DDMs assume that decision makers (DMs) act or make their decision once they have accumulated enough evidence over time to reach a threshold that justifies their choice (*45*). These models are widely used in cognitive process modeling, particularly for simple two-choice tasks such as deciding whether to overtake a vehicle, pass through an intersection, or accept a gap in traffic (*46*). DDMs have been shown to effectively predict human behavior in various scenarios, including left-turn gap acceptance and pedestrian street crossing (*47–49*).

Traffic fatalities have become a major concern, especially in developed and densely populated countries. These incidents highlight the vulnerability of pedestrians, who are the most at risk among roadway users (*50*). Implementing a complete streets design is one approach to enhance safety and reduce traffic fatalities. Complete streets is an approach to urban street design with a main objective of facilitating travel and access for all roadway users in terms of convenience, safety, and comfort, particularly for more vulnerable users like pedestrians, and cyclists (*51*). In order to understand the impacts of various street designs on the more vulnerable users, pedestrian behavior needs to be modeled jointly with all other roadway users. Analysis of the mechanisms of interaction between vehicles, pedestrians, and micromobility users allows a better understanding of the dynamics at play. A joint modeling approach is essential for the development and assessment of design strategies that ensure all users, regardless of mode, can

share the road safely and comfortably. Advancements in vehicle sensors, transportation infrastructure, and connected and autonomous vehicles (CAVs) have the potential to contribute to a safer, less stressful, and more equitable environment for all roadway users, particularly when developed within the framework of complete streets. AVs have many advantages over regular human-driven vehicles. They can improve traffic flow and throughput of highways, enhance safety by reducing reaction times, reduce environmental impacts, and improve stability of traffic flow (*52*). Although incorporating AVs may simplify driving and benefit drivers, their impact on more vulnerable users in urban settings remains uncertain (*53*).

To effectively capture the shared dynamics of the roadway, models of pedestrian decision-making must be integrated with representations of vehicle movement. Pedestrian crossing choices are shaped not only by their own risk perception and time-to-cross but also by the trajectories and maneuvers of surrounding vehicles. Thus, vehicle movement modeling becomes a necessary counterpart to pedestrian behavior models, ensuring that the interactions are described jointly rather than in isolation. While pedestrians adjust their actions based on anticipated vehicle acceleration, deceleration, or lane changes, vehicles—whether human-driven or automated—must likewise respond to unpredictable pedestrian decisions. Establishing this two-way dependency creates a foundation for joint modeling frameworks where vehicle control strategies, both longitudinal and lateral, can be linked directly to pedestrian crossing behavior, yielding more realistic assessments of safety under different street designs.

In developing a model for vehicle behavior, AVs' lateral and longitudinal movement should be considered. Longitudinal movement of vehicles can be captured using car-following models (*54*), but lateral movement is considerably more complex (*55*, *56*). Unlike human-driven vehicles, AVs are equipped with a number of sensors and control algorithms that impact their lane changing and car-following behavior, so different models are needed to capture the behavior of these technologies (*57*). Cooperative Adaptive Cruise Control is an advanced cruise control embedded in AVs. It adjusts the vehicle's speed automatically based on the speed of the leading vehicle, incorporating vehicle-to-vehicle communication to enhance its capability because of the shared information. One of the first car-following models considering CACC was proposed in (*58*). The driving logic used in (*58*) is based on choosing the suitable acceleration, which is calculated based on the difference between the current and intended speed for the vehicle or the distance and speed difference between the ego vehicle (CACC-equipped vehicle) and the target vehicle (predecessor). The model was used in (*59*) and extended to consider sensor specifications for each AV. They assumed that the speed of the AV should be low enough to allow the vehicle to stop completely once a stopped object is detected at the furthest point of the detection radius.

1 Network-Level Analysis: Active Mobility Infrastructure and Flow Efficiency

By reallocating road space to bicycles and other micromobility options, cities can reduce car dependency and promote more efficient use of the network. This section examines the effects of different street configurations—ranging from shared lanes to fully separated bike paths—on the network fundamental diagram to better understand the role of active mobility in alleviating congestion.

1.1 Experimental Design

One of the challenges of micromobility research is the limited data, especially at volumes high enough to exhibit flow breakdown. While there are also limitations in the realism of simulation data, the benefits of being able to incorporate enough bicycles, e-bikes, and scooters to reach flow breakdown outweigh the drawbacks. The traffic simulator SUMO was chosen for its inclusion of these multiple modes, as well as the flexibility to modify their parameters (*60*). As this section aims to analyze the effects of micromobility in general, multiple micromobility vehicles were included. These vehicles reflect common shared micromobility options available in major US cities. The modes included and their parameters can be seen in Table 1.1.

Table 1.1 Vehicle Type Parameters

Vehicle Type	Desired Speed (km/h)	Speed Standard Deviation (km/h)	Acceleration (m/s^2)	Deceleration (m/s^2)	Max Speed (km/h)
E-Scooter	20	4	4	4	20
E-Bike	32	6.4	4	4	32
Bike	22	4.4	2	4	32
Fast Pedestrian	5.4*	0.93*	1.5	2	20
Slow Pedestrian	3.8*	0.72*	1.5	2	10
Passenger Vehicle	40	8	2.6	4.5	200

Two classes of pedestrians were used to further increase realism and capture variations across individual movement speeds. The pedestrian parameters indicated with "*" reflect speeds found in the literature (*61*).

The network used is a 6 x 6 grid where each link is 100m long. The layout can be seen in Figure 1.1.

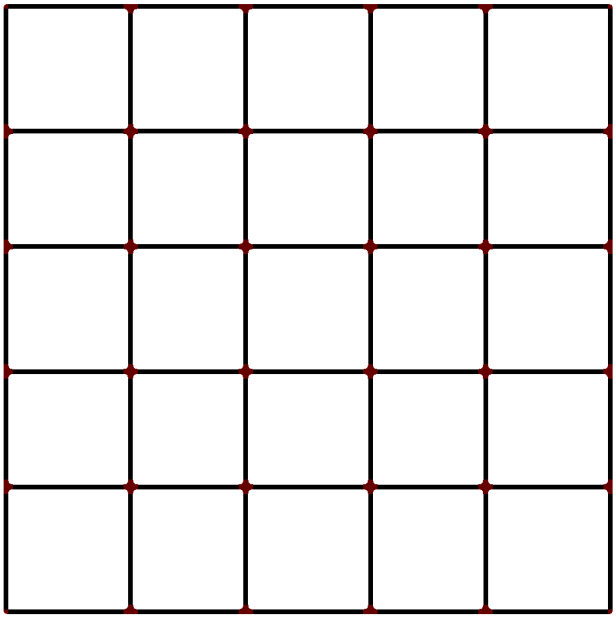

Figure 1.1 Grid Network Layout

1.1.1 Complete Streets Scenario Development

Four different scenarios which represent different levels of "completeness" of the street were tested. These networks and their properties are shown in Table 1.2, where the example cross-section was applied homogeneously to every link.

Table 1.2 Complete Street Network Scenarios

Network	Separation	Vehicle Lane Width	Micro Mobility Lane Width	Pedestrian Lane Width	Cross Section
A	None	16.8	0	0	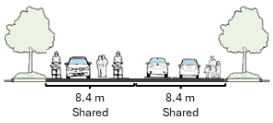
B	Sidewalk	12.8	0	4	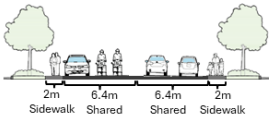
C	Sidewalk + Bike Lane	6.4	6.4	4	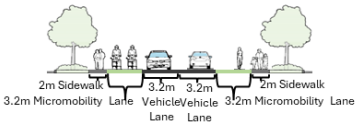
D	Sidewalk + Bike Lane (Exclude Bikes on Roadway)	6.4	6.4	4	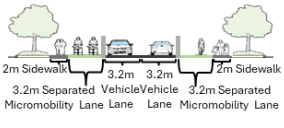

Network A serves as a baseline network where all modes share the entire area. In Network B, more separation is introduced for pedestrians, while cars and micromobility vehicles share the remainder of the space. In Networks C and D, micromobility vehicles are given their

own space. Network D has stronger separation than Network C, reflecting CS tools like bollards and curbs, meaning that micromobility vehicles cannot spill over into the car lane and vice versa.

For each of the scenarios, the same demand pattern was used. While the literature suggests changes in demand due to the implementation of CS (*3*), for the purposes of the experiment, the static demand was used as a control. The demand was generated using the RandomTrips tool in SUMO, which randomly selects origin and destination points across the network. The vehicles are all inserted over a 3-hour time period in 5 intervals of uniformly distributed departures. The insertions for each time period can be seen in Table 1.3.

Table 1.3 Insertion Rates by Vehicle Type

Vehicle Type	Period 1	Period 2	Period 3	Period 4	Period 5	Total
E-Scooter	135	180	270	540	1080	2,205
E-Bike	135	180	270	540	1080	2,205
Bike	135	180	270	540	1080	2,205
Fast Pedestrian	270	360	540	1080	2160	4,410
Slow Pedestrian	270	360	540	1080	2160	4,410
Passenger Vehicle	135	180	270	540	1080	2,205

The path traveled for the trip is chosen using a fastest-path router at the time of each vehicle insertion. SUMO models bicycle and scooter traffic flow using the Intelligent Driver Model (*62*). Though this model is based on automobile traffic, it has been validated for cyclist behavior as well and thus deemed acceptable for these micromobility vehicles (*63*).

1.1.2 Area-Based Definitions

Each network has the same total width for travel but varies in the level of separation between modes. This results in different areas available for each mode and gives rise to the use of area-wide metrics to define flow and density. These come from the area-based implementation of Edie's definitions for flow and density as found in (*64*) or additional decomposition into directional definitions as found in (*65*).

For the link-based definitions, L defines the total length of the network, notably constant across scenarios; d_i is the distance traveled by bicycle i during the time window, ΔT; and t_i is the time spent by the vehicles during that same ΔT. Based on these variables, Equations 1.1 and 1.2 show the computation for flow and density, respectively:

$$q_{length} = \sum_{i=0}^{N} d_i / (\Delta T * L) \quad \text{(Eq 1.1)}$$

$$k_{length} = \sum_{i=0}^{N} t_i / (\Delta T * L) \quad \text{(Eq 1.2)}$$

In the area-based definitions, the major change is in the inclusion of area rather than lane-miles. The network area is defined by the product of the length and width of each link, l_j and w_j, summed over all links in the network:

$$A = \sum_{j=0}^{J} l_j * w_j \quad \text{(Eq 1.3)}$$

Area is then applied instead of length in the denominator of flow and density, based on Edie's definitions:

$$q_{area} = \sum_{i=0}^{N} d_i \,/(\Delta T * A) \quad \text{(Eq 1.4)}$$

$$k_{area} = \sum_{i=0}^{N} t_i \,/(\Delta T * A) \quad \text{(Eq 1.5)}$$

Additionally, an alternative density measure was developed to account for vehicle size, capturing the proportion of the network area occupied by each mode *k*. This occupancy metric, denoted O_k, is calculated as:

$$O_k = ((n_k\, a_k)/(A_k\, \Delta \mathrm{T})) * 100 \quad \text{(Eq 1.6)}$$

where n_k is the number of vehicles of mode *k,* a_k the size of the vehicle measured as area, and A_k is the area of the network available to mode *k,* and ΔT is the observation time window. This occupancy-based density measure is introduced to better capture the spatial impact of different vehicle types, particularly in multimodal networks where modes vary significantly in size. Beyond characterizing network usage, it can also serve as a proportional equity or equality indicator by quantifying how much of the network is used by each mode relative to its size.

1.2 Network Fundamental Diagram Results

After running the four simulation scenarios, NFDs were generated first for each mode. Figure 1.2 shows the NFDs constructed using area-based metrics for mode-specific flow and density across each network scenario (A, B, C, and D), with each color representing a different mode.

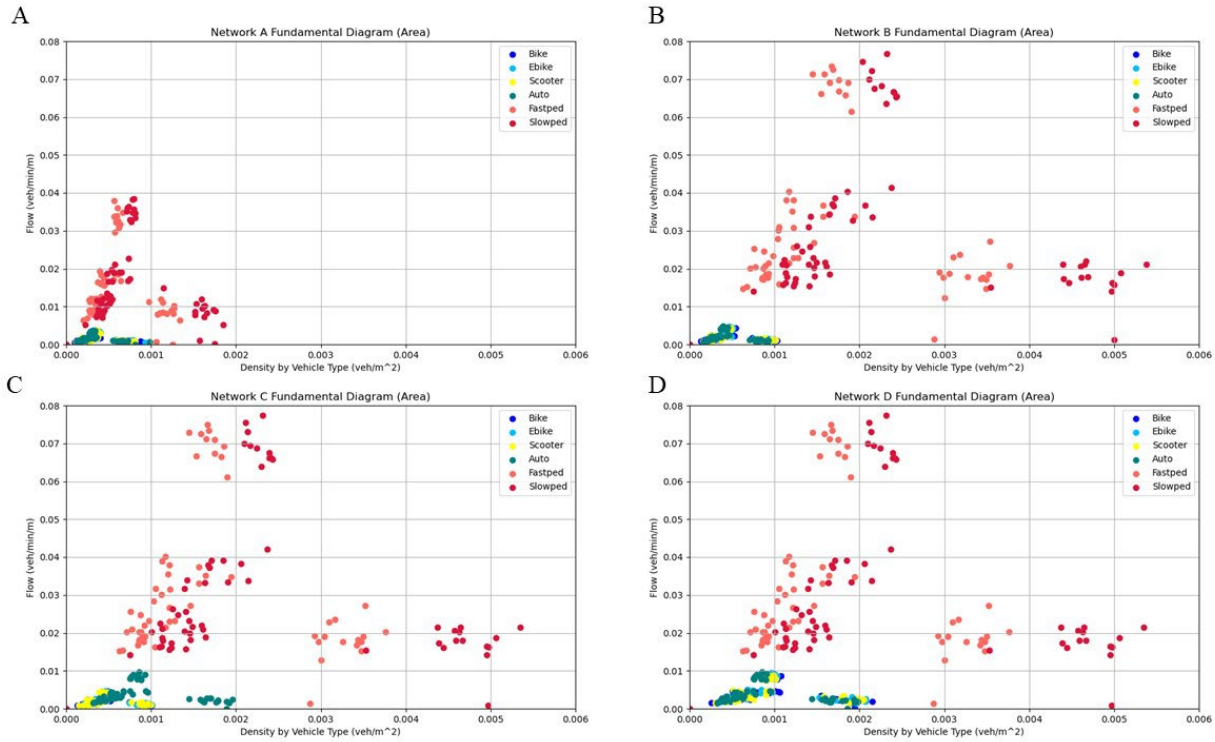

Figure 1.2 Network Fundamental Diagrams by Mode for Networks A, B, C, and D

Between Network A and Network B, the most dramatic shifts come from the separation of pedestrians. Both pedestrian classes have much higher flow than the other vehicle types, both due to their higher insertion rate but also due to their space efficiency. Once sidewalks are introduced, the pedestrians continue to reach even higher flow rates despite having a relatively small share (2m wide sidewalks) of the total road space.

Since the pedestrian NFD shapes dominate this representation, Figure 1.3 presents the same diagrams without pedestrians.

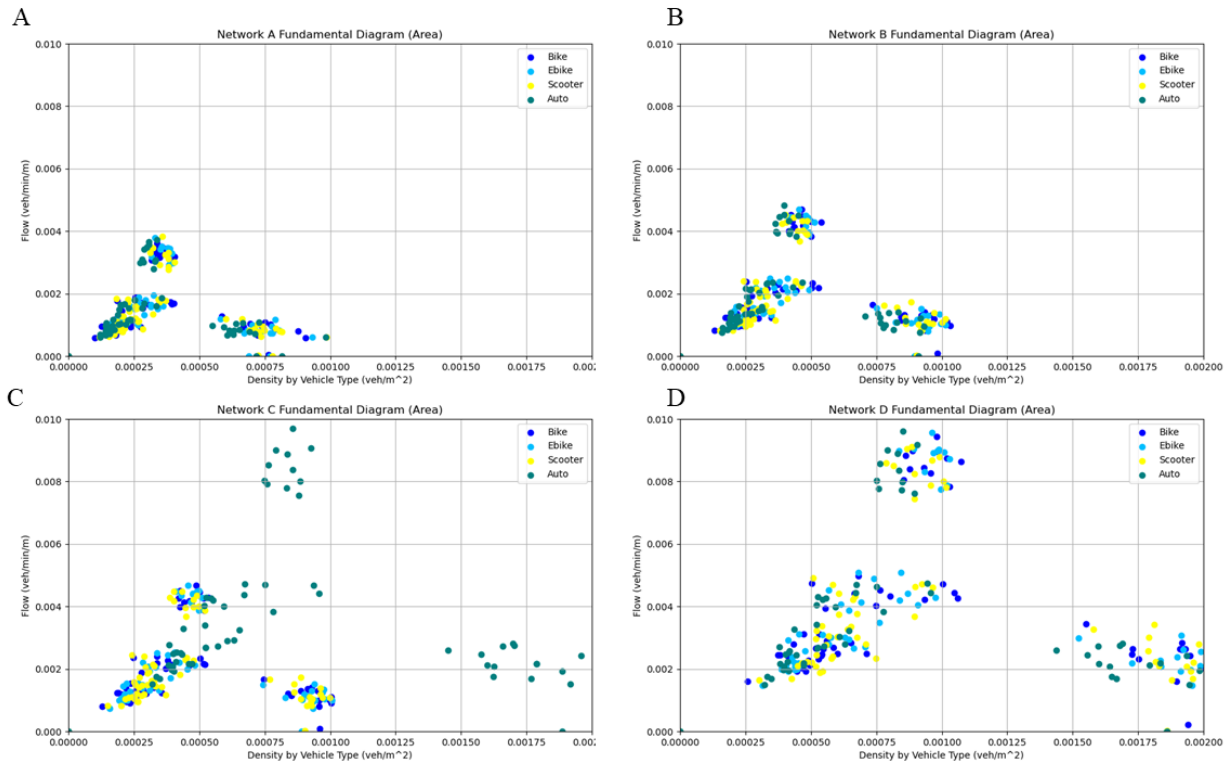

Figure 1.3 Network Fundamental Diagrams for Non-Pedestrian Modes in Networks A, B, C, and D

By removing the pedestrian curves, the shapes of the NFDs for micromobility vehicles and cars can be more clearly seen. Between Networks A and B, there is a noticeable shift toward increased flow for these modes, suggesting that pedestrian interactions in Network A negatively impacted network efficiency. In the shared space, both micromobility vehicles and cars display almost identical patterns with minimal variation in each mode's NFD, despite differing speed distributions, indicating that the interactions that occur when space is shared may be reducing efficiency. Transitioning to increased separation in Network C results in the most significant efficiency gains for cars. By providing bikes, e-bikes, and scooters with a lane (though not permanently separated), car traffic achieves higher flows and can support greater densities before flow breakdown. Finally, Network D illustrates the full extent of flow gains due to physical separation, where micromobility vehicles reach flow levels comparable to those of cars in Network C.

Figure 1.2 and Figure 1.3 depict the individual densities of each mode. While gains are still seen due to the changes in network topology, this does not capture the interaction between the modes and their effect on the flow rate. To better analyze this, 3D- NFDs between cars and micromobility vehicles for each network are shown in Figure 1.4. In these depictions, car density is measured through the standard length-based definition (veh/m), and the micromobility modes (bikes, e-bikes, and scooters) are combined into a total micromobility density which still makes use of the area-wide measurements. The color scale represents the flow rate of each point.

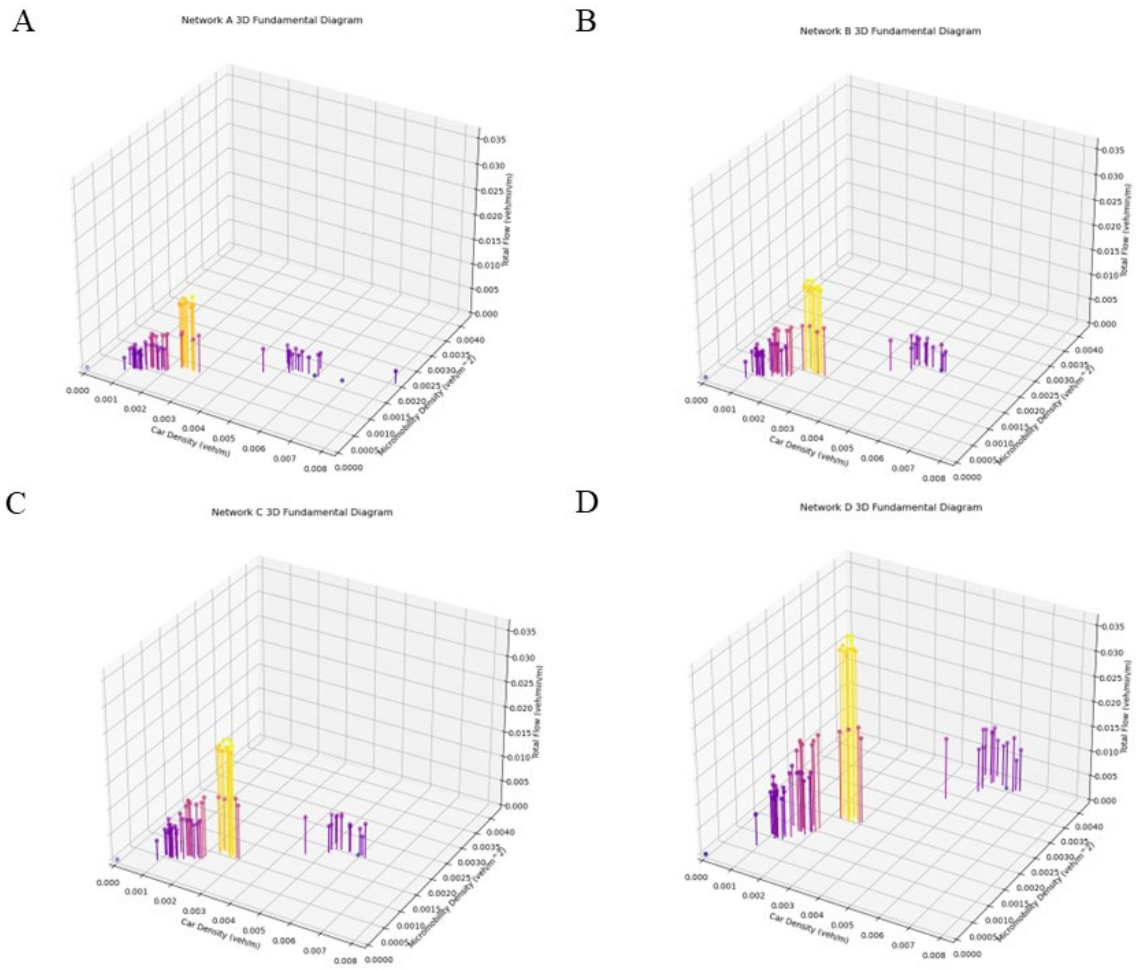

Figure 1.4 3D-NFDs for Networks A, B, C, D

Network A has the lowest peak flow rates of the four scenarios, with each subsequent network increasing in maximum flow achieved. In this representation, we can see that flow breakdown for cars, when measured through length-based metrics, occurs at about the same density across the scenarios. On the other hand, the area of flow breakdown occurs at a higher density across scenarios for micromobility vehicles. While the 3D representations help to understand more of the interactions, the overall trends are largely similar to the mode-specific measurements. With increased separation of modes, higher flow is achieved, and the density at which flow breakdown occurs is larger.

To analyze the space-size relationship between modes and their NFDs, Figure 1.5 shows the percent of the network occupied at each flow rate.

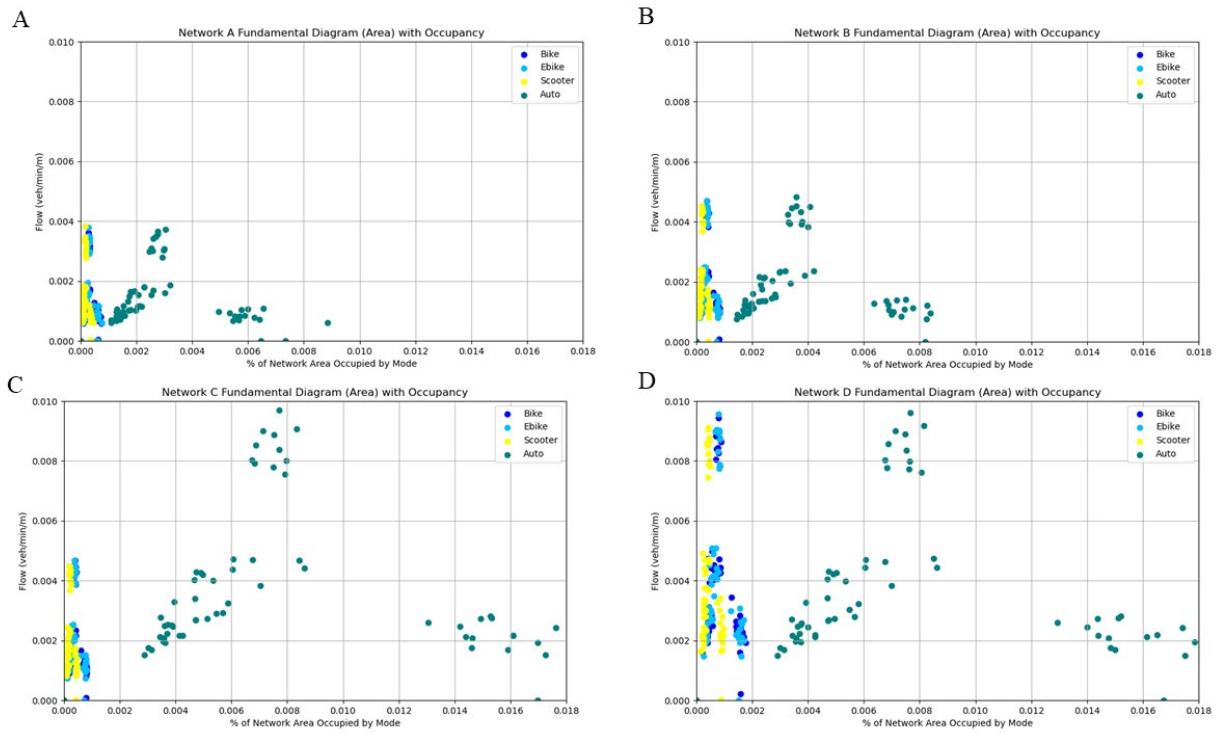

Figure 1.5 Flow vs. Percent of Network Occupied by Each Mode in Networks A, B, C, and D

In this representation, the outsized area of the network that cars occupy is clear. The pattern of increased separation creating increased efficiency for all modes continues to be prevalent in these diagrams. However, they also display the space efficiency of micromobility, where bikes, e-bikes, and scooters reach similar flow rates to cars in Network D, with much less space occupied in the network. With this increased efficiency of space, more person throughput can be achieved with separation, which is exemplified by this representation.

Figure 1.6 shows the total flow and density of all modes in each network to directly capture the network throughput.

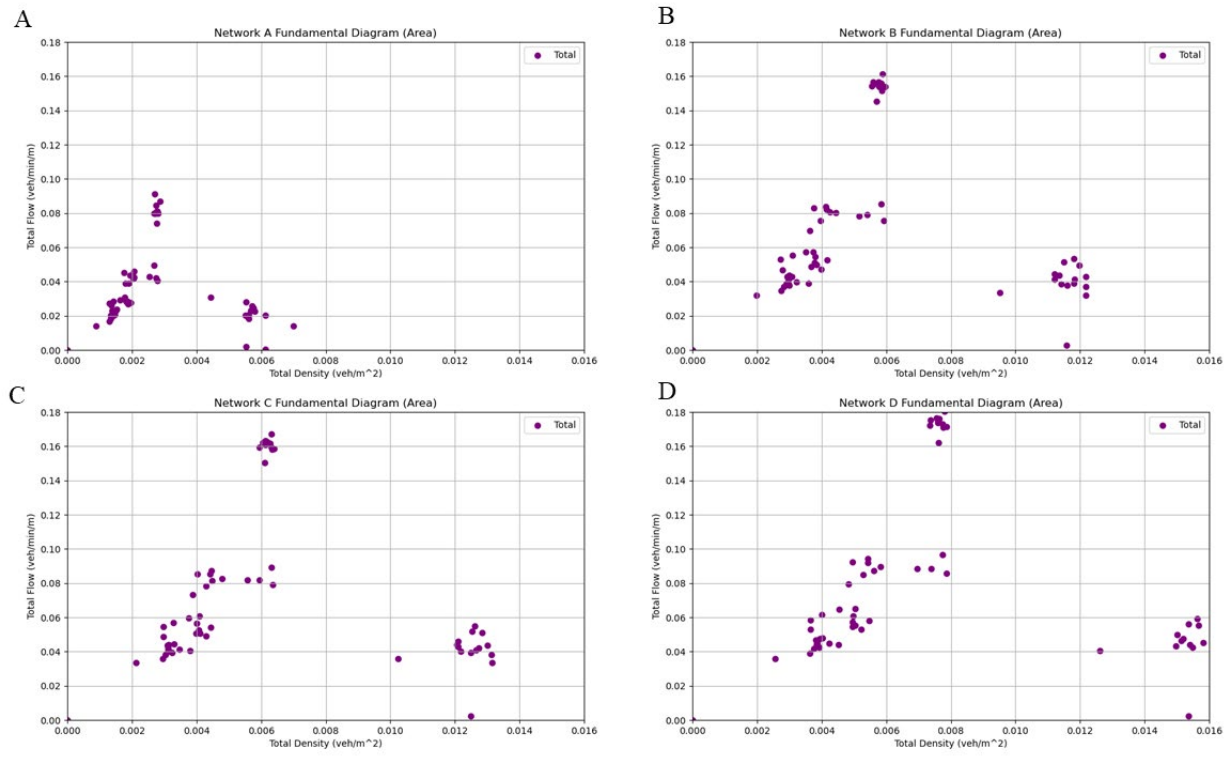

Figure 1.6 Total NFD for All Modes in Networks A, B, C, and D

Here, the relationship between network efficiency that CS interventions can create is again apparent. To compare the four scenarios, we examine the maximum flow achieved by each. In Network A, the maximum flow is 0.09 veh/min/m, while in Network B, the value is 0.16 veh/min/m- a very significant jump. In Networks C and D, there are incremental gains in maximum flow reached, with the networks achieving 0.17 veh/min/m and 0.18 veh/min/m, respectively. These figures also show the higher density reached before flow breakdown as the points shift further right in each diagram, with the maximum flow achieved in Network D at a density of approximately 0.008 veh/m^2 compared to 0.006 veh/m^2 in Network C. While previous representations have shown the individual gains in efficiency as well as pointed to an overall efficiency gain, Figure 1.6 confirms that there is more efficiency in separation created in CS for all modes in the network.

1.3 Summary

In this study, the effect of network designs on the NFD was analyzed through the use of simulation experiments over four scenarios of street configurations. These scenarios ranged from no separation between modes to fully dedicated lanes for pedestrians, micromobility, and car traffic. Comparing the diagrams across networks, we see first the inclusion of sidewalks for pedestrian separation increasing flow between Network A and B. Further separation by including both a sidewalk and a micromobility lane on each link increased flow for cars in Network C, while exclusive, physically separated lanes increased flow for micromobility in

Network D. Each method of visualizing the results of these simulations indicates that increased separation increases network efficiency. While this corroborates the results of previous studies, the quantification of the increased efficiency for micromobility vehicles through the NFD is a key contribution of this work.

2 Development of Physical Attribute Defined NFD Functional Form

2.1 Introduction

Making use of the area-based network fundamental diagram (NFD), this section outlines the development of an NFD functional form that is defined by the physical attributes of the network applied to the Evanston, IL network. The scenarios and flow-density observations developed in previously form the basis for hypothesizing a relationship between network characteristics and the shape of the NFD. To quantify these relations, the street network of Evanston, IL was implemented in SUMO with scenarios of varying active mobility infrastructure levels developed based on two characteristics: coverage, the number of links with bike lanes, and separation, the number of links with bike lanes that are fully separated. The links to meet the defined values of each characteristic were randomly selected throughout the network. These scenarios were simulated to extract resulting flow-density observations.

From these observations and using an NFD functional form adapted from the literature, values for jam density, intersection capacity, and backward wave speed for each scenario of the network were estimated (*66*). The estimated NFD parameters were then modeled as functions of the network characteristics. The network characteristics considered are shared area, which is the total space in the network where multiple modes travel together; mode-exclusive area, where only one mode operates; and the interaction plane, a custom metric for capturing the potential for modal interaction based on separation. The result of these models is a modified form of the NFD in which each parameter jam density, capacity, free-flow speed, and backward wave is expressed as a function of these network attributes. The overall methodology is shown in Figure 2.1.

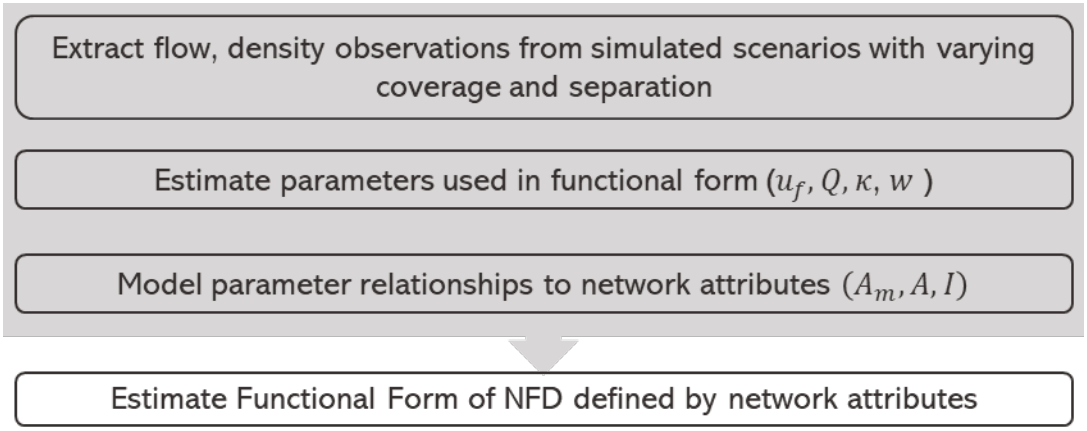

Figure 2.1 Process Flow of NFD Functional Form Development

2.2 Methodology

2.2.1 Network Scenario Simulations

The methodology begins with the development of a functional form of the NFD based on the literature updated to become a function of network attributes. The street network of Evanston, IL was extracted from Open Street Maps into SUMO using the SUMO tool OSMWebWizard (*60*, *67*). A set of links were randomly chosen at varying levels from 0% to

100% of the network links to receive a bike lane treatment. Of those selected bike lane links, another iteration of random selection, again from 0(Alozi & Hussein, 2022; Métayer & Coeugnet, 2021; Rasouli & Tsotsos, 2020; Talebpour & Mahmassani, 2016; Zhanguzhinova et al., 2023)% to 100%, selects a subset of bike lanes to be fully separated. These resulting networks were simulated in SUMO. For reference, the existing bike lane network of Evanston, IL is shown in Figure 2.2.

Figure 2.2 Existing Evanston Network from Open Street Maps

It has a handful of major corridors relevant for bikes. Identified in red is a section of roads where bikes are not allowed. Blue colored links show the locations of bike lanes, while separated bike lanes are shown in green.

To generate realistic demand patterns for the network simulations, Annual Average Daily Traffic (AADT) counts collected across the state of Illinois were used (*68*). These counts, associated to edges in the street network, serve as the basis for estimating vehicular volumes. An initial set of synthetic trips between random origins and destinations (OD) is generated to represent possible travel behavior within the network. To align these synthetic trips with observed traffic volumes, the SUMO tool *routeSampler.py* is used to sample from the OD trip pool. This tool heuristically selects trips such that the resulting vehicle routes replicate edge-level traffic counts. The route sampler adjusts the trip set to ensure that modeled flows are consistent with empirical AADT data, calibrating the demand inputs to reflect actual traffic counts. Since direct observations of bicycle demand were not available, each selected vehicle trip was duplicated and assigned to a bicycle mode to generate the corresponding bike demand. This approach enables the network design to consider scenarios in which car and bike trips are treated

as interchangeable or competitive options, supporting the development of infrastructure that allows for mode shift to be more feasible, though it is not explicitly considered in the framework.

Each simulation was conducted for a 1-hour period, corresponding to 3600 time steps with a resolution of 1 second per step. The demand set included a total of 72,000 trips, evenly split between cars and bicycles. Trips were routed using the SUMO tool *duarouter*, an approximate dynamic user equilibrium tool, while the SUMO *traci* interface was employed to collect detailed vehicle-level data, such as travel distance and trip duration (*60*). In the simulation, traffic signals are operated under actuated logic.

Performance data was collected over the full simulation period using a combination of the SUMO tripinfo outputs and real-time data gathered through SUMO traci (*60*). Key metrics extracted for analysis included vehicle travel time and total distance traveled, used to calculate flow and density values using Edie's definitions. For consistency across network configurations, data points for the network fundamental diagrams (NFDs) were averaged over four-minute intervals (240 time-steps). Each NFD developed is based on the results of three replications of the simulation of each scenario.

2.2.2 NFD Functional Form Estimation

To fit a smooth curve to each network's fundamental diagram, the function developed in the literature and shown in Equation 2.1 was employed. The function incorporates key parameters: the jam density (κ), free-flow speed (u_f), capacity (Q), and backward wave speed (w) as well as a smoothing parameter λ.

$$q(k) = -\lambda \log(\exp((-u_k\, k)/\lambda) + \exp(-Q/\lambda) + \exp(-(\kappa - k)w/\lambda)) \qquad \text{(Eq 2.1)}$$

For each scenario and vehicle type, the model was fit using Python's *differential_evolution* algorithm, which minimized the sum of squared errors between observed and predicted flow values. Among the tested values of λ, 0.5 resulted in the best fit in terms of R^2 and RMSE and was used in the remainder of the work.

The estimated values of jam density (κ), free-flow speed (u_f), capacity (Q), and backward wave speed (w) for all scenarios were next modeled as functions of network attributes (shared area, modal area, and interaction plane) for each vehicle type. Mode-exclusive area is the area where bike lanes are separated, and no interaction between modes can occur, while shared area is the total amount of area in the network where cars and bikes share space. The interaction plane is a calculated variable based on the length of a link and the amount of separation, which is then summed over the whole network. The separation is calculated based on both the number of lanes as well as characteristics of physical separation for bike lanes. Links with physical separation, like a separated bike lane, have one less interaction plane since vehicles in the separated lane cannot interact with those in the general lanes. Figure 2.3 visually represents this calculation for a single link.

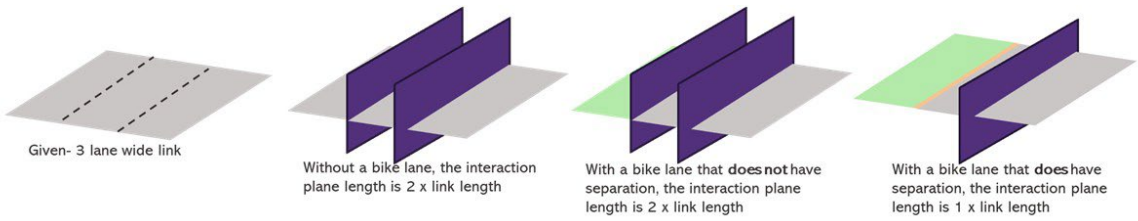

Figure 2.3 Interaction Plane Visual Definition

Over the whole network, the value of the interaction plane is then described by Equation 2.2.

$$I = \sum_L \ell_l \max(0, n_l - 1 - s) \quad \text{(Eq 2.2)}$$

where ℓ_l is the length of link l in the set of links L. The number of lanes in each link is given by n_l and s is a binary indicator of bike lane separation.

Given these network attributes and NFD function parameters, the NFD parameters were estimated as a function of network attributes. This results in a NFD functional form where jam density (κ), free-flow speed (u_f), capacity (Q), and backward wave speed (w) are replaced with their respective functions.

2.3 Results and Discussion

As outlined in the methodology, networks with varying coverage and separation for bike lanes are simulated to form the basis for NFD estimation. Figure 2.4 illustrates the resulting flow-density observations.

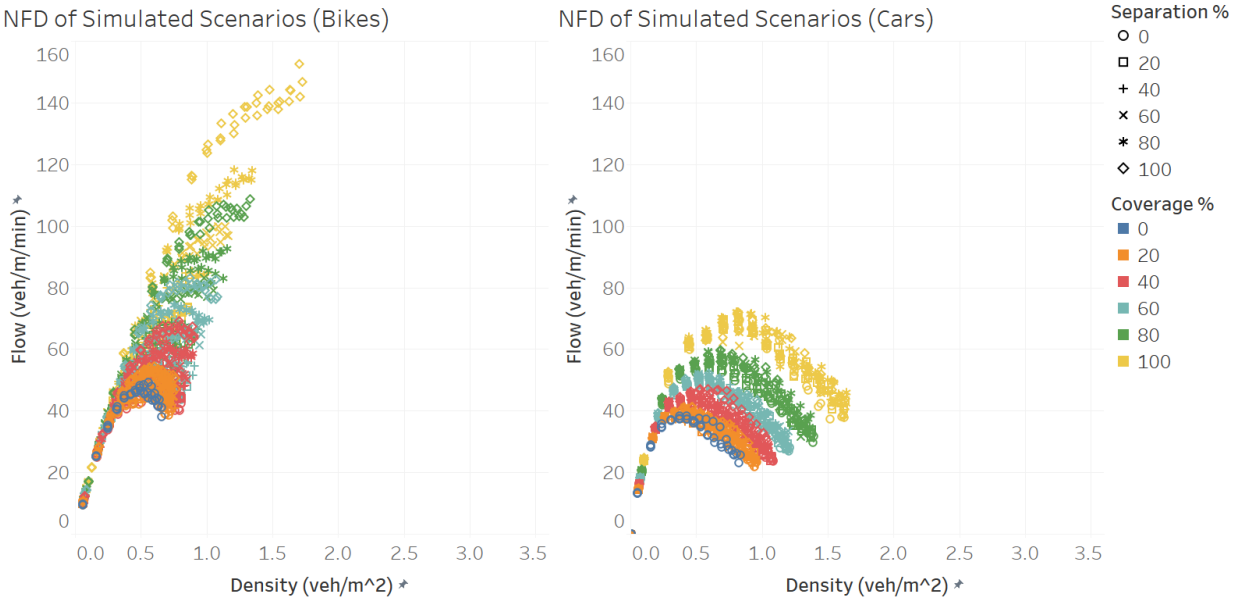

Figure 2.4 Simulated Flow-Density Relationships for Bikes and Cars

Each point represents a simulation output for a specific combination of bike lane coverage (color scale) and separation level (marker style). In the bike NFD, increasing coverage and higher levels of separation generally correspond to higher flow rates at comparable density levels. For bikes, scenarios with 100% coverage and high separation achieve the highest peak flows. This separation is also of benefit to cars, where the 100% coverage scenario achieves the highest flow as well. These NFDs also highlight the efficiency of micromobility, as cars reach congestion and flow breakdown in the second half of the curve while bikes do not.

From these flow-density observations, estimates for the parameters of Equation 2.1 were obtained. The resulting values of κ, u_f, Q, and w are shown in Table 2.1.

Table 2.1 Estimated Parameters of NFD Functional Form

Network		Bike Parameters				Car Parameters			
Coverage	Separation	κ	uf	Q	w	κ	uf	Q	W
0%	0%	1.06	140.34	46.14	93.13	1.24	192.55	36.41	54.28
20%	0%	1.20	142.43	43.44	81.84	1.50	192.26	37.62	40.31
20%	20%	1.60	142.03	45.26	59.52	1.56	191.57	37.33	42.00
20%	40%	1.60	142.02	45.68	49.98	1.52	192.06	37.24	44.64
20%	60%	1.23	139.68	48.87	50.04	1.49	192.61	38.43	43.32
20%	80%	1.70	136.65	50.83	59.36	1.46	192.65	38.04	48.03
20%	100%	1.80	137.64	52.19	56.07	1.50	190.37	39.63	44.98
40%	0%	1.40	136.83	43.75	70.99	1.68	187.21	41.02	43.72
40%	20%	1.50	134.91	47.63	65.56	1.68	187.59	42.49	40.11
40%	40%	1.60	135.75	50.99	64.55	1.72	188.91	41.56	41.22
40%	60%	1.60	134.36	55.39	69.13	1.63	186.72	43.44	44.79
40%	80%	1.60	135.34	58.13	59.64	1.71	189.13	43.78	40.71
40%	100%	1.70	134.02	65.36	92.26	1.67	190.80	44.53	48.20
60%	0%	1.40	133.96	47.83	77.77	1.87	184.03	47.79	41.33
60%	20%	1.50	136.85	52.85	86.88	1.92	185.54	48.07	41.78
60%	40%	1.60	137.33	57.74	49.68	1.86	188.30	48.49	43.47
60%	60%	1.71	136.08	63.91	78.07	1.93	187.26	49.00	44.56
60%	80%	1.80	134.98	72.01	84.30	1.92	190.10	48.55	43.76
60%	100%	2.00	137.69	79.53	83.00	1.83	190.97	49.49	46.20
80%	0%	1.40	138.66	53.28	84.25	2.01	179.14	53.87	49.03
80%	20%	1.60	133.83	59.54	95.13	2.01	184.06	53.79	48.75
80%	40%	1.80	134.79	65.81	56.79	1.77	186.78	53.97	50.58
80%	60%	2.00	134.29	77.45	75.62	2.37	186.34	55.55	49.78
80%	80%	2.20	135.59	86.78	58.58	2.23	188.00	54.56	54.68
80%	100%	2.42	139.86	101.86	70.85	2.13	188.93	55.90	62.42
100%	0%	1.60	131.50	62.29	79.13	2.65	178.40	65.08	29.76
100%	20%	1.80	134.84	69.74	46.78	2.80	184.90	64.74	78.33
100%	40%	2.20	133.08	79.62	87.16	2.55	184.24	65.96	39.73
100%	60%	2.60	137.66	92.86	76.34	2.39	186.99	64.14	35.45
100%	80%	3.00	134.83	108.98	82.57	2.88	187.26	67.18	44.08
100%	100%	3.50	133.79	136.40	85.70	2.00	187.91	65.71	51.88

Given the estimated functional form parameter values shown in Table 2.1, the next methodological step involves modeling those values with network attributes, shared area, mode-exclusive area, and interaction plane, for each mode. The resulting models for each parameter and each mode are shown in Table 2.2-Table 2.7.

Table 2.2 Model for κ_{car}

Variable	Coefficient	Standard Error	p-value
Constant	4.39	0.10	0.00
Car Area	-1.76	0.10	0.00
Shared Area	-1.61	0.06	0.00
Fit Measures			
No. of estimated parameters	3		
No. of observations	31		
R^2	0.75		

Table 2.3 Model for w_{car}

Variable	Coefficient	Standard Error	p-value
Constant	29.98	0.14	0.00
Shared Area	5.24	0.13	0.00
Car Area	12.11	0.31	0.00
Fit Measures			
No. of estimated parameters	3		
No. of observations	31		
R^2	0.95		

Table 2.4 Model for Q_{car}

Variable	Coefficient	Standard Error	p-value
Constant	63.24	0.08	0.00
Shared Area	-17.26	0.13	0.00
Interaction Plane	0.03	0.00	0.00
Fit Measures			
No. of estimated parameters	3		
No. of observations	31		
R^2	0.96		

Table 2.5 Model for κ_{bike}

Variable	Coefficient	Standard Error	p-value
Constant	4.88	0.08	0.00
Bike Area	-1.44	0.08	0.00
Shared Area	-1.90	0.04	0.00
Fit Measures			
No. of estimated parameters	3		
No. of observations	31		
R^2	0.93		

Table 2.6 Model for w_{bike}

Variable	Coefficient	Standard Error	p-value
Constant	45.85		
Shared Area	10.13	0.30	0.00
Bike Area	17.58	0.59	0.00
Fit Measures			
No. of estimated parameters	3		
No. of observations	31		
R^2	0.93		

Table 2.7 Model for Q_{bike}

Variable	Coefficient	Standard Error	p-value
Constant	120.09	0.19	0.00
Shared Area	-43.15	0.13	0.00
Interaction Plane	-0.03	0.00	0.00
Fit Measures			
No. of estimated parameters	3		
No. of observations	31		
R^2	0.95		

Table 2.2 - Table 2.4 summarize the estimated relationships between network area allocations and key macroscopic parameters for cars, while

Table 2.5 - Table 2.7 present the corresponding results for bikes. Across all models, parameter estimates are statistically significant ($p < 0.01$), and the models demonstrate good overall fit, as indicated by high R^2 values.

For cars, jam density (κ_{car}) is negatively associated with both car-exclusive area and shared area, indicating that larger car and shared spaces correspond to lower jam densities. The model explains 75% of the observed variation in κ_{car}. Both shared area and car area are positively associated with w_{car}, and the model fits the data well ($R^2 = 0.95$). Lastly, capacity (Q_{car}) is negatively associated with shared area, indicating that increases in shared area reduce maximum vehicular throughput.

The results for bikes follow similar patterns. Bike jam density (κ_{bike}) decreases with both bike area and shared area, though the effect of bike area is notably smaller in magnitude compared to shared area. The backward wave (w_{bike}) is strongly positively influenced by both bike area and shared area, with an R^2 of 0.93. Capacity (Q_{bike}) has a substantial negative association with shared area and a small negative association with interaction plane, suggesting that shared environments limit bike throughput more significantly. For bikes, more interaction planes within the network decrease capacity, which contrasts with the results for cars, where interaction planes have a small positive impact, perhaps due to cars' ability to change lanes and pass slower vehicles.

While the estimates show strong fit across all models and modes, free flow speed was not estimated due to the nearly constant relationship between free flow speed and potential model parameters, as shown in Figure 2.5.

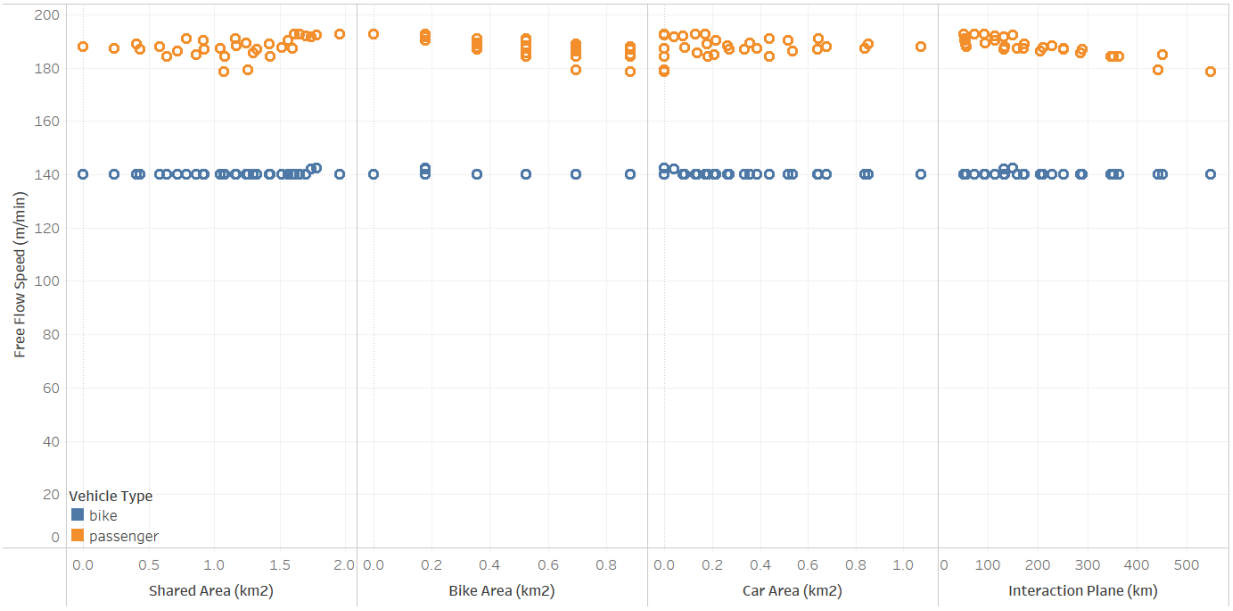

Figure 2.5 Free Flow Speed and Network Attributes

The remainder of the work uses a value for u_f of 140 m/min for bikes and 190 m/min for cars, which reflect these relationships and the speed limits of the network.

As detailed in the methodology, these estimations were then used to find an optimal form of the NFD where estimated models replaced their response variable in Equation 2.1. The resulting functional form based on network attributes is shown in Equation 2.3.

$$q_m(k_m,\ A_m,\ A,\ I) = -\lambda \log\left(\exp\left((-(u_f\ )\ k_m)/\lambda\right)\right.$$
$$+\exp\left(-((\beta_{4m} + \beta_{5m}\ A + \beta_{6m}\ I))/\lambda\right) \quad \text{(Eq 2.3)}$$
$$\left.+\exp\left(-((\beta_{7m} + \beta_{8m}\ A_m + \beta_{9m}\ I) - k_m\ )(\beta_{10m} + \beta_{11m} I + \beta_{12m}\ A)/\lambda\right)\right)$$

where I is the interaction plane, A_m is the modal area, and A is the shared area. While each network parameter was shown to fit well, the overall fit of the NFD using these estimates is also relevant. Table 2.8 shows the fit of the function for each of the scenarios used to develop the model for both micromobility and cars.

Table 2.8 R^2 of Bike and Car MNFDs for Simulated Scenarios

Network	R^2 Car	R^2 Bike
0% Bike Lanes, 0% Separated	0.97	0.91
20% Bike Lanes, 20% Separated	0.95	0.86
20% Bike Lanes, 40% Separated	0.95	0.88
20% Bike Lanes, 60% Separated	0.92	0.96
20% Bike Lanes, 80% Separated	0.94	0.98
20% Bike Lanes, 100% Separated	0.91	0.97
40% Bike Lanes, 20% Separated	0.97	0.92
40% Bike Lanes, 40% Separated	0.98	0.89
40% Bike Lanes, 60% Separated	0.97	0.81
40% Bike Lanes, 80% Separated	0.94	0.84
40% Bike Lanes, 100% Separated	0.98	0.90
60% Bike Lanes, 20% Separated	0.97	0.87
60% Bike Lanes, 40% Separated	0.97	0.82
60% Bike Lanes, 60% Separated	0.96	0.87
60% Bike Lanes, 80% Separated	0.96	0.88
60% Bike Lanes, 100% Separated	0.86	0.90
80% Bike Lanes, 20% Separated	0.96	0.92
80% Bike Lanes, 40% Separated	0.98	0.87
80% Bike Lanes, 60% Separated	0.97	0.91
80% Bike Lanes, 80% Separated	0.97	0.92
80% Bike Lanes, 100% Separated	0.92	0.98
100% Bike Lanes, 20% Separated	0.83	0.99
100% Bike Lanes, 40% Separated	0.83	0.89
100% Bike Lanes, 60% Separated	0.94	0.97
100% Bike Lanes, 80% Separated	0.93	0.99
100% Bike Lanes, 100% Separated	0.96	0.89

To validate the performance of the developed functional form, the model fit was evaluated across the simulated scenarios. The consistently high R^2 values across scenarios are shown in Table 2.8 the proposed model performs well at capturing flow–density relationships.

2.4 Summary

This section builds upon the network fundamental diagram (NFD) relationships identified in the prior section by demonstrating how network attributes such as the allocation of space to different modes and the degree of separation between them can be used to estimate the functional form of the NFD. This approach was applied to the city of Evanston, IL, where a series of simulations were conducted on varying network configurations to explicitly develop these relationships. The analysis estimates the parameters of the NFD, namely critical density, free-flow speed, maximum flow, and backward wave speed, as functions of three network attributes: exclusive modal area, shared area, and interaction plane. These relationships are modeled separately for cars and bikes. Shared areas tend to reduce maximum flow for both cars and bikes, while separated infrastructure improves flow, particularly for micromobility.

3 Microscopic Interactions - Pedestrian-CAV Decision Making

3.1 Introduction

Modeling human decision-making is challenging due to the complex mix of cognitive, psychological, and contextual factors involved. This complexity is particularly evident in urban streets without crosswalks, where pedestrian crossing behavior is influenced by vehicle interactions and life-threatening risks, making it crucial to understand these decision-making processes for improving safety and managing future interactions between pedestrians, vehicles, and autonomous vehicle (AV) systems. The effects on vulnerable users, such as pedestrians, remain uncertain as street designs evolve to accommodate Complete Street concepts. This study extends a drift diffusion model (DDM) of pedestrian crossing behavior to a two-lane urban road to provide a modeling foundation for analyzing these future designs. The model is evaluated using a micro-simulator with AVs and pedestrians, focusing on interactions affecting vulnerable users. AVs exhibit car-following and lane-changing behaviors, while pedestrians are modeled with the DDM and Cell Transmission Model (CTM). Pedestrians use sensory inputs and accumulated evidence from both lanes to make crossing decisions, while AVs adjust their behavior based on proximity to the vehicle in front and pedestrians' crossing actions. Parameter values are determined through sensitivity analysis, focusing on collision counts, conflict counts, total travel times for drivers and pedestrians, and vehicular traffic flow and density. Results reveal that equal weighting of sensory inputs from both lanes minimizes collisions and conflicts. In contrast, unequal weighting leads to unrealistic pedestrian behavior, increased collisions and conflicts, and higher travel times for vehicles, though it may decrease the travel time for pedestrians.

Human decision-making encompasses a range of scenarios, from routine choices to critical decisions, like crossing busy streets, where the stakes can be life-threatening (*69*). As urban transportation planning increasingly focuses on accommodating automated vehicles while ensuring pedestrian safety in open street environments, understanding the complex decision-making involved in human-machine interactions is crucial. Despite efforts to develop models to predict human behavior in decision-making and separate models of AVs' longitudinal and lateral movement, there is still needs for analysis techniques that jointly assess interactions between all roadway users. Efforts have been made to fill this gap ; however, a simulator that can jointly simulate the behavior of multiple vehicles and pedestrians in an identical environment and examine their interaction is still needed. In this paper, a DDM for pedestrian crossing behavior is developed and assessed through a microsimulation with AVs on a two-lane, one-way road. Analysis focuses on pedestrians' decisions to cross and the consequential effects on vehicle traffic flow. Through the simulation, we conduct a sensitivity analysis of the model parameters and assess their impact on various metrics, including conflicts, collisions, and travel times for roadway users. Our study has two main contributions. First, the micro-simulator is an extension of the simulator developed in (*59*, *70–73*) to incorporate pedestrians. Second, the pedestrian decision-making process consists of two options: cross or wait, which are modeled using the DDM. In this regard, the DDM in (*49*) is extended to a two-lane road.

3.2 Multi-Agent Platform Architecture

The microscopic analysis of pedestrian-CAV interactions was conducted using an extended micro-simulation platform that incorporates both autonomous vehicles and pedestrians in a shared urban environment. The platform was built upon an existing CAV simulation framework and expanded to include pedestrian crossing decision-making capabilities using a Drift Diffusion Model approach. The simulation environment consists of two agent types: autonomous vehicles (AVs) and pedestrians. AVs exhibit car-following and lane-changing behaviors while pedestrians are modeled using DDM for crossing decisions and Cell Transmission Model (CTM) for movement dynamics. The platform enables real-time interactions where pedestrians use sensory inputs and accumulated evidence from both lanes to make crossing decisions, while AVs adjust behavior based on proximity to lead vehicles and pedestrian crossing actions. The integrated framework allows concurrent simulation of heterogeneous agents in a shared environment, supporting complex traffic scenarios that include vehicle following dynamics, lane changes, pedestrian crossing decision behaviors, and AV collision avoidance protocols.

3.3 Road Environment and Geometry

The micro-simulator features a two-lane, one-way road environment designed specifically for AV-pedestrian interaction analysis. Each lane has a length of 1 kilometer and width of 4 meters, with 1-meter shoulders on each side designated for pedestrian use only. The shoulders serve as pedestrian waiting areas and crossing initiation zones.

The road geometry provides a controlled environment for systematic analysis of pedestrian-vehicle interactions while maintaining sufficient length to observe behavioral patterns and traffic flow effects. The two-lane configuration enables analysis of pedestrian decision-making complexity when crossing multiple lanes with potentially different traffic conditions. Grey areas in the simulation represent shoulders or sidewalks that pedestrians cross to and from, providing safe waiting areas outside the vehicle travel lanes. This configuration reflects common urban environments where pedestrians must cross multilane roads at mid-block locations.

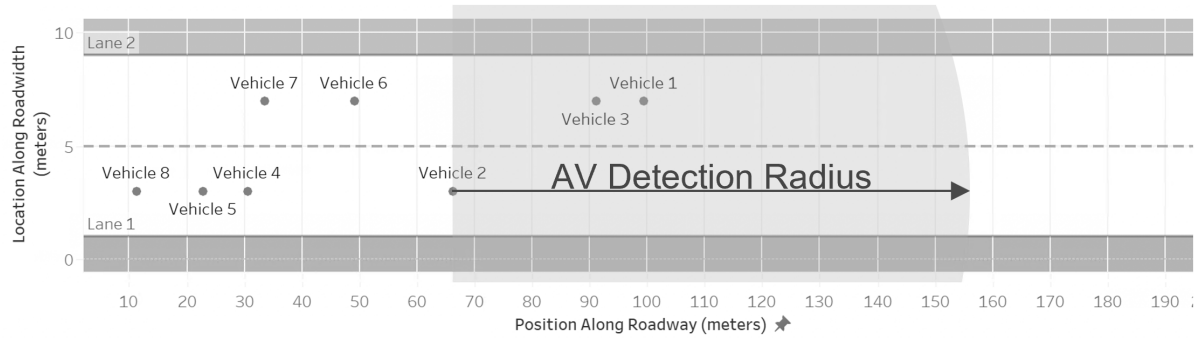

Figure 3.1 Micro-simulator's road segment properties.

The micro-simulator consists of two agent types: (1) AV and (2) Pedestrian. The AV's driving logic consists of two important maneuvers: (1) longitudinal movement (car-following

phase, or free flow speed phase) and (2) lane changes. Pedestrians are generated on both shoulders with intent to cross. The pedestrian movement is simulated after pedestrians decide to cross their path to the opposite side of the street. The following sections describe details about the formulation and assumption of different parts of our model.

3.4 AV modelling

The acceleration choice of AVs developed in (*59*) is presented with a minor modification to account for the presence of pedestrians in the simulation. The paper assumes that AVs are equipped with an automotive radar sensor with a detection range of 90m ± 2.5%. It is assumed that the vehicle's maximum speed v_{max} is decided based on spacing to the leader when they are in the car-following mode, or the detection radius, whichever is smaller. In other words, if spacing of the car-following phase is larger than the detection radius, the maximum speed is chosen assuming that there is a stopped object at a distance of the detection radius. Correspondingly, using Equations 3.1, 3.2, and 3.3 maximum safe speed can be calculated.

$$\Delta x_n = (x_{n-1} - x_n - l_{n-1}) + v_n\tau + v_{n-1}^2/(2a_{n-1}^{decc}) \quad \text{(Eq 3.1)}$$

$$\Delta x = \min(\text{SensorDetectionRange}, \Delta x_n) \quad \text{(Eq 3.2)}$$

$$v\_max = \sqrt{(-2a_n^{decc}\Delta x)} \quad \text{(Eq 3.3)}$$

n and $n-1$ denote the ID of the Target vehicle and its leader, respectively. τ denotes the reaction time of the vehicles. x_n , v_n , a_n^{decc} and l_i denote the location, speed, maximum deceleration, and length of vehicle n, respectively.

Equation 3.4 defines the acceleration choice of vehicles during car-following model, where $a_i^d(t)$ is the acceleration of vehicle n and $k_a, k_v,$ and k_d are parameters to be chosen. Furthermore, s_n is the current clearance of vehicle with n to its leader.

$$a_i^d(t) = k_a\, a_{n-1}\,(t-\tau) + k_v\,(v_{n-1}\,(t-\tau) - v_n\,(t-\tau)) + k_d\,(s_n\,(t-\tau) - s_{ref}\,) \quad \text{(Eq 3.4)}$$

s_{ref} is calculated by Equation 3.5. Furthermore, s_{min} , s_{system}, and s_{safe} are calculated based on Equations 3.6, 3.7, and 3.8, respectively.

$$s_{ref} = \max(s_{min}, s_{system}, s_{safe}\,) \quad \text{(Eq 3.5)}$$

$$s_{system} = v_n\tau \quad \text{(Eq 3.6)}$$

$$s_{safe} = v_{i-1}^2/((2 * (1 / a_n^d - 1 / a_{n-1}^d)) \quad \text{(Eq 3.7)}$$

$$s_{min} = 2m \quad \text{(Eq 3.8)}$$

In this paper, it is assumed that vehicles detect pedestrians when they are in the detection radius, then AV also consider the safe stopping deceleration for pedestrians $a_n^{ped}(t)$, as defined by Equation 3.9.

If the pedestrian is detected:

$$a_n^{ped}(t) = v_n^2/(2 \cdot d_{ped}) \quad \text{(Eq 3.9)}$$

Where v_n is the speed of the vehicle with an ID of n, d_{ped} is the distance between the vehicle with an ID of n and the closest pedestrian. The final acceleration $a_n(t)$ is defined by Equation 3.10.

$$a_n(t) = min\,(a_n(t), k(v_{max} - v_n(t), a_n^{ped}(t))) \quad \text{(Eq 3.10)}$$

We adopt the same model parameters as those proposed in (*59*), where k, k_a, k_v, and k_d are set to be 1, 1, 0.58, and 0.1, respectively.

3.5 Pedestrian Decision Modeling

In (*49*), a Gaussian DDM is used to model pedestrians' decision-making process when crossing a single-lane road. In this study, we extend the formulation in (*49*) to a two-lane case, in which the evidence is accumulated based on a pedestrian's visual perspective of the incoming vehicles in both lanes. This process can be expressed using a stochastic differential equation, as shown by Equation 3.11.

$$\mathrm{dA/dt} = -\alpha A(t) + s(t) + \epsilon(t) \quad \text{(Eq 3.11)}$$

$A(t)$ is the accumulated evidence at time t and α is the damping parameter, $s(t)$ is the time-varying sensory input, and $\epsilon(t)$ is the white noise process. As proposed in (*49*) the error distribution in this paper follows a normal distribution $\epsilon(t) \sim N(0, \sigma^2)$ with a standard deviation of σ. The pedestrian decides to cross the street if $A(t)$ surpasses a threshold value. The time that the pedestrian decides to cross the street can be calculated by Equation 3.12, where A_{th} is the evidence threshold.

$$\begin{aligned} &t' = \min\,(\mathrm{t}) \\ &\text{subject to} \quad A(t) \geq A_{th} \end{aligned} \quad \text{(Eq 3.12)}$$

The main contribution of the paper is that instead of using one sensory input, our model incorporates two of them, with one for each lane. Equation 3.13 shows the total sensory input from both lanes, where $s_1(t)$ and $s_2(t)$ are the sensory inputs for the first lane and second lane. β_1 and β_2 are the model parameters for lanes 1 and 2, respectively.

$$s(t) = \beta_1 s_1(t) + \beta_2 s_2(t) t' = \min(t) \quad \text{(Eq 3.13)}$$

To make the parameters in the sensory input compatible with the single-lane case proposed in (*49*), we assume that $\beta_1 + \beta_2 = 1$. the sensory input for the first lane is calculated using a sigmoidal transformation.

$$s_1\,(t) = \arctan\,(m((\overline{\tau_1}(t) - \overline{\tau'})) \quad \text{(Eq 3.14)}$$

$$s_2\,(t) = \arctan\,(m_p\,((\overline{\tau_2}(t) - \overline{\tau_p'}\,) \quad \text{(Eq 3.15)}$$

Where m and m' are scaling factors and $\bar{\tau}'$ and $\overline{\tau_p'}$ are parameters to be estimated. $\overline{\tau_1}(t)$ and $\overline{\tau_2}(t)$ are the generalized time to arrival signal for the first and second lanes, which can be calculated by Equations 3.16, and 3.17, respectively.

$$\overline{\tau_1}(t) = D(t)/v(t)\; + \beta_D\,(D(t)/v_1 - D(t)/v(t)\,) + \beta_\tau\;(d(D(t)/v(t)\,)/ d_t + 1) + \beta_H\,H(t) \quad \text{(Eq 3.16)}$$

$$\overline{\tau_2}(t) = (D_p\,(t))/(v_p\,(t)\,) + \beta_{Dp}\,((D_p\,(t))/v_2\; - \tau_p\,(t)) + \beta_{\tau\mathrm{p}}\,(d((D_p\,(t))/ (v_p\,(t)\,))/dt + 1)\; +\; \beta_{Hp}\,H_p\,(t) \quad \text{(Eq 3.17)}$$

Where $D(t)$ and $D_p(t)$ are the actual and predicted distances between incoming vehicle to the pedestrian, $v(t)$ and $v_p(t)$ are the actual and predicted speeds of the incoming vehicles, $H(t)$ and $H_p(t)$ are the binary variables which is 1 when there is an external human-machine interface (eHMI), and otherwise is zero. In this paper, it is assumed that $H(t)$ and $H_p(t)$ are zero. β_D, β_{Dp}, v_1, v_2, $\beta_{\dot{\tau}}$, $\beta_{\dot{\tau}p}$, β_H, and β_{Hp} are parameters of the model.

The generalized time to arrival for the second lane, as shown in Equation 3.17, represents a slightly different situation than in the first lane. The pedestrian estimates the time required to cross the first lane. Then, based on the distance it will cover during this estimated crossing time, the pedestrian predicts the position of the vehicle in the second lane. In other words, before beginning to cross, the pedestrian assesses the current situation in the closer lane and anticipates the situation in the further lane when they have finished crossing the first lane and are about to enter the second lane. Correspondingly, she forecasts her situation and the speed and the distance of the incoming vehicle in the second lane, as shown in Figure 3.2. It is also shown in Figure 3.2 that a pedestrian estimates her crossing time which is $t = \frac{4m}{v_{ped}}$, v_{ped} is the speed of the

pedestrian, and 4m is the lane width.

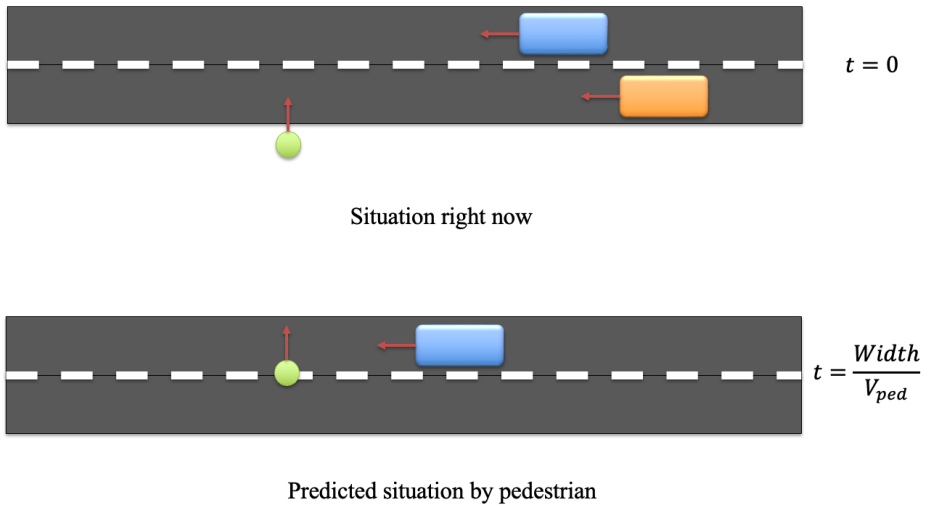

Figure 3.2 Pedestrian perspective for deciding to cross the road based on the information on both lanes.

To obtain the predicted speed of the vehicle by pedestrians it is assumed that pedestrians mainly show three different behaviors confronting a vehicle, they can be hypervigilant, neutral, or trusting; accordingly, the acceleration of the vehicle assumed by pedestrians with this type are assumed to be $2\frac{m}{s^2}, 0, -2\frac{m}{s^2}$ as shown in Figure 3.3. The rationale is that pedestrians might anticipate the approaching vehicle to either accelerate or decelerate based on their perception and their own characteristics, such as their risk tolerance, urgency, familiarity with the traffic environment, and previous experiences. Additionally, factors like age, physical ability, and cultural background can influence how a pedestrian assesses the situation. This variability in attitudes and characteristics introduces heterogeneity in their decision-making processes, leading

to diverse behaviors in similar traffic scenarios.

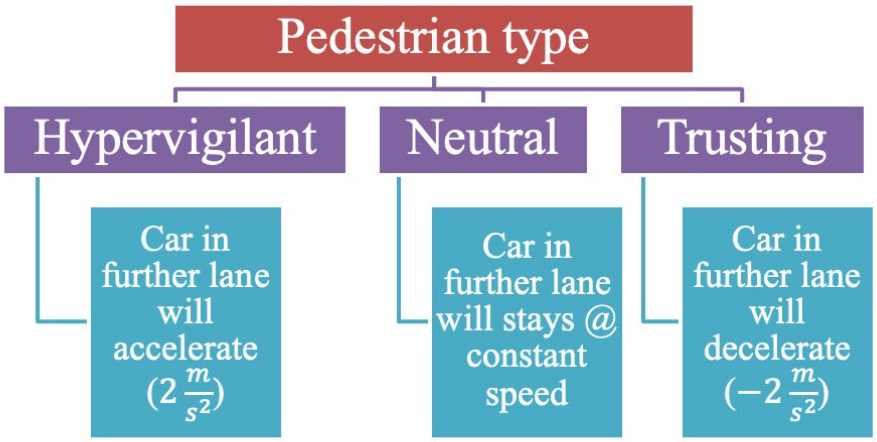

Figure 3.3 Different pedestrian types and their corresponding perspective for acceleration of incoming vehicle on the second lane.

3.6 Pedestrian Movement

Pedestrians are generated equally on both sides of the road. Their start location, x, is randomly chosen along the shoulders, and their destination is picked randomly within a set range, $[x - \alpha_d, x + \alpha_d]$, to maintain reasonable crossing angles. First, the pedestrian decides whether to cross the street. After making a decision, they move to their destination on a path generated by the CTM (*74*), as shown in Equation 3.18.

$$N_i(t+1) = N_i(t) + \sum_{j \neq i, j \in L} q_{ji}(t) - \sum_{j \neq i, j \in L} q_{ij}(t) \quad \text{(Eq 3.18)}$$

$N_i(t)$ is number of pedestrians in cell i at time t, and $q_{ji}(t)$ is flow from cell j to cell i at time t. In addition to the main CTM formula, flow constraints, as shown by Equation 3.19, are used to ensure that the number of pedestrians moving from cell i to cell j cannot be more than either demand or the available space in the adjacent cell. c_i denotes the capacity of cell j, which is chosen to be 1. Figure 3.4 shows pedestrian trajectories without vehicle interactions.

$$q_{ij}(t) = min\{(N_i(t))/c_i, (1 - (N_j(t))/c_j)\} \quad \text{(Eq 3.19)}$$

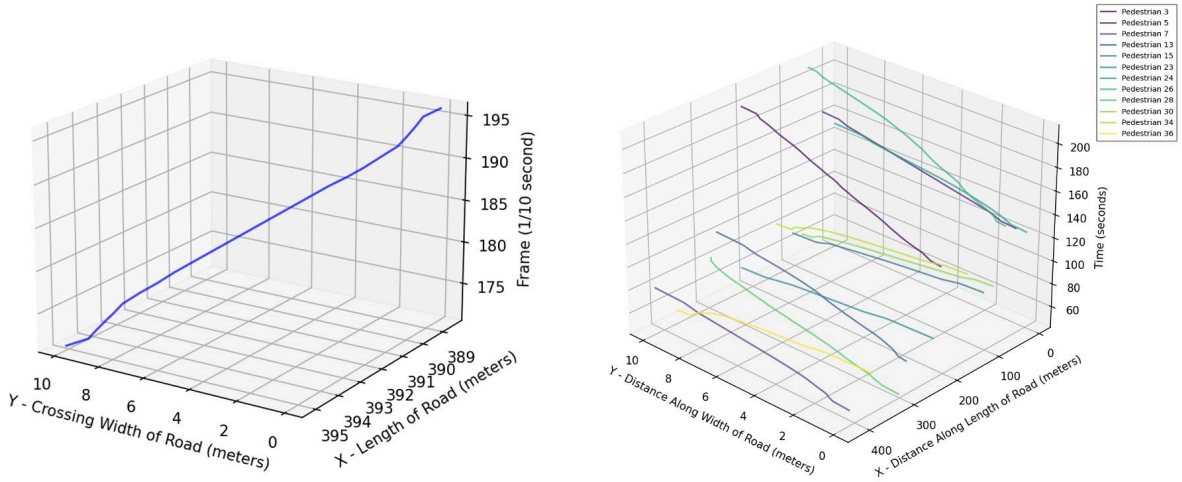

Figure 3.4 A subset of non-responsive pedestrians' trajectories.

3.7 Microsimulation Setup

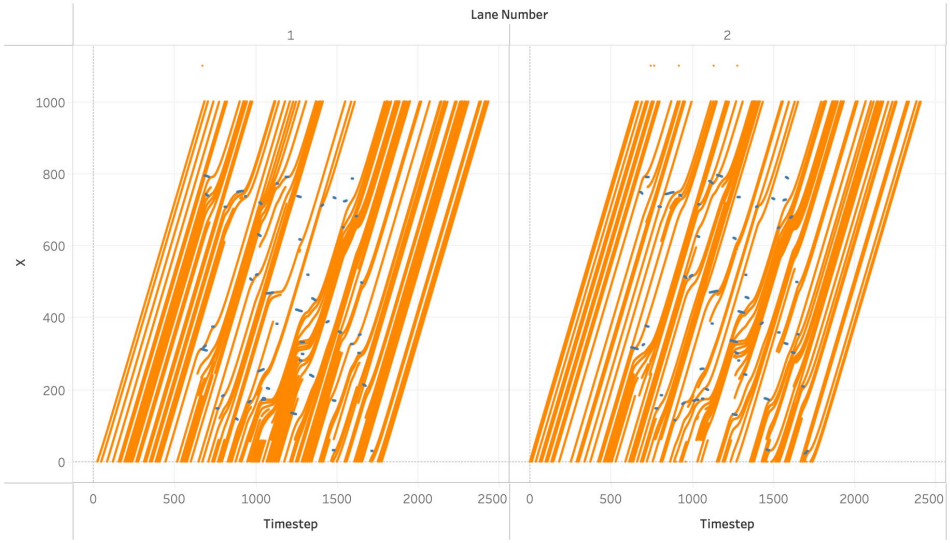

Figure 3.5 AVs trajectory when they confront non-responsive pedestrians. Vehicle's trajectory (Orange), Pedestrians trajectory (Blue).

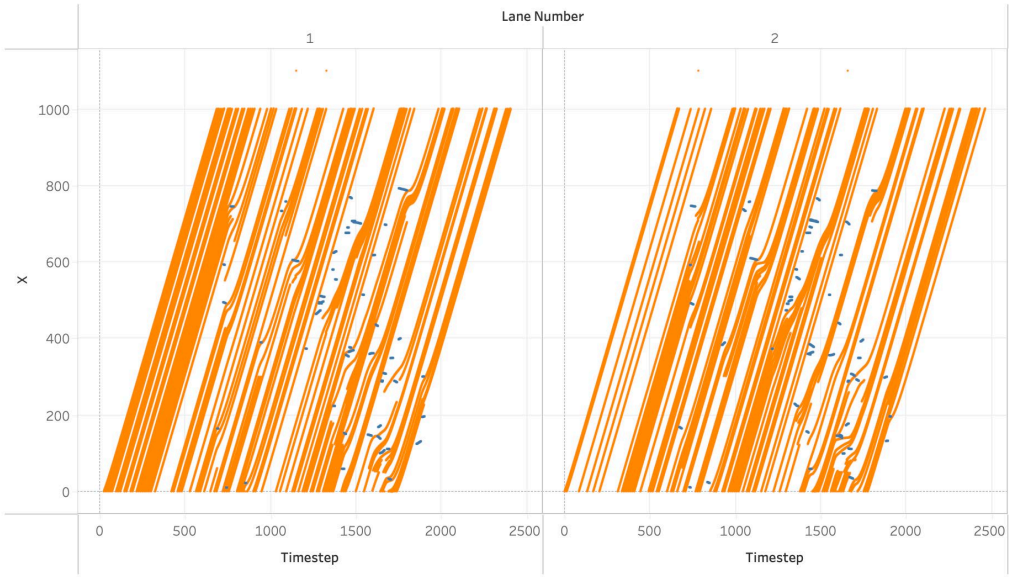

Figure 3.6 AVs trajectory when they confront responsive pedestrians. Vehicle's trajectory (Orange), Pedestrians trajectory (Blue).

3.8 Results

3.8.1 Sensitivity analysis

The sensitivity analysis aims to examine how collisions, lane conflicts, travel times, and flow-density relationships are influenced by the parameters in Equation 3.11 and Equation 3.13. Specifically, we analyze the effects of β_1, α and σ by repeating the simulation 10 times for each parameter. When the sensitivity analysis is not performed on β_1, α, and σ, their values are 0.5, 1.65 and 0.65, respectively.

To obtain the flow-density relationship for AVs on each lane, we partition the AV trajectories into position-time-windows (PTWs) of lengths of 100m and durations of 20s. We discard the first 80 s and last 80s of the simulated data to ensure that the first-generated AV has reached the end of the simulation network, and the last-generated pedestrian has not left the network. If there exist pedestrians in the range of the longitudinal locations of a PTW (including the adjacent lane), then we note that this PTW is under pedestrian influence. The average speed, flow, and density in each PTW is calculated based on Edie's definition (*75*).

3.8.2 Sensitivity analysis for β_1

β_1 is the weight for the sensory input of the lane that is closer to the pedestrian position. A higher β_1 indicates that the pedestrian's decision-making process is determined more by the closer lane than the further lane. In these experiments, β_1 was varied between 0.25 and 1 with a step size of 0.05. The performance metrics for each β_1 value is shown in Figure 3.7. According to Figure 3.7 (a), the total travel time for vehicles is lowest when $\beta_1 = 0.5$, indicating that if the pedestrians put the same weight on the sensory inputs to both lanes, their impact on vehicle traffic is the lowest. Figure 3.7 (b) shows the total travel time for pedestrians. It suggests that when $\beta_1 > 0.55$, the total travel time for pedestrians tends to decrease when β_1 increases. However, at lower β_1 values, the total travel time of pedestrian seem to fluctuate. Figure 3.7 (c) and Figure 3.7 (d) show the conflict numbers and collision numbers for both lanes respectively. These two metrics both decrease with β_1 when $\beta_1$is low and increase with β_1 when β_1 is high. It is worth noting that the collision number varies more across lanes. This is because collision is a relatively rare event and is subjected to more variation. Finally, Figure 3.7 (e) shows the number of pedestrians that decide to cross is the lowest at $\beta_1 = 0.55$. Mid-range β_1 values lead to fewer pedestrians crossing because they must evaluate crossing conditions in both lanes simultaneously. It is more challenging for pedestrians to find an optimal crossing opportunity when they need to consider both lanes rather than just one.

Regarding the speed-density and flow-density relationships of AVs for β_1 values of 0.25, 0.5, and 0.75, as shown by Figure 3.8. We notice that the vast majority of PTWs without pedestrian influence are in the free-flow state, which means the AVs are travelling at the desired speed of 55km/h. However, when the PTWs are under pedestrian influence, the speed tends to be the highest for $\beta_1 = 0.5$. This result is consistent with the vehicle travel time shown by Figure 3.7 (a). In addition, in all three β_1 values, the pedestrians tend to cross when the traffic density is medium (between 20 and 40 vehicles/km). This is because the existence of pedestrians tends to

let vehicles slow down and therefore creates a queue and increases the traffic density. When the density is high, the influence of pedestrians makes the AVs slow down more, possibly because denser traffic is more prone to breakdown under external influence.

3.8.3 Sensitivity analysis for α

As shown in Equation 3.11, α is the damping parameter, with higher values indicating a faster depreciation rate of accumulated evidence and greater dependence of the drift rate on this evidence. For the analysis, α is varied between 1.2 and 2.1 in increments of 0.1. Figure 3.9 (e) and Figure 3.9(b) illustrates the impact of different α values on the total number of pedestrians crossing the street and their total travel time, respectively. When $\alpha \leq 1.5$, all pedestrians eventually cross the street for all simulation rounds. However, when $\alpha \geq 1.6$, the number of pedestrians crossing begins to decline. This is because higher α values lead to a slower rate of evidence accumulation, resulting in longer waiting times for pedestrians, as shown in Figure 3.9(b). Consequently, some pedestrians may never reach the threshold to cross. Fewer crossing pedestrians reduce the total travel time for vehicles, as depicted in Figure 3.9(a), because they do not need to slow down. Additionally, Figure 3.9(c) and Figure 3.9(d), show that the number of conflicts and collisions decreases with higher α values. This reduction is likely due to the decreased interaction between pedestrians and AVs.

Figure 3.10 shows the speed-density and flow-density relationships for α values of 1.2, 1.7 and 2.1. When the α value is lower, more PTWs are under pedestrian influence and more of them low speed, which is possibly due to more pedestrians crossing and interaction. This observation is again consistent with the trend of the travel time shown by Figure 3.9(a). However, it is worth noting that for all three α values, the range of speed for the PTWs under pedestrian influence are similar. This is because α only dictates the decision-making process before a pedestrian decides to cross the street and is not correlated with the level of interaction between AVs and crossing pedestrians.

3.8.4 Sensitivity analysis for σ

According to Equation 3.11, sigma is the power term of the white noise process of $\epsilon(t) \sim N(0, \sigma^2)$. When σ is higher, it means that the rate of change of the accumulated evidence has higher uncertainty, possibly caused by unobserved factors. This also leads to more uncertainty in pedestrians' decision-making process. Here, we examine σ values ranging from 0.4 to 0.85 at an increment of 0.05.

Figure 3.11(e) and Figure 3.11(b) show the number of pedestrians that decide to cross and the total travel time respectively. These two metrics have decreasing trends when σ increases. Given the same sensory input, a higher σ would lead to a higher range and maximum value of the rate of change of the cumulative evidence. This potentially makes the evidence threshold more likely to be reached earlier, which also leads to a lower waiting time of pedestrians. Figure 3.11(a) shows the total travel time of the vehicles, which tends to increase with α and again shows the opposite trend as the total travel time of the pedestrians due to more AVs having to

slow down for the pedestrians. Finally, Figure 3.11(c) and Figure 3.11(d) show the number of conflicts and collisions for both lanes, which increases as the number of crossing pedestrians increases.

Now, we observe the speed-density and flow-density relationships of the PTWs as shown by Figure 3.11 when σ take different values. A higher σ is associated with more PTWs under pedestrian influence and more slowdowns. This is again consistent with the increasing travel time of the vehicles.

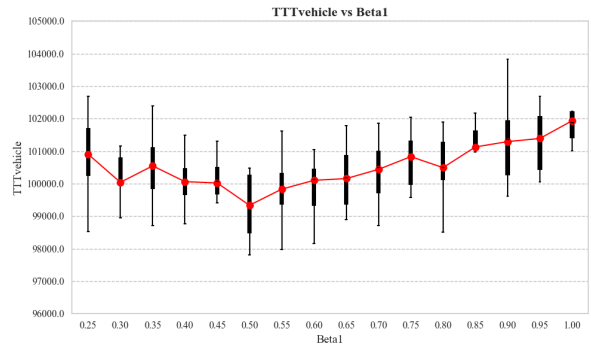

(a)

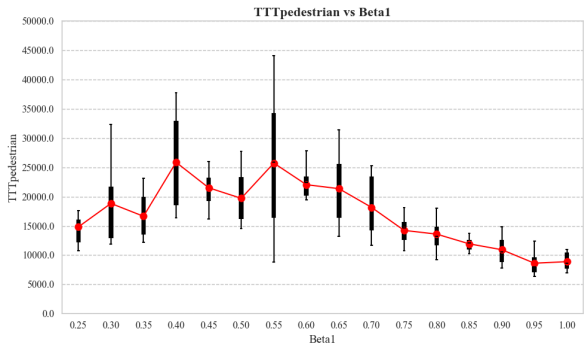

(b)

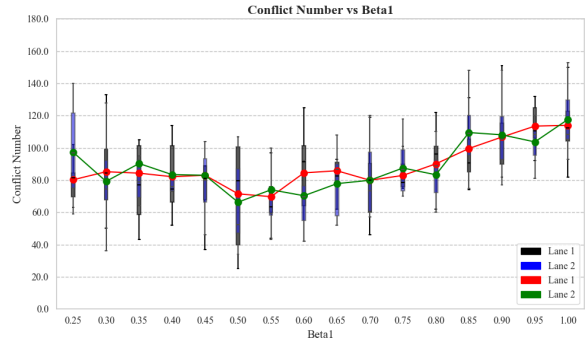

(c)

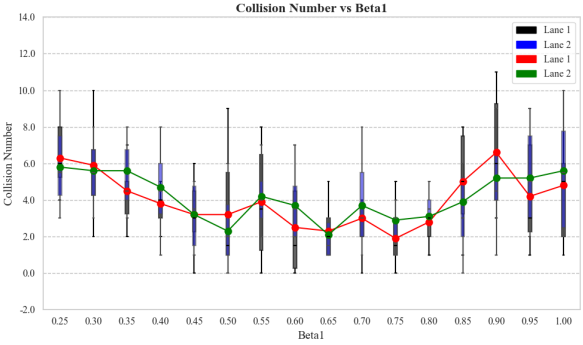

(d)

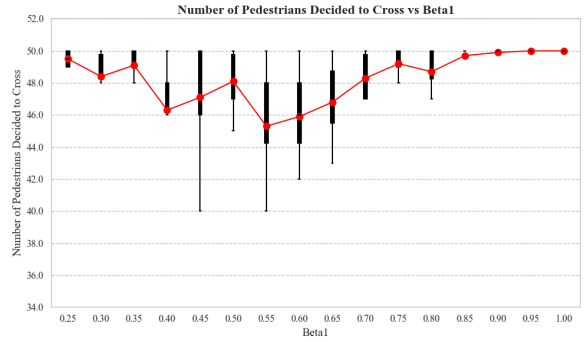

(e)

Figure 3.7 Results of the sensitivity analysis for $\beta_1 = 1 - \beta_2$:

(a) Total travel time for vehicles versus different values of beta for 10 replications for each value of beta (b) Total travel time and waiting time for pedestrians versus different values of beta for 10 replications for each value of beta (c) Conflict numbers in each lane versus different values of beta for 10 replications for each value of beta (d) Collision numbers in each lane versus different values of beta for 10 replication for each value of beta (e) Number of pedestrians that decided to cross versus different values of beta for 10 replication for each value of beta (Note: Outliers are considered in the calculation of averages (red points), though they are not shown in the plots).

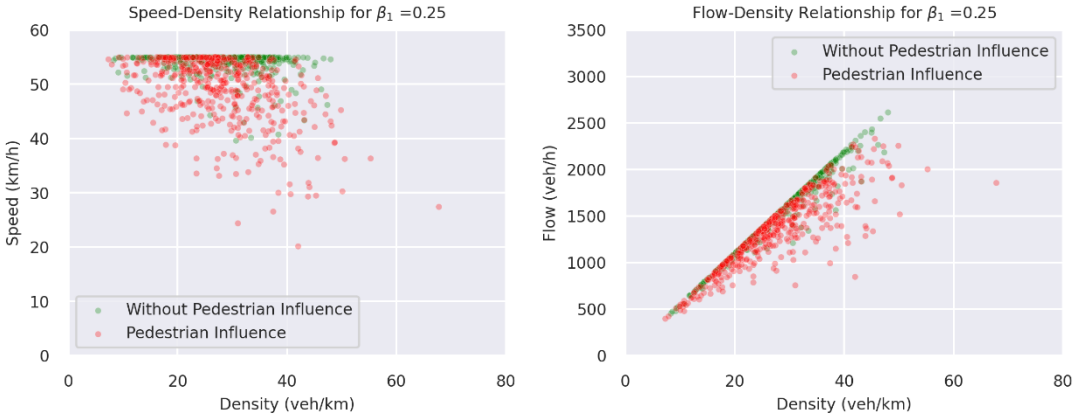

$\beta_1 = 0.25$

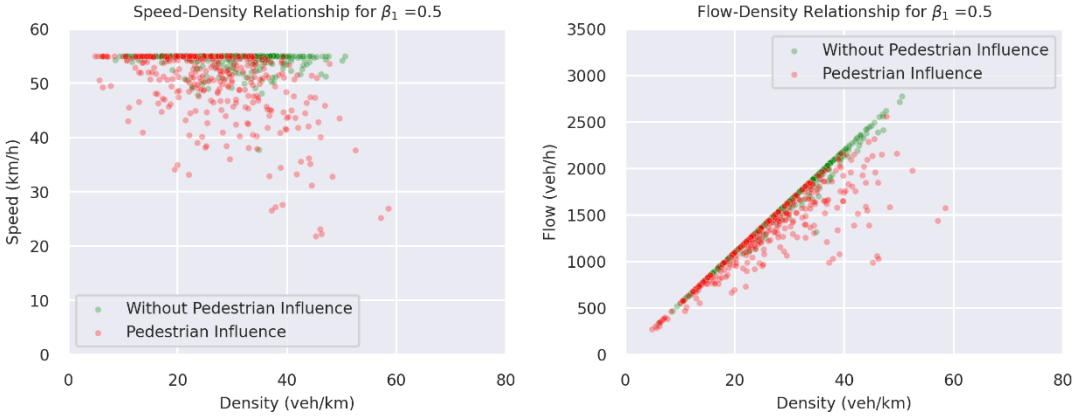

$\beta_1 = 0.5$

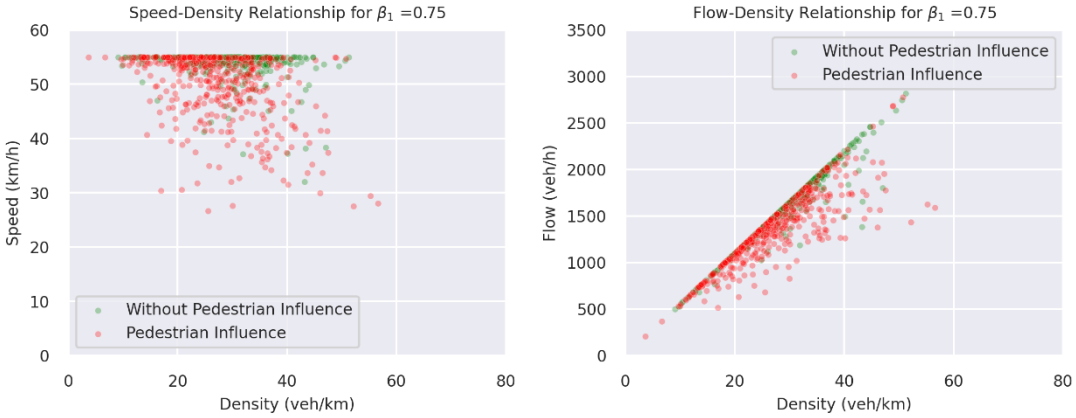

$\beta_1 = 0.75$

Figure 3.8 Effects of β_1 on Speed-Density and Flow-Density Relationships.

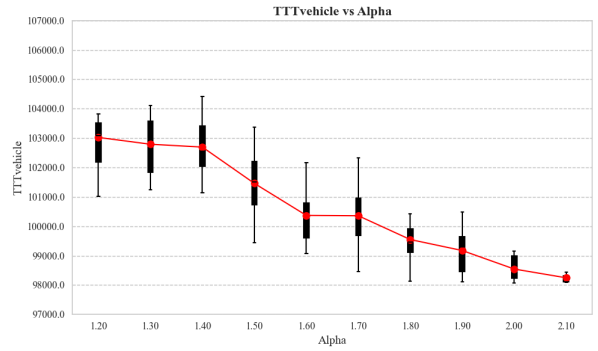

(a)

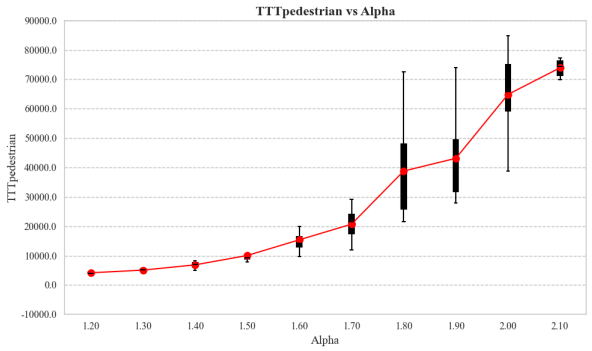

(b)

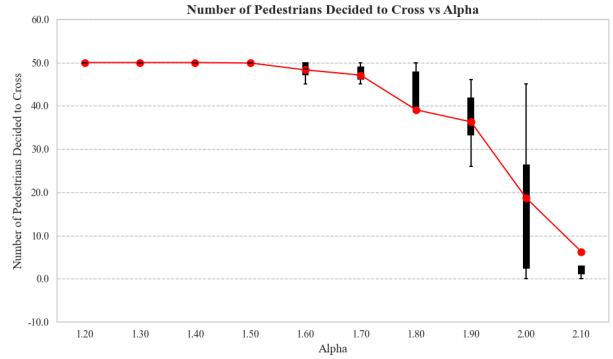

(c)

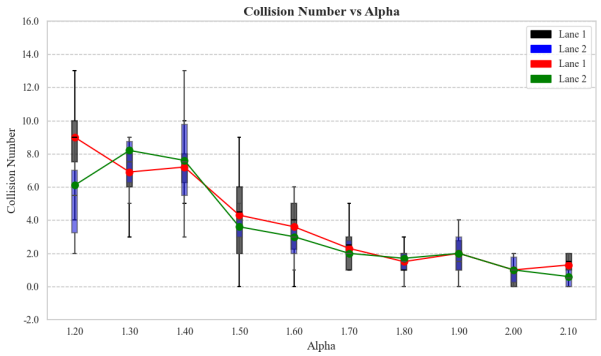

(d)

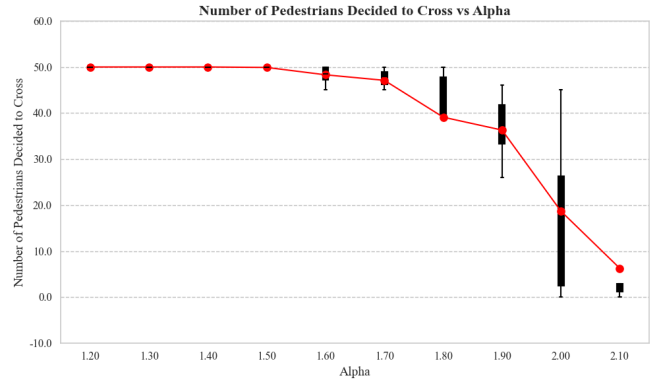

(e)

Figure 3.9 Results of the sensitivity analysis for α.

(a) Total travel time for vehicles versus different values of alpha for 10 replications for each value of alpha (b) Total travel time and waiting time for pedestrians versus different values of alpha for 10 replications for each value of alpha (c) Conflict numbers in each lane versus different values of alpha for 10 replications for each value of alpha (d) Collision numbers in each lane versus different values of alpha for 10 replication for each value of alpha (e) Number of pedestrians that decided to cross versus different values of alpha for 10 replication for each value of alpha

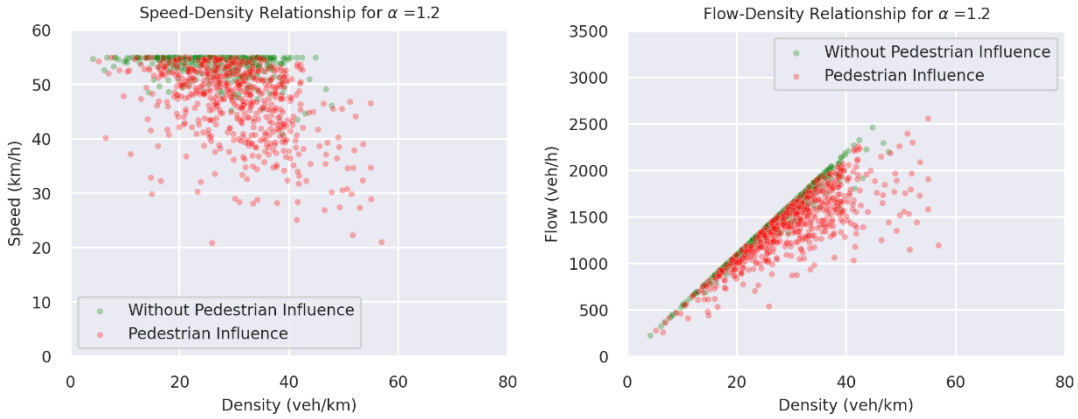

$\alpha = 1.2$

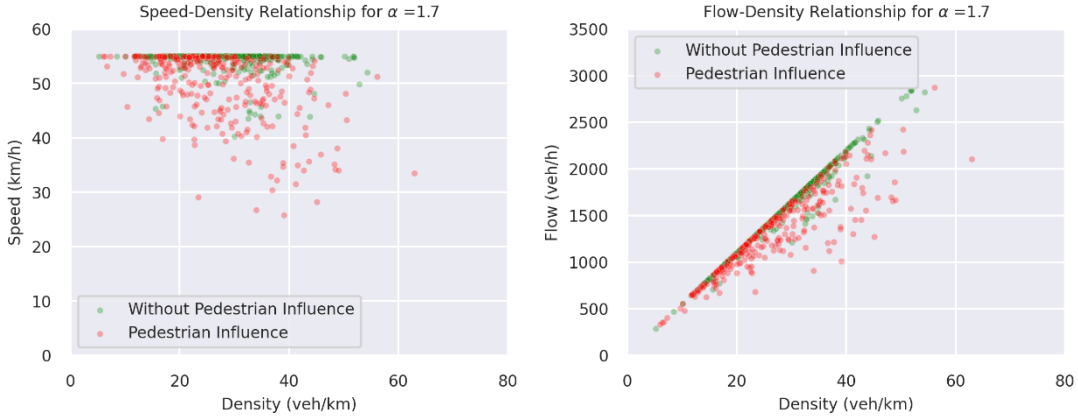

$\alpha = 1.7$

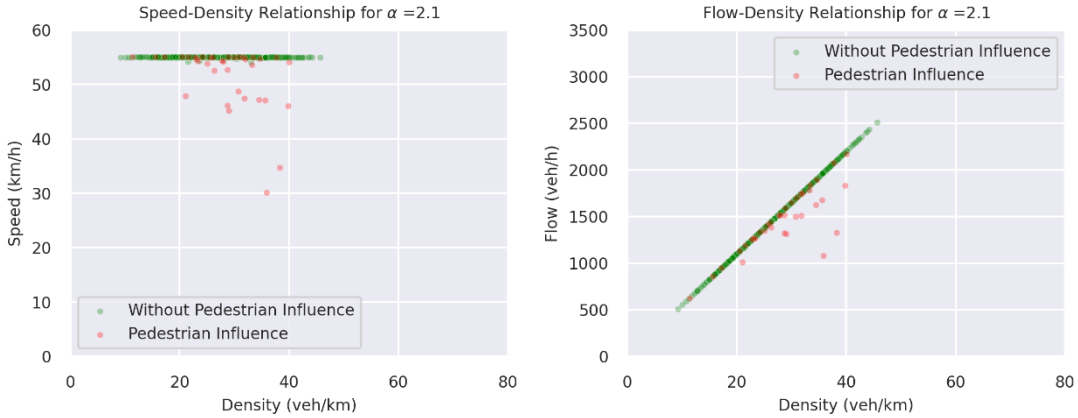

$\alpha = 2.1$

Figure 3.10 Effects of α on Speed-Density and Flow-Density Relationships.

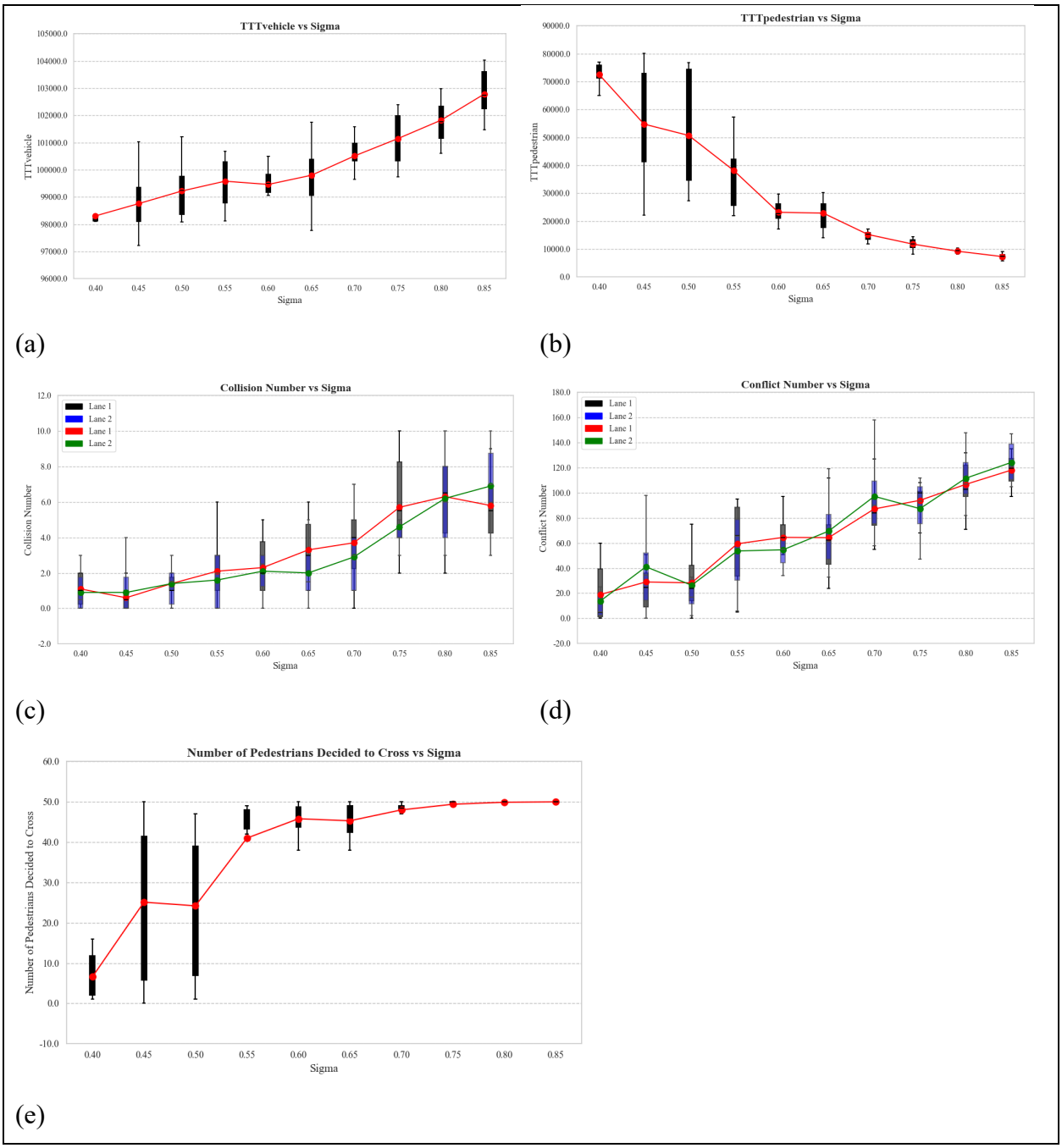

Figure 3.11 Results of the sensitivity analysis for σ :

(a) Total travel time for vehicles versus different values of sigma for 10 replications for each value of sigma (b) Total travel time and waiting time for pedestrians versus different values of sigma for 10 replications for each value of sigma (c) Conflict numbers in each lane versus different values of sigma for 10 replications for each value of sigma (d) Collision numbers in each lane versus different values of sigma for 10 replication for each value of sigma (e) Number of pedestrians that decided to cross versus different values of sigma for 10 replication for each value of sigma.

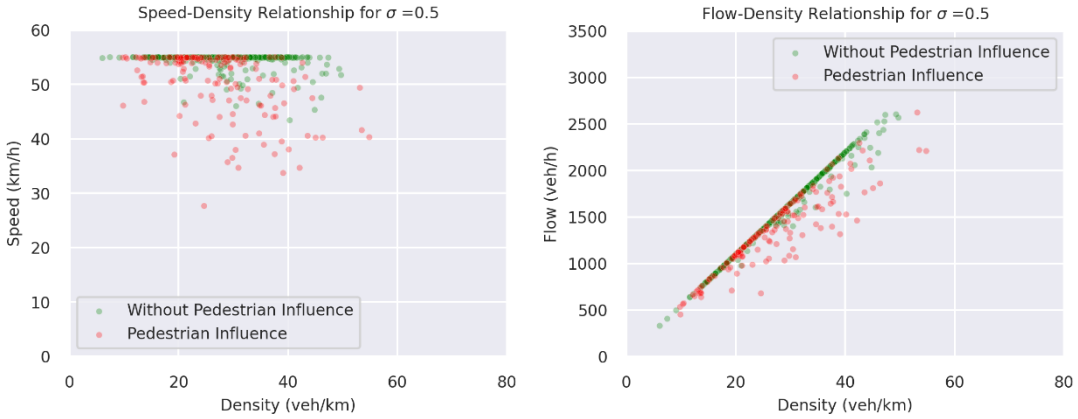

$\sigma = 0.5$

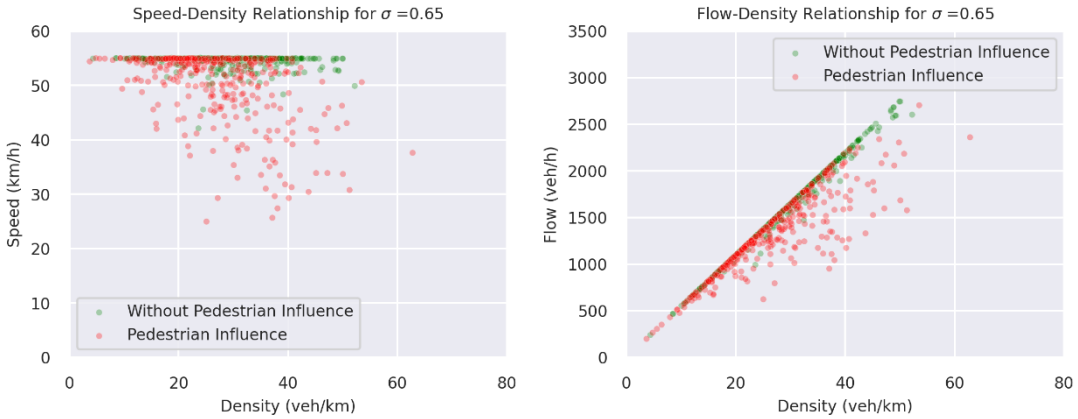

$\sigma = 0.65$

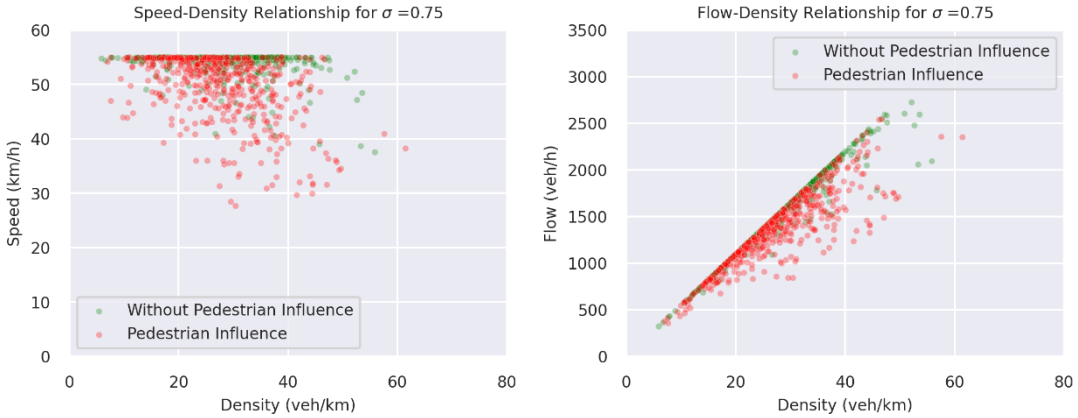

$\sigma = 0.75$

Figure 3.12 Effects of σ on Speed-Density and Flow-Density Relationships.

3.8.5 Case study

Predicting human behavior is challenging, making it impractical to use a single set of parameters to represent pedestrian behavior. Heterogeneity among pedestrians results in many valid parameter combinations. While real data and calibration are ideal for refining the model, this study uses a specific parameter set to evaluate how the DDM functions as shown in Table 1. This includes assessing model's ability to capture different expected phenomena and interactions between pedestrians and vehicles. This approach helps evaluate whether the DDM can effectively capture pedestrian decision-making and interactions in the presence of heterogeneity among pedestrians.

Figure 3.13 illustrates accumulated evidence, sensory inputs, and distance to the nearest vehicle for pedestrians with IDs 1 and 2. Pedestrian 1 decided to cross in about 10 seconds, whereas Pedestrian 2, who showed significant fluctuations in accumulated evidence, took approximately 150 seconds.

TABLE 1 chosen parameters for the simulation in the case study

Parameter	α	σ	β_1, β_2	β_D, β_{Dp}	$\beta_{\dot{\tau}}, \beta_{\dot{\tau}p}$	v_1, v_2	$\overline{\tau'}, \overline{\tau'_p}$	m, m_p	A_{th}
Chosen value	1.65	0.65	0.5	0.8	0.5	50 km/hr (13.89 m/s)	-0.1	0.6	0.8

In this case it is expected to see that there is not a sufficient gap for the pedestrian to cross the street and density of the vehicles close to the second pedestrian is higher. In order to have fair comparison, the plot is cropped to show same time steps for pedestrian with an ID of 2 compared to the pedestrian with ID of 1 as shown in Figure 3.14(b). According to the distance of closest vehicle to the pedestrian's plot for pedestrians ID 1 and 2, the density of vehicle close to the second pedestrian is higher and the first pedestrian, and also the distance of the vehicle to the first pedestrian is higher than the second one; hence, the first pedestrian accepted a gap, and crossed the street. Though, for the second pedestrian, it takes much longer to decide to cross the segment.

In order to better understand how pedestrian 1 found a large gap and accepted it, it worth visualizing the result of the simulator. Figure 3.15 (a) shows that there is a large gap behind pedestrian 1, and she decided to accept the current gap. Moreover, there are other pedestrians that decided to accept this large gap, pedestrian ID 18, 19, and 30. Evidence accumulation of pedestrian ID 18 and 19 are shown in Figure 3.15(b) and Figure 3.15(c), suggesting their accumulated evidence reached the threshold during this large gap.

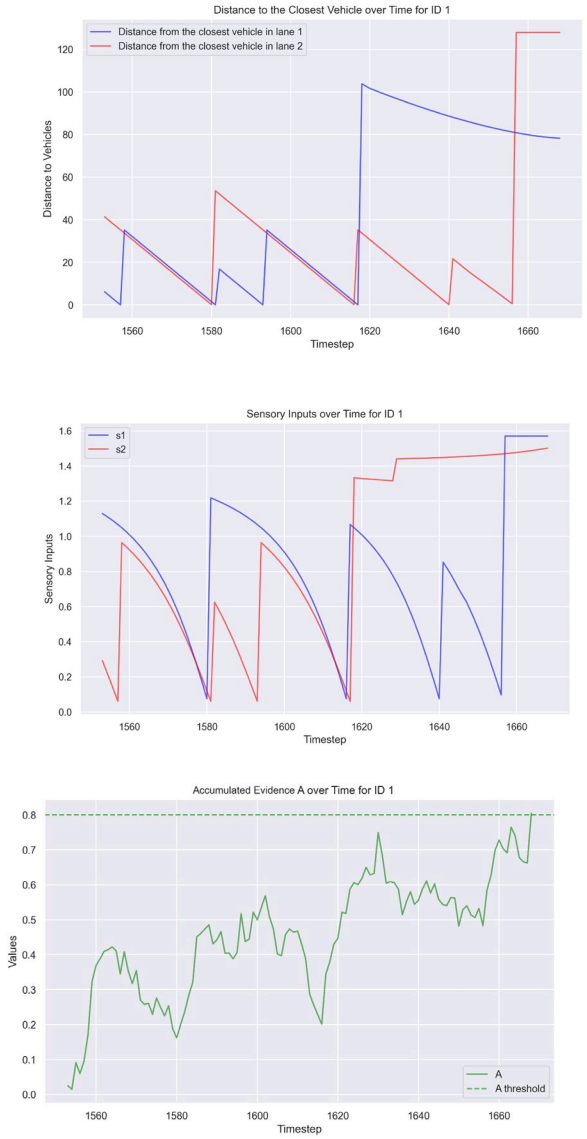

Top panel: Distance of the closest vehicle to the pedestrian ID 1, for lane 1 and lane 2, versus timestep. Middle panel: Sensory inputs for the pedestrian ID 1 for both lanes. Bottom panel: Accumulated evidence (A) over time for pedestrian ID 1

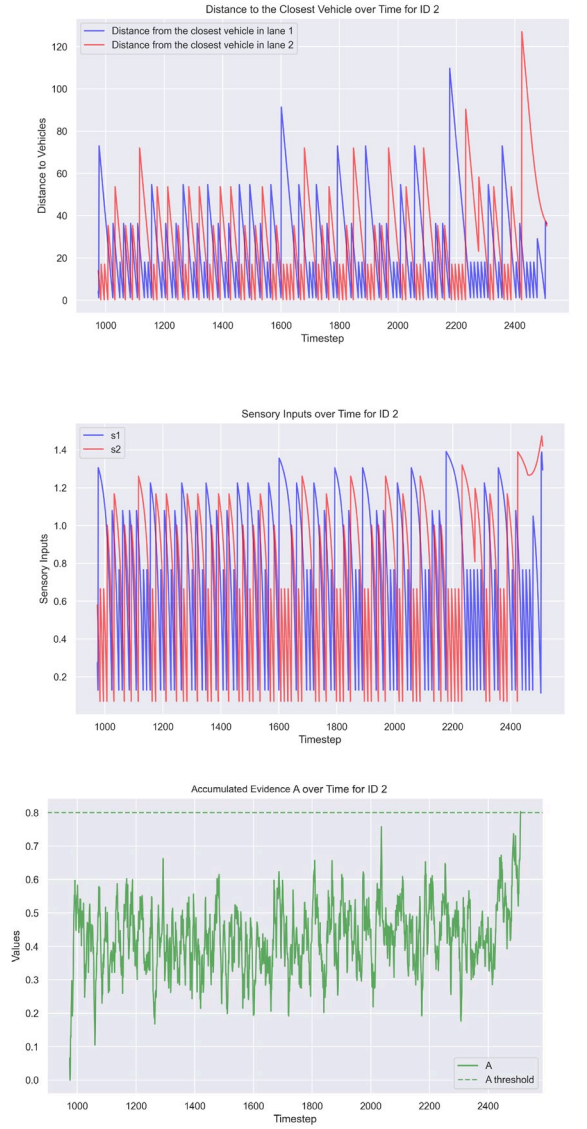

(b) Top panel: Distance of the closest vehicle to the pedestrian ID 2, for lane 1 and lane 2, versus timestep. Middle panel: Sensory inputs for the pedestrian ID 2 for both lanes. Bottom panel: Accumulated evidence (A) over time for pedestrian ID 2

Figure 3.13 Results of the simulation with selected parameters for pedestrian ID 1 and 2.

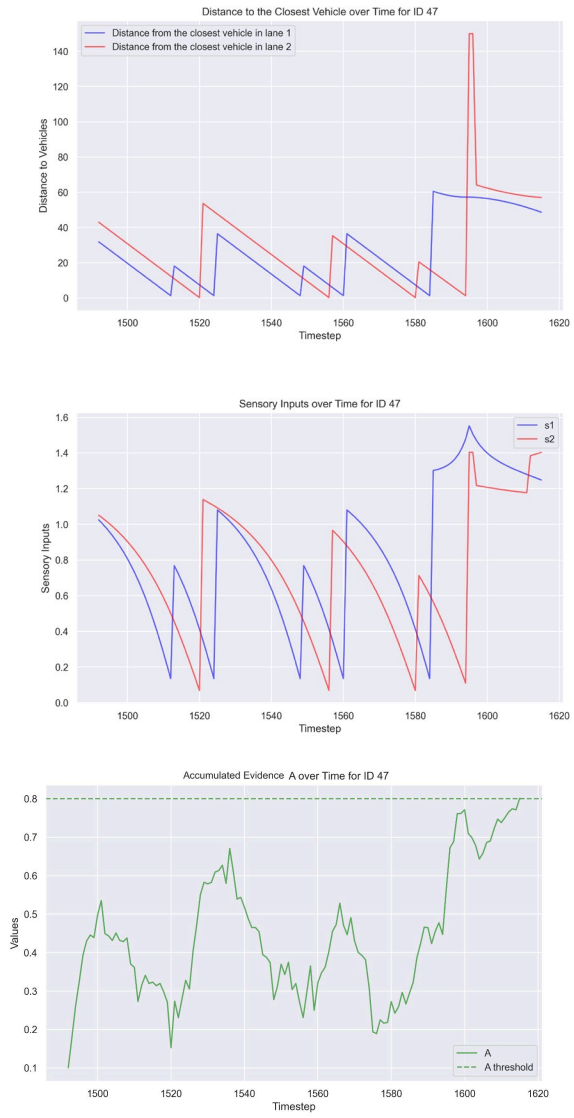

Top panel: Distance of the closest vehicle to the pedestrian ID 47, for lane 1 and lane 2, versus timestep. Middle panel: Sensory inputs for the pedestrian ID 47 for both lanes. Bottom panel: Accumulated evidence (A) over time for pedestrian ID 47

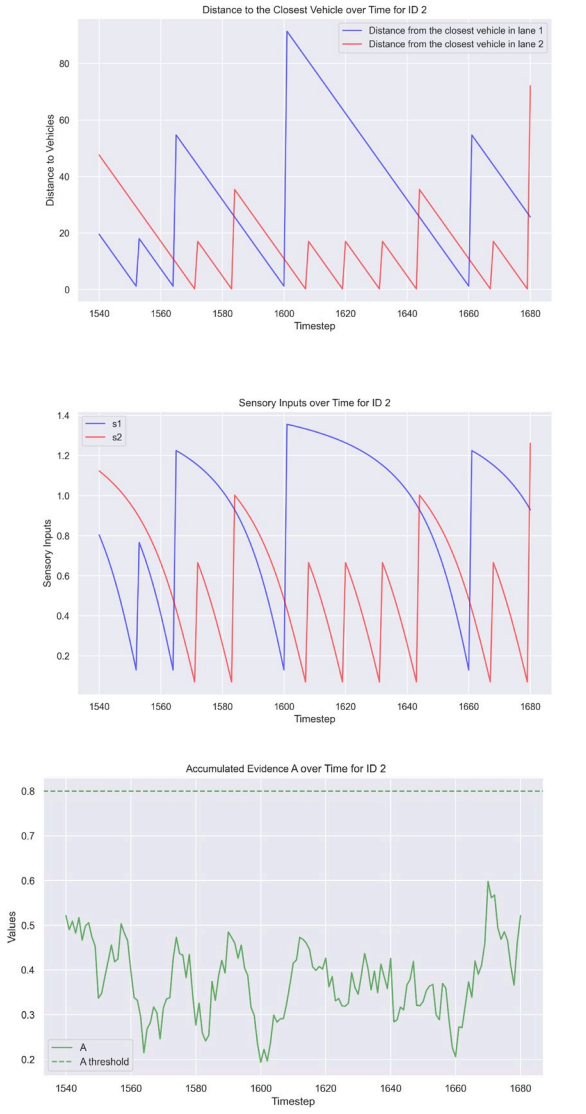

Top panel: Distance of the closest vehicle to the pedestrian ID 2, for lane 1 and lane 2, versus timestep. Middle panel: Sensory inputs for the pedestrian ID 2 for both lanes. Bottom panel: Accumulated evidence (A) over time for pedestrian ID 2, (Timestep are cropped to be comparable to pedestrian ID 1)

Figure 3.14 Results of the simulation with selected parameters for pedestrian ID 47 and 2

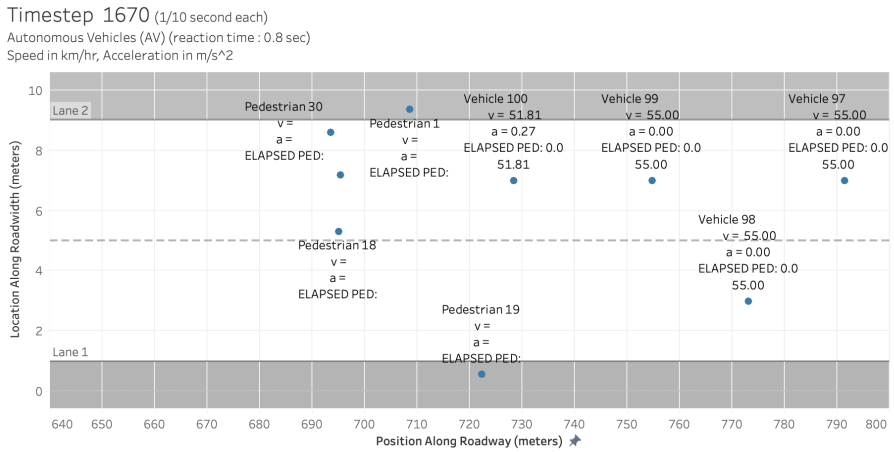

Visualization of the result, segment is cropped from 640 to 800 horizontally, for the timestep of 1670 (167 second)

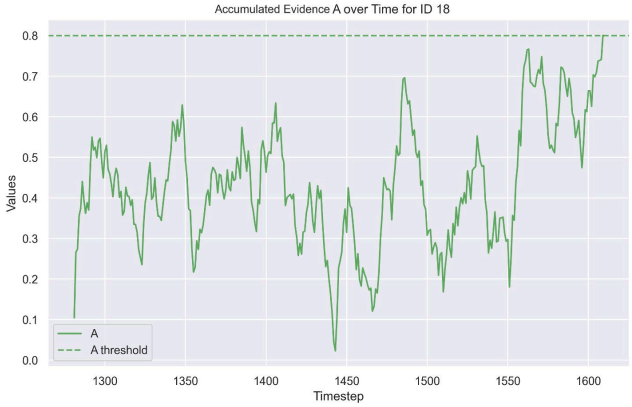

Accumulated evidence (A) for the pedestrian ID 18 over timestep

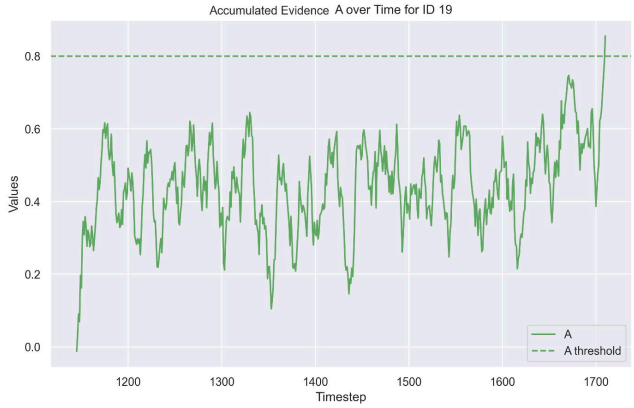

Accumulated evidence (A) for the pedestrian ID 19 over timestep

Figure 3.15 Results of the visualization for pedestrians with ID of 1, 18, 19.

On the other hand, for the pedestrian ID 2, the density of the surrounding area is expected to be high enough that prevent pedestrian from crossing the street. Figure 3.16(a) shows the time that pedestrian ID 2 has not decided to cross the street yet, and as expected the density of the vehicle is high in the second lane from which pedestrian ID 2 start crossing the segment. After encountering a gap that is large enough, pedestrian ID 2 as well as pedestrians ID 15, and 26 decide to cross the road as shown in Figure 3.16(b). Furthermore, Figure 3.16(c) shows how pedestrian ID 2 successfully cross the segment and reaching the other shoulder of the segment.

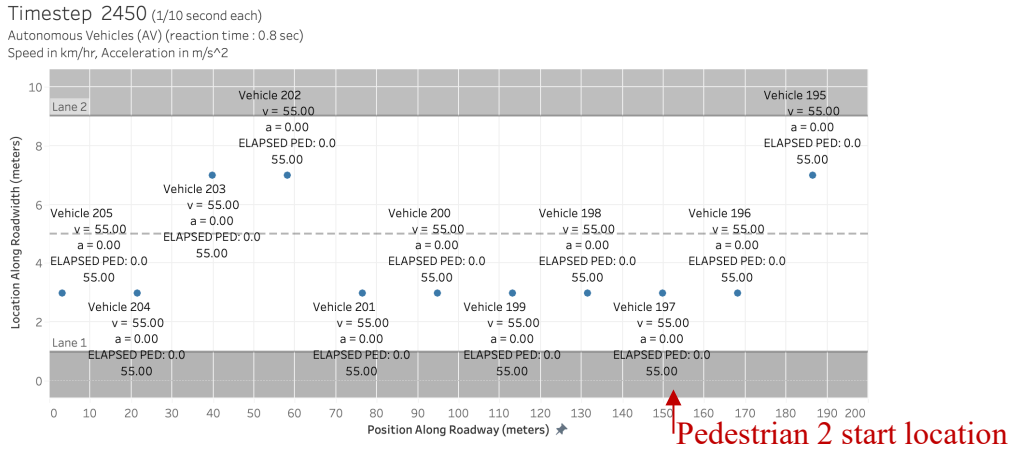

Visualization of the result, segment is cropped from 0 to 200 horizontally, for the timestep of 2450 (245 second)

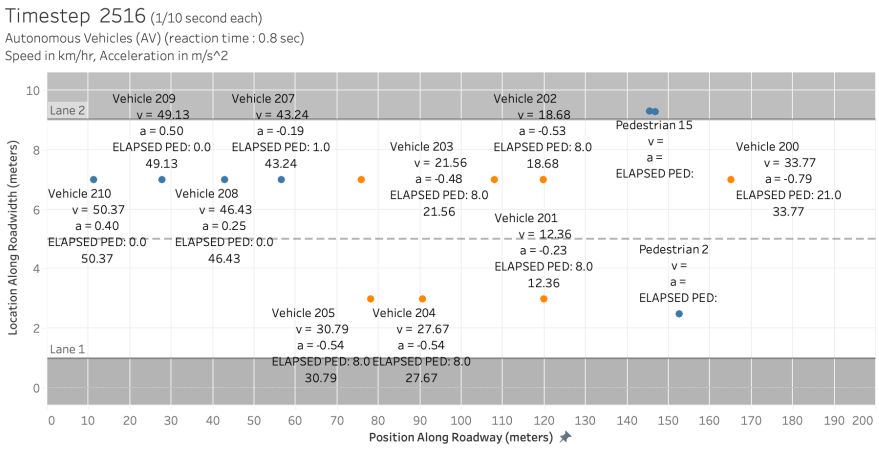

Visualization of the result, segment is cropped from 0 to 200 horizontally, for the timestep of 2516 (252 second)

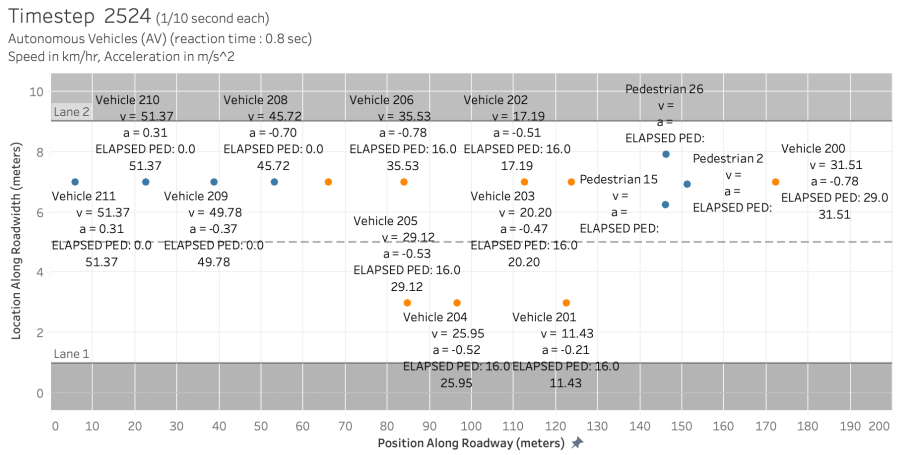

Visualization of the result, segment is cropped from 0 to 200 horizontally, for the timestep of 2524 (252 second)

Figure 3.16 Results of the visualization for pedestrians with ID of 2.

Figure 3.14(a) shows the result of the simulation for pedestrian ID 47. As shown in Figure 3.14(a) the top panel, after timestep 1580 abruptly the sensory input of both lanes ($s_1$and s_2) increased.

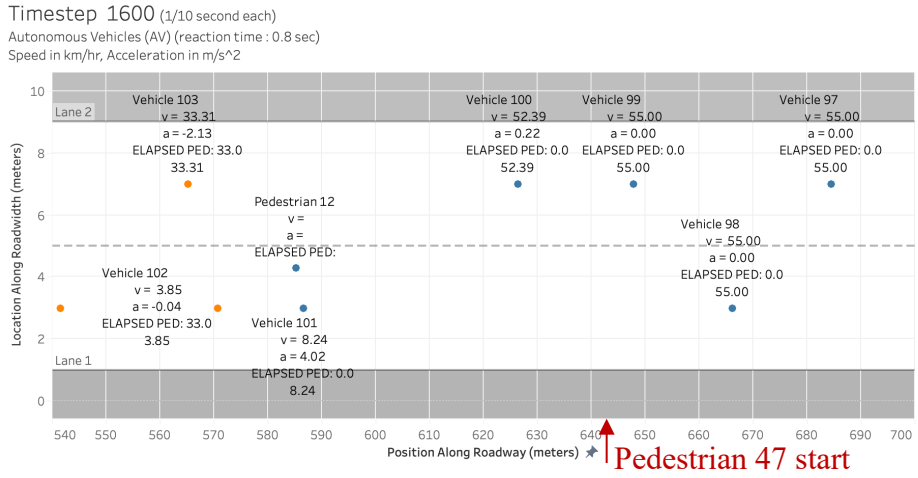

Visualization of the result, segment is cropped from 540 to 700 horizontally, for the timestep of 1600 (160 second)

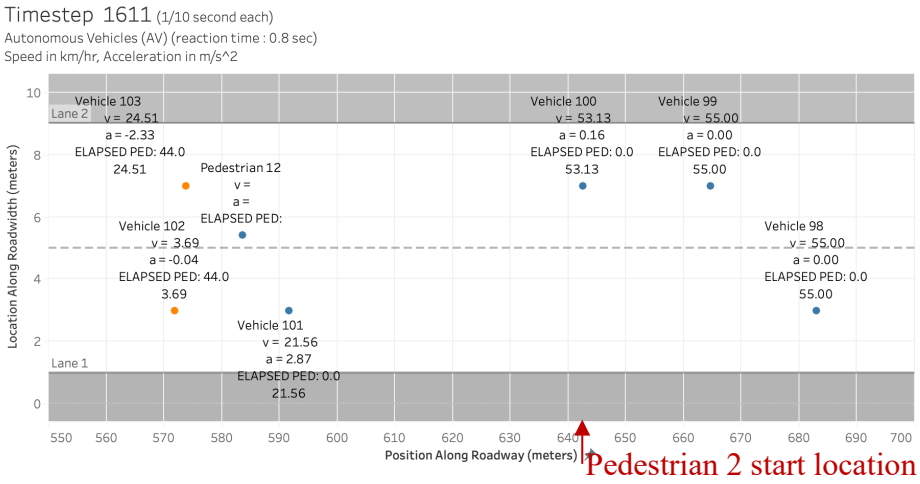

(a) Visualization of the result, segment is cropped from 550 to 700 horizontally, for the timestep of 1611 (161 second)

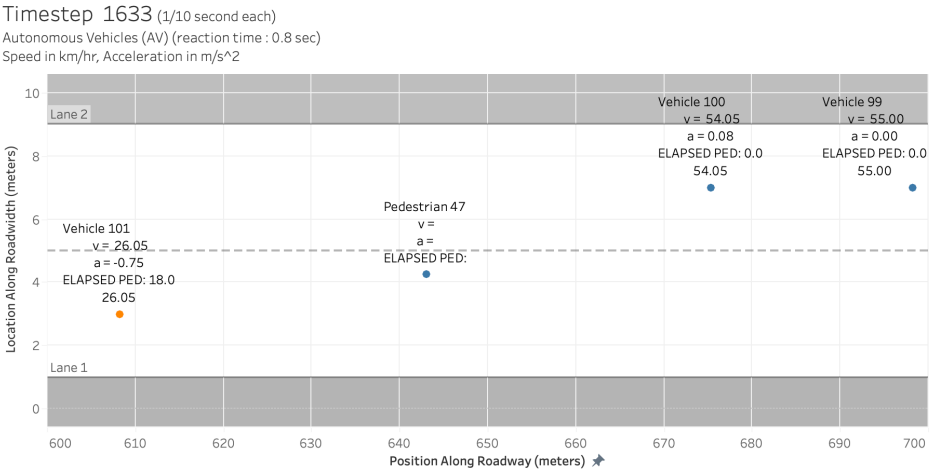

(b) Visualization of the result, segment is cropped from 600 to 700 horizontally, for the timestep of 1633 (163 second)

Figure 3.17 Results of the visualization for pedestrians with ID of 47.

Figure 3.14(a) the middle panel shows that there is indeed a large gap in the second lane, for the first lane there is not such a gap. Hence, we expect a reduction in a vehicle speed in this case in the first lane that made the sensory input for first lane be high enough to cause the pedestrian to cross the street. Figure 3.17 shows the result for the visualization for the pedestrian ID 47. As shown in Figure 3.17(a) there is already a pedestrian that decided to cross the street. According to Figure 3.17(a), pedestrian 12 is already in the middle of the segment, and the vehicles slowed down for this pedestrian. This reduction in speed of the vehicle impacted the sensory input of pedestrian 47. Then, a large gap was available between vehicle ID 100 and 101 as shown in Figure 3.17(b), which was accepted by pedestrian ID 47. Correspondingly pedestrian ID 47 successfully crossed the street as shown in Figure 3.17(c).

3.9 Conclusions

As cities navigate the era of shared spaces and open streets, integrating advanced technologies with human-centered urban design becomes increasingly critical. The rise of connected and automated vehicles promises significant traffic flow and safety improvements. Still, it must be balanced with the growing demand for walkable, sustainable neighborhoods that accommodate pedestrians, cyclists, and micromobility users. Current trends reveal a patchwork of infrastructure investments and measures that often fail to address the needs of all roadway users, particularly the most vulnerable. This highlights the need for comprehensive simulation and modeling approaches to rigorously assess and address the complex interactions between emerging technologies and traditional urban mobility needs. This paper provides a foundation for developing a methodological toolkit for analyzing interactions between AVs, pedestrians, and other roadway users.

Our sensitivity analysis provides insights into how different parameters affect interactions between pedestrians and vehicles. Variations in β_1, which controls the balance that pedestrians place on traffic in different lanes, α, which specifies the depreciation of the accumulated evidence, and σ, which represents increased uncertainty in pedestrian decision-making, all demonstrate the trade-off between pedestrian waiting times, safety, and vehicle flow efficiency. Furthermore, the analysis results suggest that collisions and conflicts in both lanes are roughly identical during the sensitivity analysis. Flow-density and speed-density diagrams indicate how pedestrians' decisions are made when the traffic density is low to medium and how more pedestrians deciding to cross adversely affects the traffic density behind them. In the case study, our model demonstrated the strong performance in depicting real-world phenomena related to gap acceptance by pedestrians. However, our micro-simulator has a few drawbacks. First, the assumption that DDM parameters for all pedestrians are identical is unrealistic because pedestrians may consider their surrounding traffic environment differently. In addition, due to the lack of data, the DDM model parameters and the speed of pedestrians have not been accurately calibrated. To address these limitations, it would be promising to construct a pedestrian crossing simulator and collect data from the participants to calibrate our model.

This research aims to support the creation of multimodal, connected, equitable, and safe urban environments by building a simulation framework for evaluation. By focusing on how different parameters affect travel times, conflicts, and pedestrian behavior, we offer valuable insights that can help city planners and engineers integrate technological advancements with the goals of creating more human-centered and sustainable urban spaces. Future work in this area will focus on incorporating human-driven vehicles and connected vehicles into the simulation, implementing V2V and V2I communication, and studying their impact on safety, capacity, and equity. Additionally, adding more vulnerable agents to the simulation, including scooters and bikes, considering the heterogeneity among users, conducting network-level analysis of the simulation, and exploring other dimensions of urban mobility will be potential future directions. This approach is crucial as cities continue to incorporate emerging technologies while striving to meet the diverse needs of all residents.

4 An Integrated Framework for Multimodal Space Utilization Planning

4.1 Conceptual Framework Development

Urban transportation systems comprise multiple modes and layers, each serving distinct functions while competing for limited space on city streets. These systems can be understood through three categories of models that provide comprehensive understanding of urban mobility dynamics.

Movement & Flow Models describe the physics and behavioral decisions influencing how individuals and goods traverse urban spaces. Movement occurs across various temporal and spatial scales, shaped by choices regarding travel modes, routes, and schedules. Temporal patterns, such as demand forecasting and mode choice, offer insights into transportation preferences over time. Traffic flow and dynamics models capture interactions between vehicles and infrastructure, addressing routing behavior, traffic adaptation, and congestion emergence. These models operate on macroscopic levels analyzing overall traffic organization and shockwave generation, and microscopic levels examining interactions among traveling agents to avoid conflicts.

Matching & Scheduling Models tackle logistical challenges of coordinating transportation resources to meet user demand. Examples include vehicle matching for ride-sharing services, which aim to minimize wait times while optimizing fleet availability. By predicting vehicle availability and expected demand, these models effectively manage dynamic demand in urban environments. Scheduling models address time-sensitive operations, such as last-mile deliveries and public transit schedules, mitigating issues like bus bunching and delays in service.

Design & Control Models address how urban spaces must be designed to accommodate a wide range of transportation modes while ensuring safety and efficiency. Strategic placement and network design involve planning key infrastructure, such as transit stops and bike docks, to ensure equitable access across the city. At the operational level, traffic control models optimize signals, lane assignments, speed limits, and congestion pricing strategies to manage urban traffic flows.

A fundamental question addressed by many models is: "When and where will something be?" Each model provides various levels of confidence in answering this question, but a unified approach is necessary to guide strategies for optimizing coexistence of various transportation modes within urban streetscapes.

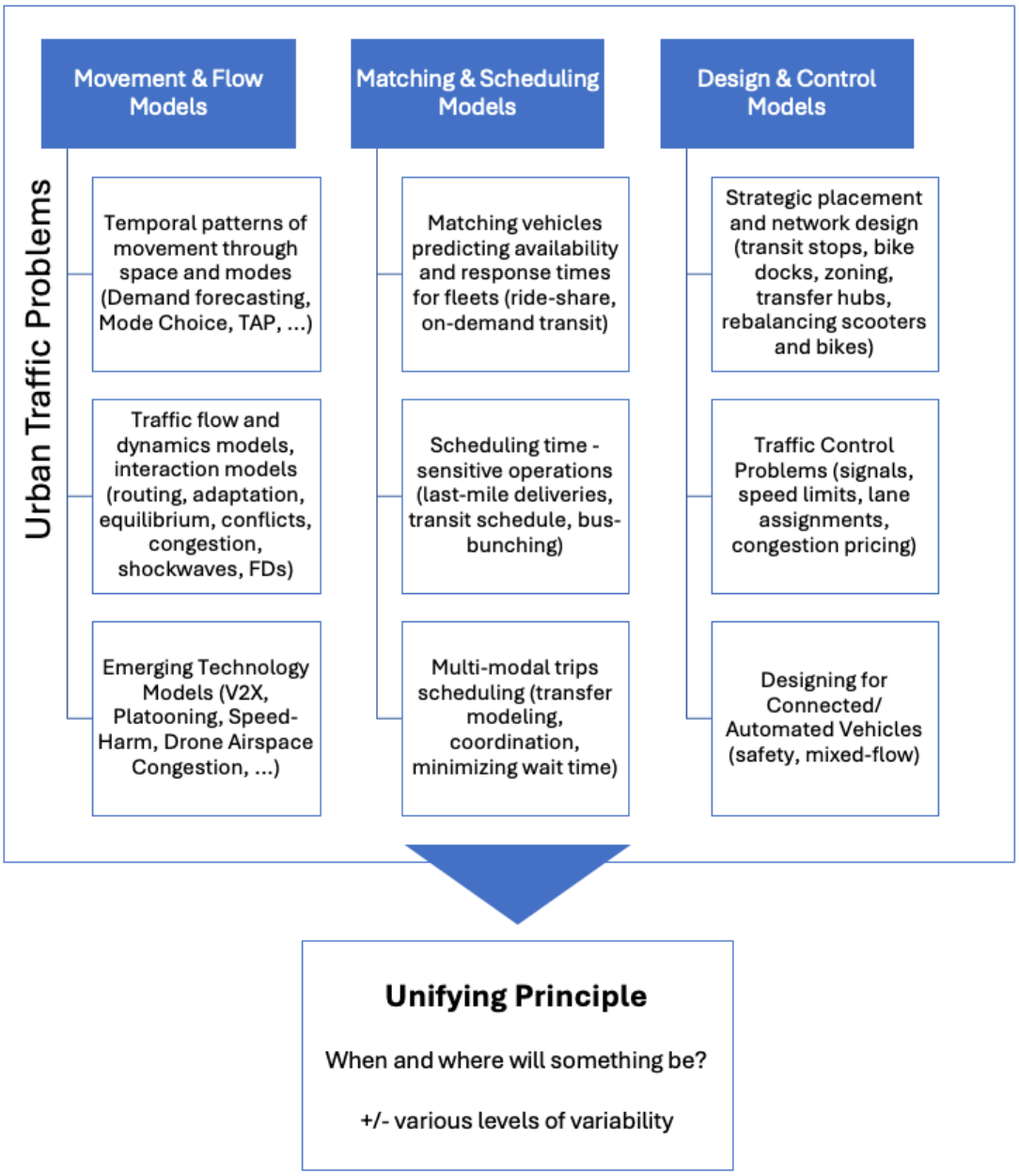

Figure 4.1 Overview of Urban Transportation Models

4.1.1 Spatial Competition Mechanisms

Urban streets accommodate cars, bikes, pedestrians, transit, and delivery services that navigate shared streets, sidewalks, and bike lanes, often overlapping in their use of these spaces. An efficient urban environment requires coordination among these transportation layers to minimize wasted space, enhance flow, and ensure safety. Current ad-hoc practices often fall short, leading to dominance by certain modes or excessive roadway allocations that leave space underutilized.

As various component models converge spatially on urban streets, competition for limited roadway space becomes critical. This spatial competition manifests differently depending on mode type. Event-Based Modes (e.g., delivery trucks, drone landings) require temporary, location-specific space. Flow-Based Modes (e.g., vehicle traffic, pedestrians, cyclists) exhibit continuous movement, creating dynamic yet overlapping demands on space.

Variability in timing and spatial usage complicates coordination of urban transportation modes, influenced by factors such as transit schedule adherence, initial traffic conditions, and peak demand fluctuations. Models with finer detail levels and fixed infrastructure, such as e-scooter rebalancing, tend to have tighter bounds on time and location, allowing more precise predictions of space use. Less detailed models, such as aggregate flow-based approaches, may have broader variability in initial conditions, leading to less predictable outcomes for how flows manifest as vehicles on roadway links.

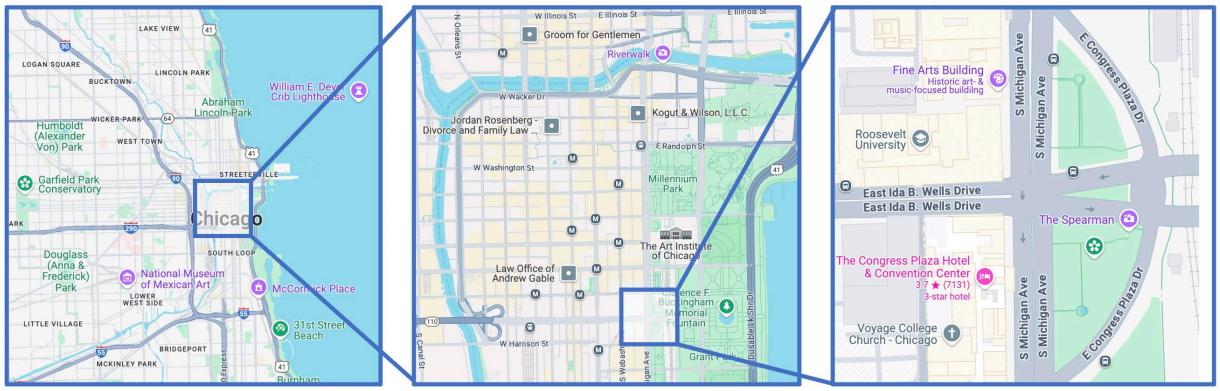

Large-Scale Network Models
- Vehicle Flows
- Public Transit Network Design
- SAV Repositioning
- Vertiport Design

Sub Network / Corridor Models
- Bike lane placement
- Corridor Signal Timing
- Bike / Scooter Dock Placement
- BRT Design

Street-Level Coordination
- Managing Conflicts
- Negotiation between Users
- Curb Space Allocation

Figure 4.2 Hierarchy of Traffic Problem Spatial Resolutions

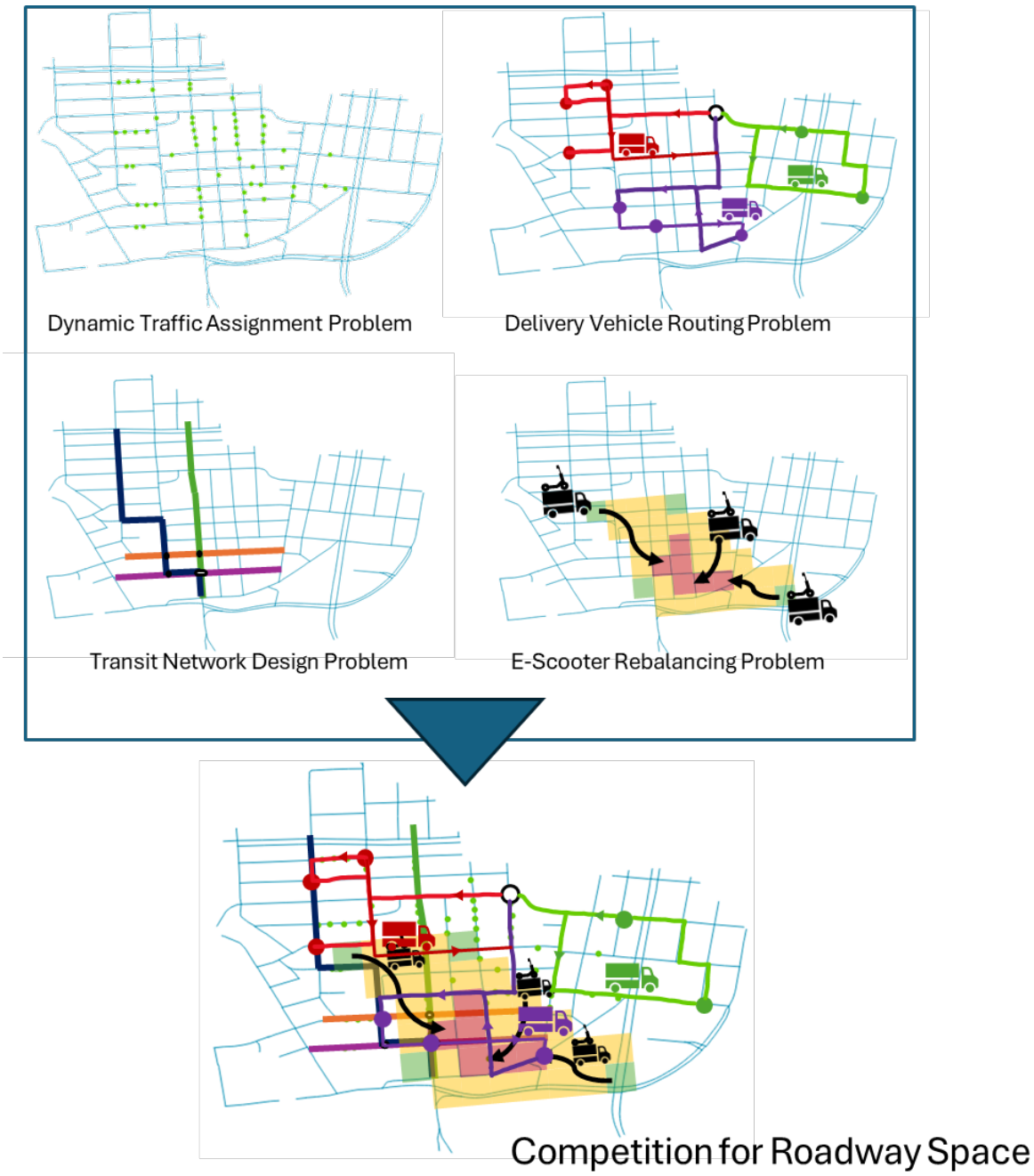

Figure 4.3 Competition Among Component Models for Roadway Space

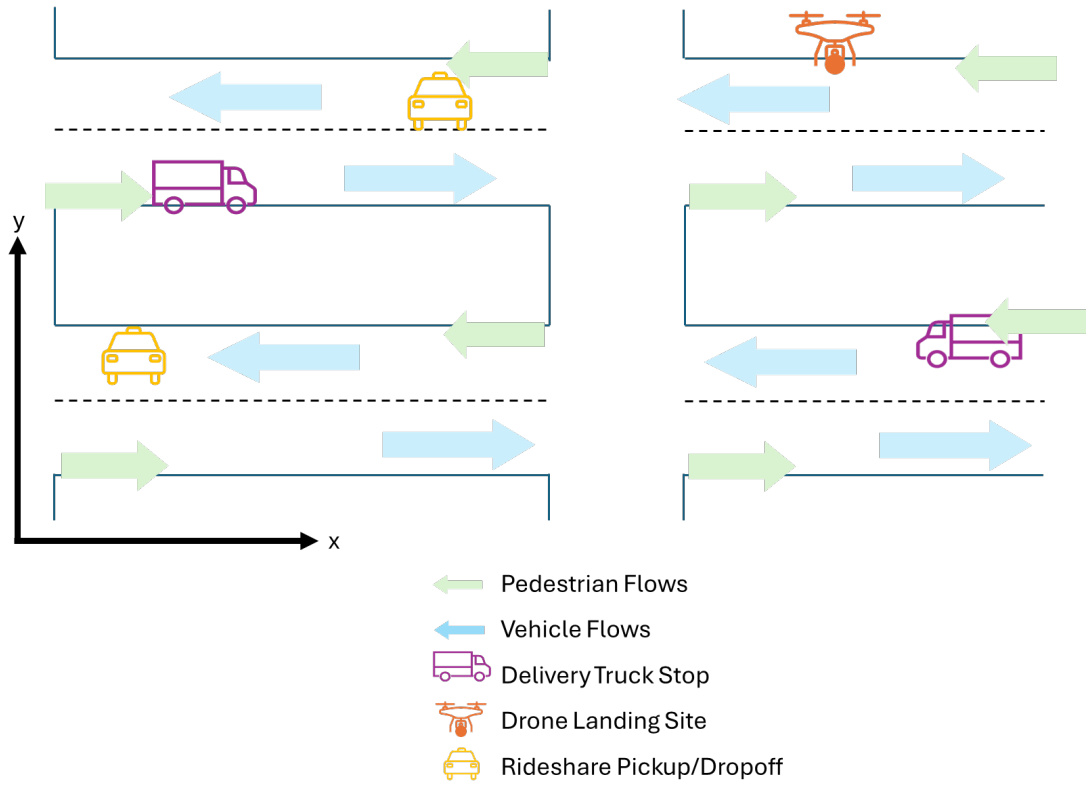

Figure 4.4 Example Spatial Demands in an Urban Block

4.1.2 Uncertainty and Variability Characterization

Inherent uncertainty presents challenges in effectively managing interactions among competing modes. Variations in transit schedules can disrupt expected traffic patterns, while fluctuations in demand during peak periods can intensify competition for limited roadway space. This variability is illustrated through distributions in both x and y locations, as well as in time, representing how factors like schedule adherence and initial traffic flow conditions influence predictability. The distributions show that some modes have tight spatial and temporal bounds while others exhibit significant variability in their actual manifestation on street infrastructure.

Models with different fidelity levels produce varying degrees of prediction uncertainty. High-fidelity event-based models may be necessary to capture dynamic elements like delivery trucks stopping or rideshare drop-offs, while coarser macro models may be sufficient for vehicular flow analysis. This hierarchy of model resolution affects the precision with which space utilization can be predicted and managed.

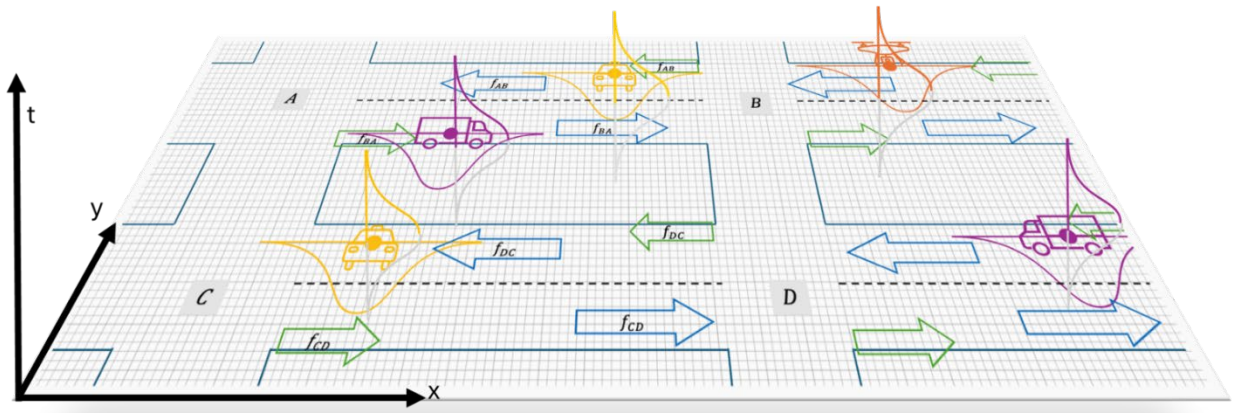

Figure 4.5 Variability Predicting Street Usage showing temporal and spatial uncertainty distributions

4.2 Monte Carlo Simulation Methodology

4.2.1 Grid-Based Space Representation

Given the variability in arrival times and spatial demands among different transportation modes, predicting street usage remains challenging. Each component model contributes to space utilization plans for the street, creating a loose schedule that dictates how various modes are expected to use street space. To address these uncertainties, micro-simulations are proposed to capture intricate interactions between component models within a defined urban area. These simulations incorporate essential infrastructural and control elements to create realistic operational environments. By overlaying a grid onto the urban streetscape, space utilization can be systematically assessed.

A Monte Carlo-style approach models varying conditions and entity placements across this grid. In each simulation, at most one entity, or none, can occupy a given grid point at any time. The combined results provide insights into expected space utilization across modes, assessing space usage and potential conflicts in shared urban streetscapes.

For each Monte Carlo simulation run n, an indicator function $I^{(n)}_{m,x,y,t}$ denotes whether mode m occupies cell (x,y) at time t during simulation run n:

$$I^{(n)}_{m,x,y,t} = 1 \text{ (if mode } m \text{ is in cell } (x,y) \text{ at time } t \text{ in simulation } n\text{); 0 otherwise} \quad \text{(Eq 4.1)}$$

where

$m =$ mode of transport (pedestrian, bike, delivery, rideshare etc.)

$(x, y) =$ grid cell on the urban streetscape

$t =$ simulation time

$n =$ Monte-Carlo simulation iteration

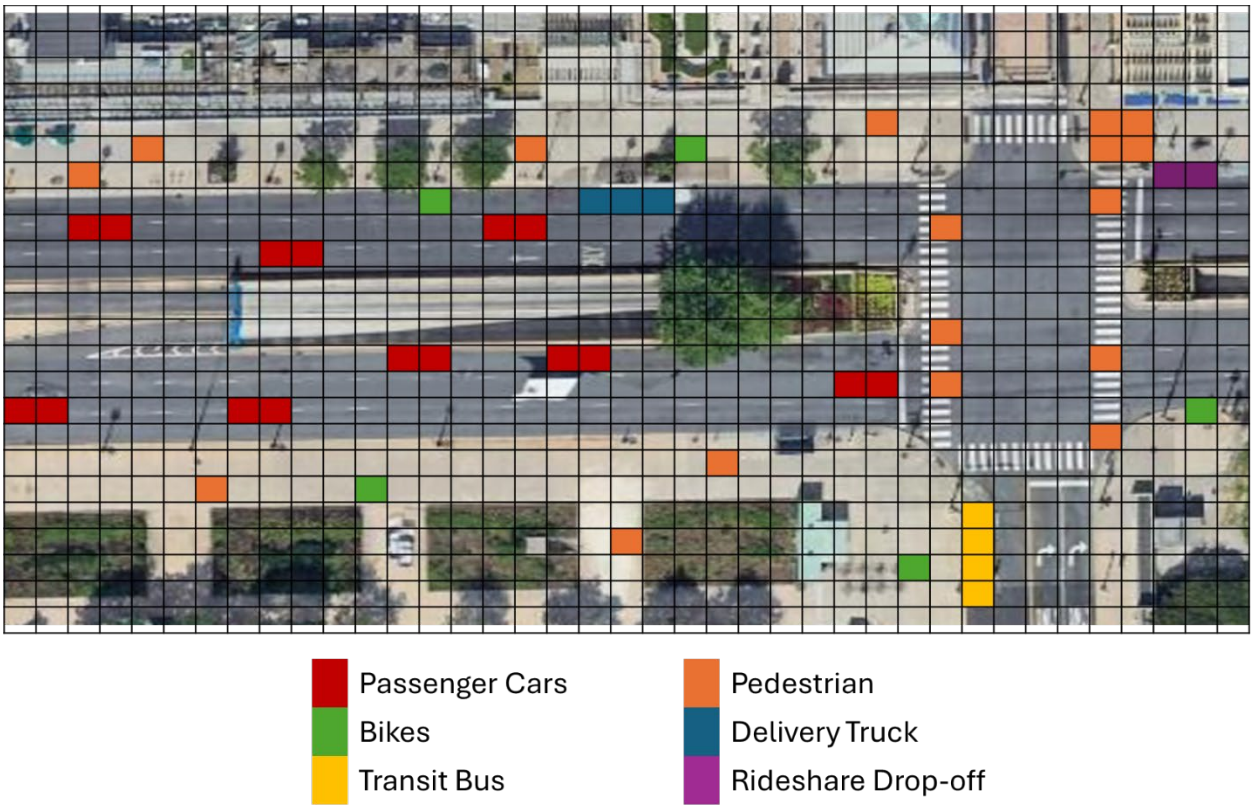

Figure 4.6 Sample Instant in Time of a Single Simulation Run showing grid cells colored by occupying mode

4.2.2 Probabilistic Occupancy Modeling

Across multiple simulations, the probability that mode m occupies cell (x,y) at time t, denoted as P(m,x,y,t), is calculated by averaging the indicator function across all N Monte Carlo simulation runs:

$$P(m,x,y,t) = \frac{1}{N}\sum_{n=1}^{N} I_{m,x,y,t}^{(n)} \quad \text{(Eq 4.2)}$$

where

$P(m,x,y,t) =$ probability that mode m occupies the cell (x,y) at time t

$N =$ total number of Monte Carlo simulation runs

$I_{m,x,y,t}^{(n)} =$ indicator function for mode m in run n

$P(m,x,y,t)$ represents the fraction of simulations in which mode m occupies cell (x,y) at time t. It is empirically derived through repeated simulations that account for randomness and demand variability associated with each mode.

It is possible that no mode occupies cell (x,y) at time t in some Monte Carlo simulations, therefore the total probability across all modes can be less than 1:

$$0 \leq P(total,x,y,t) = \sum_m P(m,x,y,t) \leq 1 \quad \text{(Eq 4.3)}$$

This occurs because in some simulations, the location may not be occupied by any mode at time t.

4.2.3 Monte Carlo Implementation Strategy

The framework implementation follows a systematic process integrating component models through Monte Carlo simulation. Each simulation run samples from the uncertainty distributions of different component models, creating realistic scenarios of space competition and utilization.

The methodology addresses the fundamental challenge of predicting "when and where something will be" by explicitly modeling the uncertainty in these predictions. Rather than assuming deterministic outcomes, the framework acknowledges that transportation systems exhibit inherent variability that must be captured for effective analysis.

Computational efficiency considerations require careful balance between simulation resolution and analytical tractability. The grid-based approach enables systematic analysis while maintaining computational feasibility for practical applications.

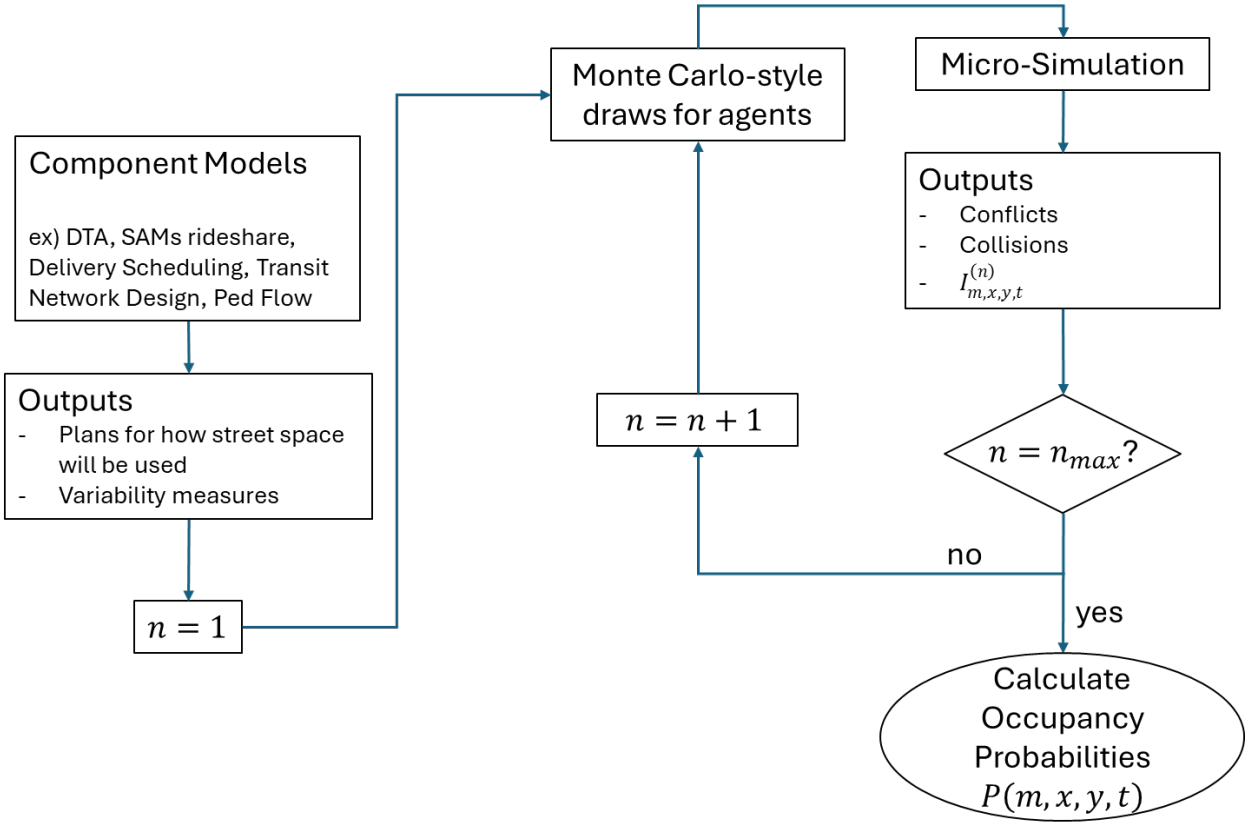

Figure 4.7 Framework Flowchart showing the complete methodology from component models through analysis

4.3 Conflict Identification and Space Utilization Analysis

4.3.1 Activity and Conflict Classification

The framework distinguishes between different types of cells based on their utilization patterns and potential for conflicts. Non-Active Cells have low $P(total, x, y, t)$ values,

indicating locations that are often unoccupied across Monte Carlo simulations. Low values could signal underutilization of space, suggesting cells not in high demand for any mode. This may highlight parts of the street network that are underused relative to their design intent, pointing to opportunities to optimize space allocation.

However, low values could also indicate intentional design features, such as buffer zones between bike lanes and traffic or pedestrian safety islands, which are meant to be less occupied to promote safety and comfort. Low $P(total, x, y, t)$ values in specific periods could merely reflect time-based factors, such as reduced demand during off-peak hours.

Active Cells have higher $P(total, x, y, t)$ values. A threshold value θ_{occ} can distinguish between the two. The condition for an active cell is:

$$P(total, x, y, t) \geq \theta_{occ} \quad \text{(Eq 4.4)}$$

where

θ_{occ} = minimum cell occupancy probability threshold, such as .1

Once a cell (x,y) is deemed active at time t, it can be identified as a conflict zone based on mode occupancy distribution. Non-Conflict Cells occur when a single mode dominates occupancy, as in one mode has occupancy probability $\geqslant \theta_{\text{dom}}$, so this cell is not considered a contested area. Conflict Cells occur when no single mode dominates and each mode's occupancy is more evenly distributed, $\max_m P(m, x, y, t) < \theta_{\text{dom}}$, classifying the cell as a conflict zone due to significant competition between modes.

4.3.2 Spatial Efficiency Metrics

The criteria for conflict in cell (x,y) at time t is:

$$P(total, x, y, t) \geq \theta_{\text{occ}} \quad \text{and} \quad \max_m P(m, x, y, t) < \theta_{\text{dom}} \quad \text{(Eq 4.5)}$$

where

θ_{dom} = mode dominance probability dominance threshold, such as .8

Threshold values may be set as planners see fit, with θ_{occ}used to assess basic activity level in a cell and θ_{dom} for determining when one mode is dominant, minimizing likelihood of spatial conflicts. Depending on safety or design priorities, even cells deemed relatively inactive should be analyzed, especially when pedestrians are present, as this may necessitate larger safety buffers.

The framework enables evaluation of modal space-use efficiency by examining modal-specific probabilities such as P(ped,x,y,t). This assessment determines whether space allocated for specific modes, like pedestrians or bikes, is underutilized. Low pedestrian probabilities in designated pedestrian spaces may suggest suboptimal space use, indicating opportunities for alternative utilization.

4.3.3 Design Optimization Framework

The framework can integrate known stationary elements, such as trees or permanent street furniture, modeled with probability of 1 at fixed locations. This enables comprehensive space utilization analysis that accounts for both dynamic transportation demands and fixed infrastructure elements.

Areas frequently occupied by unintended modes—such as delivery trucks regularly utilizing pedestrian areas—suggest need for layout reconsideration to accommodate mixed use more effectively. By adjusting street layouts, sidewalk widths, or bike lane placements based on actual usage patterns, planners can dynamically reconfigure spaces as needs change over time.

The temporal dimension supports dynamic allocation approaches, where single spaces may host different modes at different times, fostering more efficient, adaptable use of urban space.

4.4 Application Framework and Design Implications

The proposed framework offers metrics for conflict prediction and spatial efficiency assessment to aid in urban design and planning. Simulation results allow prediction of areas with potential conflict through likelihood of different modes overlapping in the same space at the same time. Identifying such "hotspot" areas can help planners target high-conflict zones for design improvements, such as adding pedestrian crosswalks or bike lane separation, potentially improving user safety.

Conflict probabilities serve as effective measures for assessing efficacy of different design strategies in reducing inter-modal conflict and thereby enhancing urban safety and usability. The framework enables systematic evaluation of design alternatives based on quantitative conflict prediction rather than qualitative assessment alone.

By identifying critical insights, like conflict hotspots, underused spaces, and mode split probabilities, the framework fosters a feedback loop that guides iterative urban design adjustments. High pedestrian usage may prompt improvements like wider sidewalks or more frequent crosswalks. Conversely, if spaces designated for one mode are regularly occupied by another, it may indicate need for reallocating street space or adjusting signage.

Through this iterative design cycle, planners can continuously adapt street layouts based on efficiency and conflict data, leading to gradual and evidence-based improvements in urban design. The framework enables data-driven insights to guide spatial redesign based on actual usage patterns rather than design assumptions.

4.5 Future Considerations

The framework raises questions about design priorities, including the order in which modes are considered and whether safety concerns should prioritize pedestrians and cyclists. Additionally, selecting and integrating appropriate models can be complex, especially given different temporal and spatial resolutions required.

High-resolution event-based models may be necessary to capture dynamic elements like delivery trucks stopping or rideshare drop-offs impacting sidewalks, while coarser macro models may be sufficient for vehicular flow. A larger challenge lies in balancing space allocation and demand, as space allocation impacts demand, which in turn informs future space requirements—a dynamic interaction that potentially evolves toward equilibrium over time.

This feedback loop could reveal daily or seasonal adaptation patterns, helping planners refine designs that meet changing demands. With expanded feedback systems, the model could track day-to-day dynamics and long-term adaptations, providing robust foundation for responsive, sustainable urban planning.

Findings

This research demonstrates that Connected and Autonomous Vehicle (CAV) deployments are compatible with Complete Streets objectives through systematic infrastructure design, interaction analysis, and space allocation strategies.

Infrastructure Separation Enhances All Mode Performance: Strategic modal separation creates substantial efficiency gains across all transportation modes. Maximum network flow increased from 0.09 veh/min/m² in shared configurations to 0.18 veh/min/m² with complete separation which is a near-doubling of throughput. Pedestrian separation through sidewalks generates the most dramatic improvements, while micromobility lane additions provide meaningful gains for all modes. The area-based Network Fundamental Diagram methodology effectively captures multimodal performance relationships that traditional measures cannot detect. Micromobility modes achieve comparable flow rates to automobiles while occupying significantly less network area.

Network Attributes Enable Predictive Modeling: Physical attribute-defined NFD functional forms establish quantitative relationships between infrastructure and performance. Three key variables: shared area, modal-exclusive area, and interaction plane, predict fundamental diagram parameters with high accuracy ($R^2 > 0.90$). Shared area consistently reduces maximum flow, while separated infrastructure improves capacity, particularly for micromobility.

Pedestrian-CAV Interactions Require Parameter Balance: Extended Drift Diffusion Model analysis reveals optimal parameter ranges for minimizing conflicts while maintaining crossing opportunities. Equal weighting of sensory inputs from both lanes ($\beta_1 = 0.5$) produces the lowest collision rates. Values of damping parameter α above 1.6 substantially reduce crossing attempts, while pedestrian decision uncertainty critically influences system safety.

Probabilistic Framework Identifies Conflict Hotspots: The integrated space utilization framework uses Monte Carlo simulation to identify spatial and temporal conflicts. Grid-based representation captures competing demands while modeling inherent system uncertainty. Occupancy thresholds and dominance parameters provide quantitative measures for distinguishing contested urban spaces.

Synergistic Solutions Achieve Dual Objectives: CAV efficiency and Complete Streets objectives create synergistic rather than competing outcomes when systematically approached. The methodological toolkit enables quantitative evaluation based on comprehensive performance metrics spanning safety, efficiency, and equity. Evidence challenges assumptions about trade-offs between technological efficiency and human-centered design.

Recommendations

The research demonstrates that effective management of interactions between transportation modes is essential for optimizing urban space utilization and achieving both CAV efficiency and Complete Streets objectives. Cities should prioritize strategic modal separation as the primary mechanism for reducing conflicts and enhancing network performance. The evidence shows that infrastructure separation, beginning with pedestrian facilities and progressing to dedicated micromobility lanes, creates synergistic benefits that improve safety and throughput for all users.

Transportation agencies should adopt the integrated analytical framework developed in this research to systematically evaluate street design alternatives based on quantitative performance metrics. The combination of network-level flow analysis, microscopic interaction modeling, and probabilistic space utilization assessment provides the comprehensive evaluation capability needed to balance competing demands for limited urban street space. This evidence-based approach enables planners to move beyond ad-hoc design decisions toward systematic optimization of multimodal infrastructure.

Future CAV deployment should be coordinated with Complete Streets infrastructure development to ensure compatibility and maximize benefits. CAV systems must be designed with sophisticated pedestrian interaction models that account for decision-making uncertainty while maintaining reasonable crossing opportunities. The framework developed here provides the foundation for this integration, enabling cities to realize the full potential of both autonomous vehicle technology and human-centered urban design through strategic interaction management and evidence-based space allocation.

Outputs

Publications and Presentations

- Khakpour, A., Hegde, S. J., Li, N., & Mahmassani, H. S. (2025). *A drift diffusion model of pedestrian-crossing interactions with AVs on two-lane complete streets.* Presented at the TRB Annual Meeting 2025.
- Raymer M. *Urban growth, congestion, and equity: Leveraging multi-mobility and active infrastructure investments for livable cities.* [Order No. 32165003]. Northwestern University; 2025.

Methodologies and Technologies Developed

- Area-based Network Fundamental Diagram methodology for multimodal traffic flow analysis
- Physical attribute-defined NFD functional form for predicting network performance based on infrastructure characteristics
- Extended Drift Diffusion Model for pedestrian crossing decisions in two-lane CAV environments
- Custom microsimulator modeling AV, HV, and pedestrian interactions in urban spaces
- Conflict detection algorithm using generalized time-to-collision metrics
- Monte Carlo simulation framework for multimodal space utilization analysis using MESA platform
- Agent-based simulation with continuous space representation incorporating AREM model for autonomous vehicles
- Optimization framework for bike lane allocation based on macroscopic flow optimization
- Real-time conflict detection system for identifying safety issues between CAVs and vulnerable users

Software and Simulation Tools

- Custom microsimulator with AV response modeling and pedestrian decision-making capabilities
- Repeatable process for building and modifying real-world transportation networks for multimodal performance testing
- Scenario generation tools for systematically varying infrastructure attributes
- Comprehensive behavioral model capturing non-traditional movement patterns between diverse agents

Outcomes

Increased Understanding and Awareness: The research significantly expanded understanding of multimodal traffic interactions through development of area-based flow and density measures that explicitly capture trade-offs in multimodal streets. The microsimulator enhanced comprehension of AV-pedestrian interaction dynamics, advancing knowledge on AV safety responses and informing safer design practices for mixed urban traffic environments.

Body of Knowledge Expansion: The work contributed substantial advances to transportation science by demonstrating how Complete Streets infrastructure configurations affect network performance across multiple modes simultaneously. The development of physics-based movement and interaction models enables evidence-based evaluation of urban street design effectiveness considering diverse roadway demands.

Improved Processes and Technologies: The research produced data-driven processes for network design that systematically consider trade-offs between transportation modes. The framework provides cities with quantitative tools for evaluating existing street designs, identifying improvement opportunities, and justifying street redesign projects through before-and-after analysis capabilities.

Enhanced Decision Support: The optimization framework serves as a practical decision support tool for planners and policymakers to strategically allocate bike lanes and other infrastructure. The methodology enables transportation agencies to develop CAV-compatible street design guidelines and evidence-based recommendations for urban CAV programming standards.

Impacts

Transportation System Safety And Reliability: The program contributed to safer and more reliable transportation by enhancing AV response modeling for complex pedestrian interactions, supporting AV design improvements that reduce collision risks in urban settings. The conflict detection models enable identification and characterization of conflicts throughout simulations, supporting alternative road designs that reduce conflicts and promote greater equity for vulnerable users.

Infrastructure Design And Planning: The research provides cities with tools to optimize street space allocation based on observed usage patterns and supports planners in creating more equitable distribution of street space among user groups. The evidence-based approach helps justify redesign initiatives that balance vehicle throughput with multimodal accessibility, incorporating safety as a core objective of complete street design.

Policy And Decision-Making: The work enables cities to quantitatively assess how CAV operations might impact Complete Streets objectives, supporting proactive planning for emerging transportation technologies. The framework helps transportation departments make data-driven decisions about street design effectiveness and provides metrics for evaluating both efficiency and accessibility outcomes.

Challenges and Lessons Learned

This research encountered significant computational, data, and methodological challenges that provide valuable insights for future work in multimodal transportation analysis and CAV-Complete Streets integration.

Computational and Performance Challenges: The most substantial challenge involved computational intensity of simulating multimodal networks with diverse behavioral models simultaneously. The microscopic pedestrian-CAV interaction simulator initially exhibited prohibitively long runtimes that required code optimization focused on spatial indexing algorithms. Network-level simulations for NFD functional form development faced similar demands, requiring careful balance between simulation resolution and analytical tractability.

Data Limitations and Calibration Issues: A critical limitation emerged from lack of empirical data for model calibration, particularly for pedestrian-CAV interactions in mixed-traffic environments. The Drift Diffusion Model parameters were initially formulated without proper calibration due to insufficient real-world observations. Additionally, realistic bicycle demand patterns required assumptions due to absence of comprehensive bike demand data, with vehicle trips duplicated and assigned to bicycle modes as a workable but potentially inaccurate solution.

Model Integration Complexity: Integrating models operating at different temporal and spatial resolutions proved more complex than anticipated. The challenge of ensuring compatible assumptions and parameter ranges across network-level NFD analysis, microscopic interaction modeling, and probabilistic space utilization components required iterative refinement. The heterogeneity assumption for pedestrian behavior, treating all pedestrians with identical DDM parameters, oversimplifies diverse real-world decision-making patterns.

Key Lessons Learned: Several important lessons emerged: computational performance considerations must be integrated into research design from the outset rather than as post-hoc solutions; empirical data for model validation is critical and future research should prioritize data collection or partnerships with CAV pilot programs; model integration across scales requires systematic attention to assumption consistency; and simulation-based analysis provides valuable policy insights when empirical data is limited, but results must be interpreted with appropriate caution regarding real-world applicability.

References

1. Appleyard, D. Livable Streets: Protected Neighborhoods? *The ANNALS of the American Academy of Political and Social Science*, Vol. 451, No. 1, 1980, pp. 106–117. https://doi.org/10.1177/000271628045100111.
2. LaHood, R. Recommended Actions: USDOT Policy Statement on Bicycle and Pedestrian Accommodation Regulations and Recommendations | FHWA. https://highways.dot.gov/safety/pedestrian-bicyclist/safety-tools/recommended-actions-usdot-policy-statement-bicycle-and. Accessed Jul. 29, 2024.
3. Bas, J., M. B. Al-Khasawneh, S. Erdoğan, and C. Cirillo. How the Design of Complete Streets Affects Mode Choice: Understanding the Behavioral Responses to the Level of Traffic Stress. *Transportation Research Part A: Policy and Practice*, Vol. 173, 2023, p. 103698. https://doi.org/10.1016/j.tra.2023.103698.
4. Hass-Klau, C. A Review of the Evidence from Germany and the UK. *Transport Policy*, Vol. 1, No. 1, 1993, pp. 21–31. https://doi.org/10.1016/0967-070X(93)90004-7.
5. Perk, V., M. Catalá, M. Mantius, K. Corcoran, and University of South Florida. Center for Urban Transportation Research. *Capturing the Benefits of Complete Streets.* Publication BDV26-977–04. 2015.
6. Vandegrift, D., and N. Zanoni. An Economic Analysis of Complete Streets Policies. *Landscape and Urban Planning*, Vol. 171, 2018, pp. 88–97. https://doi.org/10.1016/j.landurbplan.2017.11.004.
7. Shapard, J., and M. Cole. Do Complete Streets Cost More than Incomplete Streets? *Transportation Research Record*, Vol. 2393, No. 1, 2013, pp. 134–138. https://doi.org/10.3141/2393-15.
8. Hui, N., S. Saxe, M. Roorda, P. Hess, and E. J. Miller. Measuring the Completeness of Complete Streets. *Transport Reviews*, Vol. 38, No. 1, 2018, pp. 73–95. https://doi.org/10.1080/01441647.2017.1299815.
9. Gregg, K., and P. Hess. Complete Streets at the Municipal Level: A Review of American Municipal Complete Street Policy. *International Journal of Sustainable Transportation*, Vol. 13, No. 6, 2019, pp. 407–418. https://doi.org/10.1080/15568318.2018.1476995.
10. Mahmassani, H., J. C. Williams, and R. Herman. Performance of Urban Traffic Networks. *Proceedings of the 10th International Symposium on Transportation and Traffic Theory*, 1987, pp. 1–20.
11. Daganzo, C. F., and N. Geroliminis. An Analytical Approximation for the Macroscopic Fundamental Diagram of Urban Traffic. *Transportation Research Part B: Methodological*, Vol. 42, No. 9, 2008, pp. 771–781. https://doi.org/10.1016/j.trb.2008.06.008.
12. Johari, M., M. Keyvan-Ekbatani, L. Leclercq, D. Ngoduy, and H. S. Mahmassani. Macroscopic Network-Level Traffic Models: Bridging Fifty Years of Development toward the next Era. *Transportation Research Part C: Emerging Technologies*, Vol. 131, 2021, p. 103334. https://doi.org/10.1016/j.trc.2021.103334.
13. Gould, G., and A. Karner. Modeling Bicycle Facility Operation: Cellular Automaton Approach. *Transportation Research Record*, Vol. 2140, No. 1, 2009, pp. 157–164. https://doi.org/10.3141/2140-17.
14. Zhao, Y., and H. M. Zhang. A Unified Follow-the-Leader Model for Vehicle, Bicycle and Pedestrian Traffic. *Transportation Research Part B: Methodological*, Vol. 105, 2017, pp. 315–327. https://doi.org/10.1016/j.trb.2017.09.004.

15. Zhang, J., W. Mehner, S. Holl, M. Boltes, E. Andresen, A. Schadschneider, and A. Seyfried. Universal Flow-Density Relation of Single-File Bicycle, Pedestrian and Car Motion. *Physics Letters A*, Vol. 378, No. 44, 2014, pp. 3274–3277. https://doi.org/10.1016/j.physleta.2014.09.039.
16. Guo, N., R. Jiang, S. Wong, Q.-Y. Hao, S.-Q. Xue, and M.-B. Hu. Bicycle Flow Dynamics on Wide Roads: Experiments and Simulation. *Transportation Research Part C: Emerging Technologies*, Vol. 125, 2021, p. 103012. https://doi.org/10.1016/j.trc.2021.103012.
17. Wierbos, M. J., V. L. Knoop, F. S. Hänseler, and S. P. Hoogendoorn. A Macroscopic Flow Model for Mixed Bicycle–Car Traffic. *Transportmetrica A: Transport Science*, Vol. 17, No. 3, 2021, pp. 340–355. https://doi.org/10.1080/23249935.2019.1708512.
18. Huang, Y., D. Sun, A. Li, and K. W. Axhausen. Impact of Bicycle Traffic on the Macroscopic Fundamental Diagram: Some Empirical Findings in Shanghai. *Transportmetrica A: Transport Science*, Vol. 17, No. 4, 2021, pp. 1122–1149. https://doi.org/10.1080/23249935.2020.1832157.
19. Schön, P., Heinen ,Eva, and B. and Manum. A Scoping Review on Cycling Network Connectivity and Its Effects on Cycling. *Transport Reviews*, Vol. 44, No. 4, 2024, pp. 912–936. https://doi.org/10.1080/01441647.2024.2337880.
20. Xu, S. J., and J. Y. J. and Chow. A Longitudinal Study of Bike Infrastructure Impact on Bikesharing System Performance in New York City. *International Journal of Sustainable Transportation*, Vol. 14, No. 11, 2020, pp. 886–902. https://doi.org/10.1080/15568318.2019.1645921.
21. Liu, B., D. Bade, and J. Y. J. Chow. Bike Count Forecast Model with Multimodal Network Connectivity Measures. *Transportation Research Record*, Vol. 2675, No. 7, 2021, pp. 320–334. https://doi.org/10.1177/03611981211021849.
22. Griswold, J. B., M. Yu, V. Filingeri, O. Grembek, and J. L. Walker. A Behavioral Modeling Approach to Bicycle Level of Service. *Transportation Research Part A: Policy and Practice*, Vol. 116, 2018, pp. 166–177. https://doi.org/10.1016/j.tra.2018.06.006.
23. Aziz, H. M. A., N. N. Nagle, A. M. Morton, M. R. Hilliard, D. A. White, and R. N. Stewart. Exploring the Impact of Walk–Bike Infrastructure, Safety Perception, and Built-Environment on Active Transportation Mode Choice: A Random Parameter Model Using New York City Commuter Data. *Transportation*, Vol. 45, No. 5, 2018, pp. 1207–1229. https://doi.org/10.1007/s11116-017-9760-8.
24. Schoner, J. E., and D. M. Levinson. The Missing Link: Bicycle Infrastructure Networks and Ridership in 74 US Cities. *Transportation*, Vol. 41, No. 6, 2014, pp. 1187–1204. https://doi.org/10.1007/s11116-014-9538-1.
25. Smith, H. L., and A. Haghani. A Mathematical Optimization Model for a Bicycle Network Design Considering Bicycle Level of Service. Presented at the Transportation Research Board 91st Annual MeetingTransportation Research Board, 2012.
26. Duthie, J., and A. Unnikrishnan. Optimization Framework for Bicycle Network Design. *Journal of Transportation Engineering*, Vol. 140, No. 7, 2014, p. 04014028. https://doi.org/10.1061/(ASCE)TE.1943-5436.0000690.
27. Mesbah, M., R. Thompson, and S. Moridpour. Bilevel Optimization Approach to Design of Network of Bike Lanes. *Transportation Research Record*, Vol. 2284, No. 1, 2012, pp. 21–28. https://doi.org/10.3141/2284-03.

28. Correa, J., A. Mauttone, and F. Robledo. Maximizing Modal Shift in Bicycle Network Design. *Procedia Computer Science*, Vol. 220, 2023, pp. 226–234. https://doi.org/10.1016/j.procs.2023.03.031.
29. Mauttone, A., G. Mercadante, M. Rabaza, and F. Toledo. Bicycle Network Design: Model and Solution Algorithm. *Transportation Research Procedia*, Vol. 27, 2017, pp. 969–976. https://doi.org/10.1016/j.trpro.2017.12.119.
30. Akbarzadeh, M., S. S. Mohri, and E. Yazdian. Designing Bike Networks Using the Concept of Network Clusters. *Applied Network Science*, Vol. 3, No. 1, 2018, p. 12. https://doi.org/10.1007/s41109-018-0069-0.
31. Lim, J., K. Dalmeijer, S. Guhathakurta, and P. Van Hentenryck. The Bicycle Network Improvement Problem. *Journal of Transportation Engineering, Part A: Systems*, Vol. 148, No. 11, 2022, p. 04022095. https://doi.org/10.1061/JTEPBS.0000742.
32. Wiedemann, N., C. Nöbel, L. Ballo, H. Martin, and M. Raubal. Bike Network Planning in Limited Urban Space. *Transportation Research Part B: Methodological*, Vol. 192, 2025, p. 103135. https://doi.org/10.1016/j.trb.2024.103135.
33. Ballo, L., M. Raubal, and K. W. Axhausen. Designing an E-Bike City: An Automated Process for Network-Wide Multimodal Road Space Reallocation. *Journal of Cycling and Micromobility Research*, Vol. 2, 2024, p. 100048. https://doi.org/10.1016/j.jcmr.2024.100048.
34. Liu, H., W. Y. Szeto, and J. Long. Bike Network Design Problem with a Path-Size Logit-Based Equilibrium Constraint: Formulation, Global Optimization, and Matheuristic. *Transportation Research Part E: Logistics and Transportation Review*, Vol. 127, 2019, pp. 284–307. https://doi.org/10.1016/j.tre.2019.05.010.
35. Guerreiro, T. de C. M., Kirner Providelo ,Janice, Pitombo ,Cira Souza, Antonio Rodrigues Ramos ,Rui, and A. N. and Rodrigues da Silva. Data-Mining, GIS and Multicriteria Analysis in a Comprehensive Method for Bicycle Network Planning and Design. *International Journal of Sustainable Transportation*, Vol. 12, No. 3, 2018, pp. 179–191. https://doi.org/10.1080/15568318.2017.1342156.
36. Natera Orozco, L. G., F. Battiston, G. Iñiguez, and M. Szell. Data-Driven Strategies for Optimal Bicycle Network Growth. *Royal Society Open Science*, Vol. 7, No. 12, 2020, p. 201130. https://doi.org/10.1098/rsos.201130.
37. Olmos, L. E., M. S. Tadeo, D. Vlachogiannis, F. Alhasoun, X. Espinet Alegre, C. Ochoa, F. Targa, and M. C. González. A Data Science Framework for Planning the Growth of Bicycle Infrastructures. *Transportation Research Part C: Emerging Technologies*, Vol. 115, 2020, p. 102640. https://doi.org/10.1016/j.trc.2020.102640.
38. Castiglione, M., R. D. Vincentis, M. Nigro, and V. Rega. Bike Network Design: An Approach Based on Micro-Mobility Geo-Referenced Data. *Transportation Research Procedia*, Vol. 62, 2022, pp. 51–58. https://doi.org/10.1016/j.trpro.2022.02.007.
39. Ospina, J. P., J. C. Duque, V. Botero-Fernández, and A. Montoya. The Maximal Covering Bicycle Network Design Problem. *Transportation Research Part A: Policy and Practice*, Vol. 159, 2022, pp. 222–236. https://doi.org/10.1016/j.tra.2022.02.004.
40. Hwang, U., I. Kim, S. Guhathakurta, and P. Van Hentenryck. Comparing Different Methods for Connecting Bike Lanes to Generate a Complete Bike Network and Identify Potential Complete Streets in Atlanta. *Journal of Cycling and Micromobility Research*, Vol. 2, 2024, p. 100015. https://doi.org/10.1016/j.jcmr.2024.100015.

41. Tian, K., G. Markkula, C. Wei, Y. M. Lee, R. Madigan, N. Merat, and R. Romano. Explaining Unsafe Pedestrian Road Crossing Behaviours Using a Psychophysics-Based Gap Acceptance Model. *Safety science*, Vol. 154, 2022, p. 105837.
42. Lin, Q., G. Li, Y. Lyu, H. Xue, and J. Ou. Pedestrian Crossing Decision-Making Model at Uncontrolled Mid-Block Locations Based on Pedestrian Simulator. 2023.
43. Singh, A., and U. Suddamalla. Multi-Input Fusion for Practical Pedestrian Intention Prediction. 2021.
44. Schumann, J. F., A. R. Srinivasan, J. Kober, G. Markkula, and A. Zgonnikov. Using Models Based on Cognitive Theory to Predict Human Behavior in Traffic: A Case Study. Presented at the 2023 IEEE 26th International Conference on Intelligent Transportation Systems (ITSC), 2023.
45. Fudenberg, D., W. Newey, P. Strack, and T. Strzalecki. Testing the Drift-Diffusion Model. *Proceedings of the National Academy of Sciences*, Vol. 117, No. 52, 2020, pp. 33141–33148. https://doi.org/10.1073/pnas.2011446117.
46. Giles, O., G. Markkula, J. Pekkanen, N. Yokota, N. Matsunaga, N. Merat, and T. Daimon. At the Zebra Crossing: Modelling Complex Decision Processes with Variable-Drift Diffusion Models. https://osf.io/cgj7r. Accessed Aug. 1, 2024.
47. Mohammad, S. H., H. Farah, and A. Zgonnikov. Modeling Gap Acceptance in Overtaking: A Cognitive Process Approach. 2023.
48. Zgonnikov, A., D. Abbink, and G. Markkula. Should I Stay or Should I Go? Cognitive Modeling of Left-Turn Gap Acceptance Decisions in Human Drivers. *Human Factors: The Journal of the Human Factors and Ergonomics Society*, Vol. 66, No. 5, 2024, pp. 1399–1413. https://doi.org/10.1177/00187208221144561.
49. Pekkanen, J., O. T. Giles, Y. M. Lee, R. Madigan, T. Daimon, N. Merat, and G. Markkula. Variable-Drift Diffusion Models of Pedestrian Road-Crossing Decisions. *Computational Brain & Behavior*, Vol. 5, No. 1, 2022, pp. 60–80. https://doi.org/10.1007/s42113-021-00116-z.
50. Jain, A., A. Gupta, and R. Rastogi. Pedestrian Crossing Behaviour Analysis at Intersections. *International Journal for Traffic and Transport Engineering*, Vol. 4, No. 1, 2014, pp. 103–116.
51. Tolford, T. M. Complete Streets Policy in Louisiana: Insights from a Decade of State DOT Implementation. *Case studies on transport policy*, Vol. 12, 2023, p. 101012.
52. Mahmassani, H. S. 50th Anniversary Invited Article—Autonomous Vehicles and Connected Vehicle Systems: Flow and Operations Considerations. *Transportation Science*, Vol. 50, No. 4, 2016, pp. 1140–1162. https://doi.org/10.1287/trsc.2016.0712.
53. Theisen, M., C. Schießl, W. Einhäuser, and G. Markkula. Pedestrians' Road-Crossing Decisions: Comparing Different Drift-Diffusion Models. *International Journal of Human-Computer Studies*, Vol. 183, 2024, p. 103200.
54. Brackstone, M., and M. McDonald. Car-Following: A Historical Review. *Transportation Research Part F: Traffic Psychology and Behaviour*, Vol. 2, No. 4, 1999, pp. 181–196.
55. Ma, C., and D. Li. A Review of Vehicle Lane Change Research. *Physica A: Statistical Mechanics and its Applications*, 2023, p. 129060.
56. Zheng, Z. Recent Developments and Research Needs in Modeling Lane Changing. *Transportation research part B: methodological*, Vol. 60, 2014, pp. 16–32.
57. Ammourah, R., and A. Talebpour. Deep Reinforcement Learning Approach for Automated Vehicle Mandatory Lane Changing. *Transportation Research Record: Journal of the*

Transportation Research Board, Vol. 2677, No. 2, 2023, pp. 712–724. https://doi.org/10.1177/03611981221108377.
58. Van Arem, B., C. J. Van Driel, and R. Visser. The Impact of Cooperative Adaptive Cruise Control on Traffic-Flow Characteristics. *IEEE Transactions on intelligent transportation systems*, Vol. 7, No. 4, 2006, pp. 429–436.
59. Talebpour, A., and H. S. Mahmassani. Influence of Connected and Autonomous Vehicles on Traffic Flow Stability and Throughput. *Transportation research part C: emerging technologies*, Vol. 71, 2016, pp. 143–163.
60. Alvarez Lopez, P., M. Behrisch, L. Bieker-Walz, J. Erdmann, Y.-P. Flötteröd, R. Hilbrich, L. Lücken, J. Rummel, P. Wagner, and E. Wießner. Microscopic Traffic Simulation using SUMO. Presented at the The 21st IEEE International Conference on Intelligent Transportation Systems, Maui, USA, 2018.
61. Daamen, W., and S. P. Hoogendoorn. Free Speed Distributions — Based on Empirical Data in Different Traffic Conditions. Berlin, Heidelberg, 2007.
62. Treiber, M., A. Hennecke, and D. Helbing. Congested Traffic States in Empirical Observations and Microscopic Simulations. *Physical Review E*, Vol. 62, No. 2, 2000, pp. 1805–1824. https://doi.org/10.1103/PhysRevE.62.1805.
63. Kurtc, V., and M. Treiber. Simulating Bicycle Traffic by the Intelligent-Driver Model-Reproducing the Traffic-Wave Characteristics Observed in a Bicycle-Following Experiment. *Journal of Traffic and Transportation Engineering (English Edition)*, Vol. 7, No. 1, 2020, pp. 19–29. https://doi.org/10.1016/j.jtte.2019.03.005.
64. Saberi, M., and H. Mahmassani. Exploring Areawide Dynamics of Pedestrian Crowds: Three-Dimensional Approach. *Transportation Research Record Journal of the Transportation Research Board*, Vol. 2421, 2014, pp. 31–40. https://doi.org/10.3141/2421-04.
65. Mjahed, L. B., H. S. Mahmassani, and A. Talebpour. Macroscopic Directional Analysis of Pedestrian Flow. *Transportation Research Record*, Vol. 2561, No. 1, 2016, pp. 64–72. https://doi.org/10.3141/2561-08.
66. Ambühl, L., A. Loder, M. C. J. Bliemer, M. Menendez, and K. W. Axhausen. A Functional Form with a Physical Meaning for the Macroscopic Fundamental Diagram. *Transportation Research Part B: Methodological*, Vol. 137, 2020, pp. 119–132. https://doi.org/10.1016/j.trb.2018.10.013.
67. OpenStreetMap contributors. Planet Dump Retrieved from Https://Planet.Osm.Org. , 2017.
68. Average Annual Daily Traffic. https://idot.illinois.gov/transportation-system/network-overview/highway-system/maps/average-annual-daily-traffic.html. Accessed May 15, 2025.
69. Johnson, J. Designing with the Mind in Mind: The Psychological Basis of User Interface Design Guidelines. New York, NY, USA, 2021.
70. Rasouli, A., and J. K. Tsotsos. Autonomous Vehicles That Interact With Pedestrians: A Survey of Theory and Practice. *IEEE Transactions on Intelligent Transportation Systems*, Vol. 21, No. 3, 2020, pp. 900–918. https://doi.org/10.1109/TITS.2019.2901817.
71. Zhanguzhinova, S., E. Makó, A. Borsos, Á. P. Sándor, and C. Koren. Communication between Autonomous Vehicles and Pedestrians: An Experimental Study Using Virtual Reality. *Sensors (Basel, Switzerland)*, Vol. 23, No. 3, 2023, p. 1049. https://doi.org/10.3390/s23031049.

72. Alozi, A. R., and M. Hussein. Evaluating the Safety of Autonomous Vehicle–Pedestrian Interactions: An Extreme Value Theory Approach. *Analytic Methods in Accident Research*, Vol. 35, 2022, p. 100230. https://doi.org/10.1016/j.amar.2022.100230.
73. Métayer, N., and S. Coeugnet. Improving the Experience in the Pedestrian's Interaction with an Autonomous Vehicle: An Ergonomic Comparison of External HMI. *Applied Ergonomics*, Vol. 96, 2021, p. 103478. https://doi.org/10.1016/j.apergo.2021.103478.
74. Daganzo, C. F. The Cell Transmission Model: A Dynamic Representation of Highway Traffic Consistent with the Hydrodynamic Theory. *Transportation research part B: methodological*, Vol. 28, No. 4, 1994, pp. 269–287.
75. Edie, L. C. *Discussion of Traffic Stream Measurements and Definitions*. Port of New York Authority, 1963.